

SOLAR GENERATED STEAM INJECTION IN HEAVY OIL RESERVOIRS

A THESIS SUBMITTED TO
THE GRADUATE SCHOOL OF NATURAL AND APPLIED SCIENCES
OF
MIDDLE EAST TECHNICAL UNIVERSITY

BY

CANSU AFŞAR

IN PARTIAL FULFILLMENT OF THE REQUIREMENTS
FOR
THE DEGREE OF MASTER OF SCIENCE
IN
PETROLEUM AND NATURAL GAS ENGINEERING

SEPTEMBER 2014

Approval of the thesis:

SOLAR GENERATED STEAM INJECTION IN HEAVY OIL RESERVOIRS

submitted by **CANSU AFŞAR** in partial fulfillment of the requirements for the degree of **Master of Science in Petroleum and Natural Gas Engineering Middle East Technical University** by,

Prof. Dr. Canan Özgen _____
Dean, Graduate School of **Natural and Applied Sciences**

Prof. Dr. Mahmut Parlaktuna _____
Head of Department, **Petroleum and Natural Gas Engineering**

Prof. Dr. Serhat Akın _____
Supervisor, **Petroleum and Natural Gas Engineering Dept., METU**

Examining Committee Members:

Prof. Dr. Mahmut Parlaktuna _____
Petroleum and Natural Gas Engineering Dept., METU

Prof. Dr. Serhat Akın _____
Petroleum and Natural Gas Engineering Dept., METU

Prof. Dr. Nurkan Karahanoğlu _____
Geological Engineering Dept., METU

Asst. Prof. Çağlar Sınayuç _____
Petroleum and Natural Gas Engineering Dept., METU

Dr. Kubilay Kumsal _____
Consultant

Date: 01.09.2014

I hereby declare that all information in this document has been obtained and presented in accordance with academic rules and ethical conduct. I also declare that, as required by these rules and conduct, I have fully cited and referenced all material and results that are not original to this work.

Name, Last name: Cansu AFŞAR

Signature:

ABSTRACT

SOLAR GENERATED STEAM INJECTION IN HEAVY OIL RESERVOIRS

Afşar, Cansu

M.S., Petroleum and Natural Gas Engineering Department

Supervisor: Prof. Dr. Serhat AKIN

September 2014, 123 pages

Turkey is one of the countries having mostly heavy oil reservoirs with 10-15° API gravity. Due to high amount of residual oil in the reservoir, thermal injection methods are evaluated to increase recovery in south-east of Turkey. However, the fuel cost of steam generation, that represents 60% of the total project cost, is a major challenge for companies. Combination of solar generated steam technology and heavy oil recovery techniques encourage companies to reduce the operation costs. This solar aided steam injection system has already proven its capability to replace natural gas systems up to 80%, depending on the steam requirement and weather data.

In this study, a pilot scale area was selected in order to present an evaluation whether the solar generated steam injection is technically and economically feasible in the heavy oil reservoirs. Operational data such as injection rate, steam temperature and steam quality were determined by using published studies. Continuous steam injection together with natural gas burner back-up system was used when direct normal insolation (DNI) is intermittent to maintain required steam during troublesome climates,

nights and winter seasons. After solar collector system was designed in Transient System Simulation Tool (TRNSYS) and combined with the steam injection method, economic analyses were also carried out to determine if the solar thermal technology is feasible for the candidate pilot field.

Results indicated that existing DNI of the selected region was not high enough to maintain the continuous steam injection. It caused a requirement of natural gas back up system. Economic analyses of combined system indicated that fuel saving cannot compensate the initial cost of solar project with current oil price in 30 years period.

Keywords: Enhanced oil recovery (EOR), steam injection, heavy oil reservoir, solar generated steam technology,

ÖZ

GÜNEŞTEN ÜRETİLEN BUHARIN AĞIR PETROL REZERVUARLARINA ENJEKSİYONU

Afşar, Cansu

Yüksek Lisans, Petrol ve Doğal Gaz Mühendisliği Bölümü

Tez Yöneticisi: Prof. Dr. Serhat AKIN

Eylül 2014, 123 sayfa

10-15° API ağırlıklı petrol içeren ağır petrol rezervuarlarına sahip ülkelerden biri de Türkiye'dir. Rezervuarda kalan önemli miktardaki petrolden dolayı, Türkiye'nin güney doğusunda petrol üretimini artırmak için termal enjeksiyon methotları değerlendirilmektedir. Fakat; toplam buhar üretim maliyetlerinin %60'ını oluşturan yakıt maliyeti şirketler için büyük zorluklardan biridir. Güneşten buhar elde etme teknolojisinin ve ağır petrol kurtarım tekniklerinin beraber kullanımı şirketlere bu maliyetlerin azaltılması konusunda ümit vaat etmiştir. Güneş destekli buhar elde etme projesi, buhar ihtiyacına ve hava durumu datalarına bağlı olarak %80'e kadar doğal gaz sisteminin yerine geçebileceğini kanıtlamıştır.

Bu çalışmada güneşten buhar elde etme yönteminin teknik ve ekonomik olarak uygulanabilirliğini göstermek için Türkiye'nin güney doğusunda bulunan X sahasında pilot bir alan seçilmiştir. Operasyon parametreleri; enjeksiyon debisi, buhar sıcaklığı ve buhar kalitesi vb. yayınlanan çalışmalardan alınmıştır. Doğal gaz destek sistemi,

güneşten üretilen buhar sistemiyle beraber, direk güneş radyasyonunun kesintili olduğu zamanlarda; zorlu ilkim şartlarında, geceleri ve kış sezonlarında kullanılmıştır. Güneş kolektörlerinin Transient System Simulation Tool (TRNSYS) simülatörü kullanılarak modellenmesinden sonra buhar enjeksiyon yöntemiyle birleştirilmiştir. Bu projenin X sahasında uygulanabilir olup olmadığına karar vermek için ekonomik analizler de yapılmıştır.

Sonuçlar göstermektedir ki mevcut bulunan direk güneş radyasyonu devamlı buhar enjeksiyonunu devam ettirmek için yeterli değildir. Bu yüzden doğal gazla destekleme sistemine ihtiyaç duyulmuştur. Birleştirilmiş sistemin ekonomik analizine göre buradan yapılacak yakıt tasarrufu güneş sisteminin ilk maliyetini, günümüzdeki petrol fiyatlarıyla 30 yıl içerisinde telafi edememektedir.

Anahtar Kelimeler: İleri petrol kurtarımı (EOR), buhar enjeksiyonu, ağır petrol rezervuarları, güneşten buhar elde etme teknolojisi

Dedicated to my family

ACKNOWLEDGEMENTS

First and foremost, I wish to express my greatest respect and appreciation to my thesis advisor, Prof. Dr. Serhat Akın, for giving inspiration for the creation of this work. His suggestions shaped the dissertation and have kept me on the right path to complete this work.

Words fail me to express my special appreciation to my parents, Ümran and Metin Afşar, my sister and her husband, Duygu and Mehmet Ünlü, for their constant support and encouragement all through my life. Their unselfish cooperation and much needed help has helped me to complete this task.

My deepest gratitude goes to my biggest supporter Çağrı Arı, who has been there for me every step of the way. He has shown nothing less than perfect patience and encouragement.

Special thanks go to my best friends, Bengisu Çorakçı, Esin Durdu, İklima Şenol and İrem Doma, who have helped me to relieve so much stress over the past few years and carried me to the end of this journey. I couldn't have done this without you. I really appreciate to Gülin Başkes for her never ending and unconditional self-devotion and support.

My sincere thanks also go to Ülker Kalfa who taught me that learning is more than just a grade and Murat Kalfa for his endless support. It was them who introduced me first to “Petroleum Engineering”. Words are not enough to express my appreciation to Basak Kalfa who has always been there in sunshine and in shadow of my life.

I express my deepest thanks to Selin Güven, Aslı Satı Gündođar, Sevtaç Bülbül and Tuđçe Bayram Ertürk for their support and friendship.

I would like to thank Tufan Akba and Atalay Çalıřan for their valuable advices and crucial contribution to this thesis.

I would like to thank GÜNAM (Center for Solar Energy Research and Applications) for providing TRNSYS software and Turkish Petroleum Company for providing me their resources and technical support.

Last, but certainly not least, words cannot express my gratitude to Mustafa Kemal ATATURK, the leader of Turkey's War of Independence and the founder of Turkish Republic, for his reforms to improve the status of women and make us visible in the society.

TABLE OF CONTENTS

ABSTRACT.....	V
ÖZ.....	VII
ACKNOWLEDGEMENTS.....	X
TABLE OF CONTENTS	XII
LIST OF TABLES	XIV
LIST OF FIGURES.....	XVI
NOMENCLATURE.....	XIX
CHAPTERS	
INTRODUCTION.....	1
1.1 BACKGROUND INFORMATION.....	1
1.1.1 Solar Thermal Energy	2
LITERATURE SURVEY.....	7
2.1 SOLAR THERMAL COLLECTORS.....	7
2.2 SOLAR GENERATED STEAM FOR OIL RECOVERY	11
2.3 STEAM INJECTION METHOD	13
2.3.1 Parameters That Effect Steamflooding.....	17
2.4 STEAM INJECTION MODELLING	20
2.4.1 Field History	21
2.4.2 Characteristics of X field.....	22
2.4.3 X Field Steam Pilot Study	22
2.4.4 Numerical Model Framework.....	24

2.4.5	Semi Analytical Wellbore Model.....	25
	STATEMENT OF THE PROBLEM.....	29
	METHOD OF SOLUTION.....	31
4.1	SOLAR GENERATED STEAM INJECTION METHOD.....	31
4.1.1	Overview of Concentrating Solar System	31
4.1.2	Solar Generated Steam Injection Model.....	35
	RESULTS & DISCUSSION.....	77
5.1	RESULTS.....	77
5.1.1	Solar Field Performance and Cost Analysis	77
5.2	DISCUSSION	98
	CONCLUSIONS	101
	RECOMMENDATIONS FOR FUTURE WORK.....	103
	REFERENCES	105
	APPRENDICES	
	A.HEAT TRANSFER FLUID (THERMINOL-VP1) PROPERTIES (21).....	109
	B.SOLAR FIELD DESIGN	111
	C.HEAT EXCHANGER DESIGN.....	123

LIST OF TABLES

TABLES

Table 1. 1: Type and sources of renewable Energy System	2
Table 2. 1: The Characteristics of the SEGS Plants	10
Table 2. 2: Screening criteria for steam injection process	14
Table 2. 3: Wellbore parameters that used in the model	25
Table 4. 2: Typical Meteorological Year Data	39
Table 4. 3: Monthly average weather data.....	44
Table 4. 4: Explanation of the terms	44
Table 4. 5: Parameters of the collector	58
Table 4. 6: Input of the collector model	58
Table 4. 7: Pump Model	61
Table 4. 8: Storage tank parameters	66
Table 4. 9: Feedwater quality requirement for steam generation.....	71
Table 4. 10: Operation design of steam generator.....	75
Table 5. 1: Parameters of the collector	80
Table 5. 2: Input of the collector model	81
Table 5. 3: Pump Model	81
Table 5. 4: Storage tank parameters	81
Table 5. 5: Breakdown of the investment cost of 50 MW PTC power plant.....	93
Table 5. 6: Yearly Saving with Solar Field.....	97
Table A. 1: Therminol-VP1 properties.....	109

Table B. 1: Nomenclature of Solar Collector..... 111
Table B. 2: Default setting of TRNSYS..... 115
Table B. 3: Nomenclature of Pump 118
Table B. 4: Nomenclature of Storage Tank..... 119
Table B. 5: Default Setting of TRNSYS for Storage Tank..... 122

Table C. 1: Heat Exchanger Properties..... 123

LIST OF FIGURES

FIGURES

Figure 1. 1: Sun-Earth relationship	4
Figure 1. 2: High insolation areas in the world	5
Figure 2. 1: Parabolic Dish Collector	7
Figure 2. 2: Solar tower system	8
Figure 2. 3: Parabolic trough collector system	9
Figure 2. 4: Enhanced oil recovery methods	12
Figure 2. 5: Effect of reservoir thickness on steamflooding method	18
Figure 2. 6: Geometry of common regular pattern floods	19
Figure 2. 7: Production history of the field	21
Figure 2. 8: Five spot steam drive pilot pattern	23
Figure 2. 9: Oil production rates of 4 wells during the steam injection application	23
Figure 2. 10: Steam quality varies with depth based on the steam quality	26
Figure 2. 11: Steam temperature varies with depth based on the steam quality	26
Figure 2. 12: Steam quality varies with depth based on the steam injection rate	27
Figure 2. 13: Steam quality varies in vacuum insulated tubings	27
Figure 4. 1: Diffuse and Direct Radiation	32
Figure 4. 2: The declination angle due to Earth's tilt	33
Figure 4. 3: Declination angle variation by month, from Equation 4.1	34
Figure 4. 4: Solar Angles	35
Figure 4. 5: Steam generating solar injection model.....	36
Figure 4. 6: Monthly Global Radiation	41
Figure 4. 7: Diffuse Radiation throughout the year	42

Figure 4. 8: Temperature variation throughout the year	42
Figure 4. 9: Sunshine duration throughout the year	43
Figure 4. 10: Amount of precipitation throughout the year	43
Figure 4. 11: Direct normal insolation of Batman on both June 21,	49
Figure 4. 12: Variation of equation of time throughout the year, from Equation 4.27 ..	51
Figure 4. 13: Collector shading effect through a day	53
Figure 4. 14: Representation of end loss	54
Figure 4. 15: The parallel and counterflow design of heat exchangers	67
Figure 4. 16: Counterflow heat exchanger.....	69
Figure 4. 17: Once through steam generator	72
Figure 4. 18: Configuration of OTSG	73
Figure 4. 19: Operation Design of Conventional Steam Injection	74
Figure 5. 1: Steam quality varies with depth based on the steam quality	78
Figure 5. 2: Steam temperature varies with depth based on the steam quality	78
Figure 5. 3: Steam quality varies with depth based on the steam injection rate	79
Figure 5. 4: Steam quality varies in vacuum insulated tubings.....	79
Figure 5. 5: Produced steam by 1 parallel series	82
Figure 5. 6: Produced steam by 2 parallel series	83
Figure 5. 7: Produced steam by 3 parallel series	83
Figure 5. 8: Produced steam by 4 parallel series	84
Figure 5. 9: Produced steam by 5 parallel series	84
Figure 5. 10: Produced steam by 6 parallel series	85
Figure 5. 11: Produced steam by 7 parallel series	85
Figure 5. 12: Produced steam by 8 parallel series	86
Figure 5. 13: Produced steam by 9 parallel series	86
Figure 5. 14: Produced steam by 10 parallel series	87
Figure 5. 15: Produced steam by 11 parallel series	87
Figure 5. 16: Solar collector performance analysis	88

Figure 5. 17: Total installed cost for parabolic trough plant commissioned or 90
Figure 5. 18: Cost breakdown for parabolic trough collectors 91
Figure 5. 19: Monthly Fuel Consumption 95
Figure 5. 20: Comparison of fuel saving and fuel consumption by months in 1 year ... 95
Figure 5. 21: History and forecast of the oil price 96
Figure 5. 22: CAPEX+O&M vs Cost Saving by Years 98

NOMENCLATURE

EOR.....	Enhanced oil recovery
CSP.....	Concentrating solar power
DNI.....	Direct normal irradiance
HTF.....	Heat transfer fluid
PTC.....	Parabolic trough collector
SEGS.....	Solar energy generating systems
TMY.....	Typical meteorological year
TRNSYS.....	Transient System Simulation Tool
OOIP.....	Original oil in place
STB.....	stock tank barrel
D.....	day
WAG.....	Water alternating gas
SCF.....	Standard cubic feet
NSRDB.....	National Solar Radiation Data Base
BTU.....	British thermal unit
Ft.....	feet
F.....	Fahrenheit
C.....	Celsius
Psi.....	pound square inch
OTSG.....	Once through steam generator

CHAPTER 1

INTRODUCTION

1.1 Background Information

Energy is the basic input of our civilization and it is the most current indicator to show the level of countries in socio-economic development. Countries' policies are mostly based on to get new energy resources to meet their energy requirement.

In order to meet ever-increasing energy demand; governments are supporting the companies to discover and develop the new alternative energy sources. In addition to that, current popular resources such as coal, oil and natural gas have already shown enormous challenges including environmental impacts, foreign source dependency, increasing prices and limited sources.

Renewable energy sources do not require fuel based energy production systems therefore they are less dependent on mentioned concerns. Table 1.1 shows the type and sources of renewable energy systems.

Table 1. 1: Type and sources of renewable Energy System [1]

Renewable Energy System	Sources
Solar Energy	Sun
Wind Energy	Wind
Biomass Energy	Biological waste
Geothermal Energy	Ground water
Hydropower	Rivers
Offshore wind, wave, and tidal energy	Ocean and Sea
Hydrogen Energy	Water and Hydroxide

On a global scale; emission free energy sources has already started to replace the fossil fuels and traditional production technologies; therefore, to develop new technologies becomes essential for the future. Nowadays, massive investments have been made in renewable energies and the most promising one seems solar energy as an infinite energy source.

The following sections will give detailed information about solar energy and its applications in oil and gas industry.

1.1.1 Solar Thermal Energy

Solar energy is the most common and useful type because it has several features as following:

- An inexhaustible source of energy and never decreases.
- A kind of clean energy that does not include gas, smoke, dust or harmful substances such as carbon or sulfur.

- All the countries can benefit from sun. In this way, the energy dependence of countries can be eliminated.
- Can be achieved easily without any transportation expenses.
- Does not require any complex technology. Almost all countries, with local industry organizations easily benefit from its energy.

People has benefited from the advantage of solar energy in different utilization for many years. Firstly, concentrating sun rays were used to make fire and burn ants in 7th Century B.C. In 2nd Century B.C., Archimedes used mirrors to focus sun's rays. In 1860s, August Mouchet and Abel Pifre invented the first solar powered engines. In following years, concentrating solar power has been used for several applications such as heating and generating electricity. [2]

Solar energy can be used all over the world; however, efficiency is changing based on the region due to earth-sun relative motion. The sun with a diameter of 1.39×10^9 m completes the rotate on its axis about 1 month. Actually it shows difference between on its equator (27 days) and on the polar region (30 days). The distance between Earth and Sun is about 1.495×10^{11} m. Figure 2.1 shows the geometric relationship between earth and sun. [3]

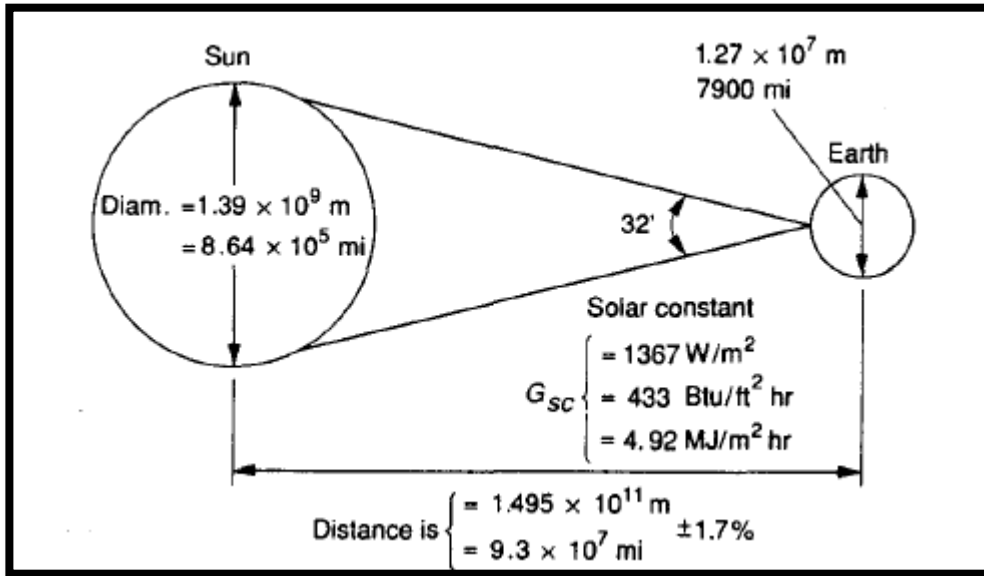


Figure 1. 1: Sun-Earth relationship [3]

The variety of wavelengths of energy (62 MW/m^2) spreads from the sun but only one in the billions of this energy is emitted by the earth surface. The approximate value of solar radiation at the outside of the atmosphere is 1367 W/m^2 . However, because of the angular position of the Earth, it shows difference of irradiance from region to region. Figure 1.2 shows highest insolation areas in the world and it seems that most encouraging area for solar energy investments are South-Western United States, Central and South America, Africa, the Middle East, the Mediterranean countries of Europe, Iran, Pakistan and the desert regions of India, the former Soviet Union, China and Australia. [4]

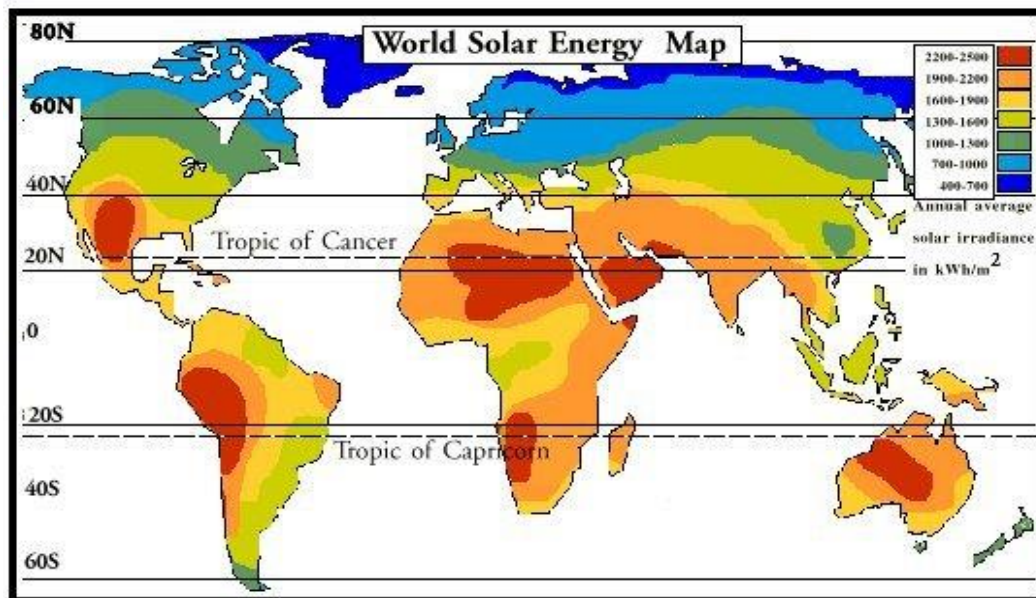


Figure 1. 2: High insolation areas in the world [4]

In order to make a design of solar system three main factors should be considered; the amount, quality, and sunset hour. In this study, as only solar thermal system will be presented, other solar system such as flat collectors or photovoltaic (PV) will not be included.

The working mechanism of solar thermal energy is as follows: Sun's rays are scattered by the atmosphere and turn in to direct solar radiation and they are concentrated by the concentration solar systems and provide heat. Heat is used in power cycle such as steam turbine and then it generates the electricity. Also, generated steam can be used for different applications and in different industries. One of these utilization areas is oil industry and in this study the application named "solar generated steam injection in heavy oil reservoirs" will be presented.

This study aims to demonstrate whether solar project is feasible or not in a selected oil field located in Southeast Turkey which is also a candidate for large scale steam injection application. First, solar field has been designed based on the steam injection's criteria. Then, economic analysis has been performed in order to evaluate the feasibility of solar generated steam injection method.

CHAPTER 2

LITERATURE SURVEY

2.1 Solar Thermal Collectors

There are 3 different mechanisms in solar thermal system. The first one is parabolic dish collectors that concentrate the sun's energy by a parabolic-shaped point focus concentrator and reflects it on to the focal point receiver. Concentrators can follow the sun's motion with a two-axis tracking system. Heat is used by a heat engine for power conversion. Approximately, 25kW of electricity can be generated with maximum 30% efficiency from one parabolic dish system. Figure 2.1 shows a photo of parabolic dish collector. [5]



Figure 2. 1: Parabolic Dish Collector [6]

The next one is solar tower system that consists of many large two axis sun tracking heliostats (large individually tracking mirrors) and a tower with a receiver at the top of it. Focusing sunlight creates heat for heat transfer fluid in the receiver to produce steam. Steam is sent to conventional steam generator to generate electricity. [5] System needs very high investment cost. Solar tower system can produce 50 to 200 MW of electricity. Operating temperature can be achieved around 1000°C. Figure 2.2 shows a photo of a solar tower system. [5]



Figure 2. 2: Solar tower system [6]

The last one is parabolic trough collector system includes trough shaped reflectors and a receiver tube mounted at trough's focal line. Concentrated solar energy heats the thermal transfer fluid flowing through the receiver pipe and is sent to the heat exchangers to generate superheated steam. In a steam turbine generator, electricity is produced by converting to steam energy. Tracking system can be north-south axis or east-west axis. Individual systems can produce about 80MW of electricity. Operating

temperature is about 400°C. Figure 2.3 shows a photo of a parabolic trough collector system. [5]



Figure 2. 3: Parabolic trough collector system [7]

In this study, solar generated steam injection model has been designed by using parabolic trough collector system. In order to understand working principle of this system, it is important to know how parabolic trough collectors have been developed until today.

The first large scale solar collectors were designed in the U.S. in the 1970s by the Energy Research and Development Administration. The collectors were able to reach temperatures up to 400°C (752°F). Then by Sandia National Laboratories in Albuquerque, New Mexico, variety in size from a few hundred to about 5000 m² of collector area were came into use. Also, in 1981 new investments were made in Europe and one of the biggest and the most successful projects with 7602 m² of mirror area was carried out in Tabernas, Spain. [8]

In 1982, Luz International Limited (Luz) built a parabolic trough collector system for industrial process heat application. In 1983, Luz had an agreement with Southern California Edison for a project called Solar Energy Generating System (SEGS) I and II plants. Then, the project was developed through SEGS IX projects. While initial systems could produce 30MW, later it was increased to 80MW. Table 2.1 shows the properties of the SEGS plants constructed by Luz. [8]

Table 2. 1: The Characteristics of the SEGS Plants [9]

SEGS Plant	1st Year of Operation	Net Output (MW _e)	Solar Field Outlet Temp. (°C/°F)	Solar Field Area (m ²)	Solar Turbine Eff. (%)	Fossil Turbine Eff. (%)	Annual Output (MWh)
I	1985	13.8	307/585	82,960	31.5	-	30,100
II	1986	30	316/601	190,338	29.4	37.3	80,500
III & IV	1987	30	349/660	230,300	30.6	37.4	92,780
V	1988	30	349/660	250,500	30.6	37.4	91,820
VI	1989	30	390/734	188,000	37.5	39.5	90,850
VII	1989	30	390/734	194,280	37.5	39.5	92,646
VIII	1990	80	390/734	464,340	37.6	37.6	252,750
IX	1991	80	390/734	483,960	37.6	37.6	256,125

Solar thermal power is commonly used in generating electricity. However, increasing in awareness regarding to solar energy has provided an increase in investment of this energy in other areas. Oil industry has a big share in solar energy market. The following part presents the new technology in enhanced oil recovery methods with solar generated steam injection technique.

2.2 Solar Generated Steam for Oil Recovery

Obviously, most of the conventional resources are approaching their end, so to create innovative solutions for getting the most out of the reservoirs is on the agenda of every country. Enhanced oil recovery (EOR) methods represent the exact solution for increasing oil recovery.

The life cycle of a field is divided into 3 stages in the development strategies. Primary oil recovery is defined as naturally producing of hydrocarbons with the pressure change of the formation or using artificial lift techniques to get pressure difference. Secondary oil recovery including water injection and immiscible gas injection is used when reservoir pressure is not enough to produce. Recovery factor can change between 20-65% according to characteristics of the reservoir. The last one tertiary oil recovery also called enhanced oil recovery (EOR) is used when secondary oil recovery methods are no longer produce economically. EOR methods include 3 main groups; thermal methods, gas methods and physicochemical methods. The selection of the method is based on the characteristics of oil and reservoir. Figure 2.4 shows the scheme of hydrocarbon recovery method. [10]

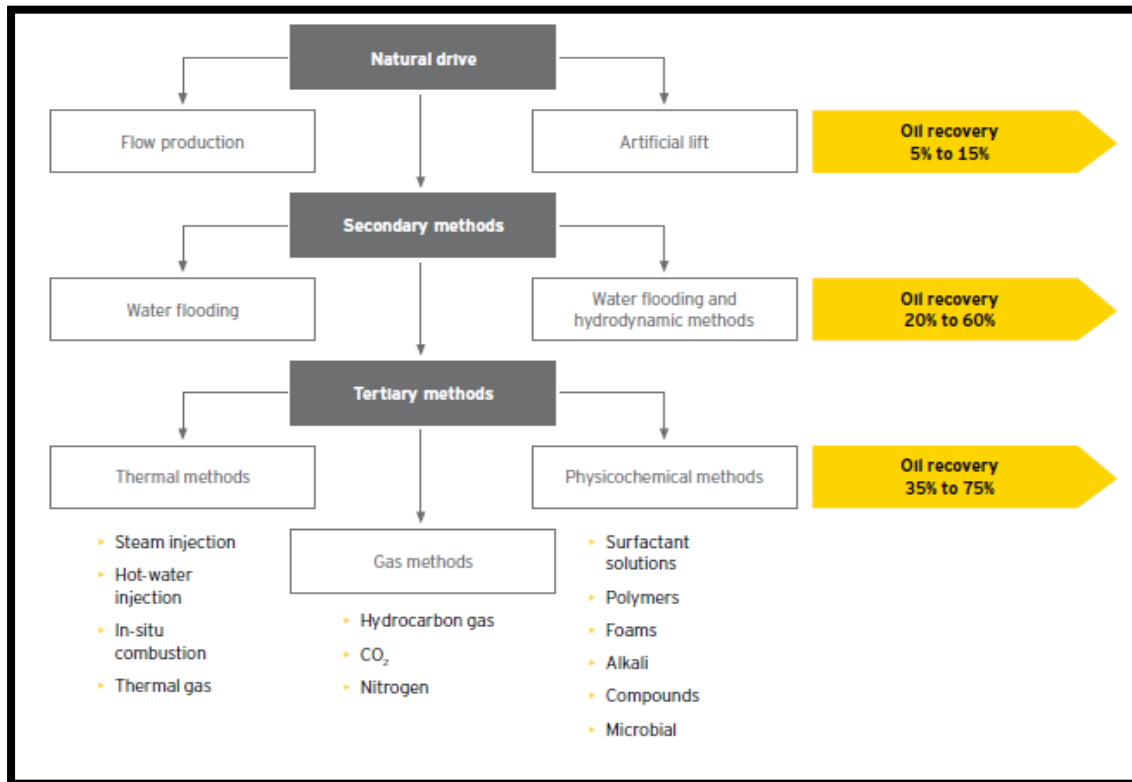


Figure 2. 4: Enhanced oil recovery methods [10]

The most promising technique in tertiary methods is thermal injection which shares 50% of the EOR market. Thermal methods are appropriate for heavy oil reservoir with API gravity with a range of 22° to 8° API and viscosities between 100-10000 centipoises. The basic principle of thermal methods is to heat the reservoir causing the increase temperature of oil so viscosity reduces and it allows the fluid to flow more easily. [10]

Steam injection method usually faces several challenges including high project cost and maintenance cost of facilities. High costs and greenhouse gas restrictions lead the companies to find a way to reduce environmental impact and investment cost.

Concentrating Solar Power (CSP) in thermal EOR project is an excellent idea that was born as a result of these challenges.

The main advantage of CSP is its ability to produce considerable amount of steam for large scale projects economically and environmentally. The first project that brought the solar thermal power and steam injection together was developed by U.S renewable energy organization, GlassPoint in California. After the success of this project, GlassPoint had an agreement with Petroleum Development Oman to construct solar thermal power in the Middle East. Since the Middle East has the biggest heavy oil fields and high solar insolation, solar thermal project has big promise in the future in that area. [11]

Turkey is one of the countries which have heavy oil reservoirs and abundant sunshine areas. Currently, continuous steam injection process is being applied in a pilot scale area in Turkey. Based on the results, more investments in steam generation may be required so CSP technology can be considered to reduce the environmental impact as well as operational cost. [11]

This study aims to demonstrate whether solar project is feasible or not in a selected oil field in some part of Turkey which is also a candidate for steam injection application. First, solar field has been designed based on the steam injection's criteria. Then, economic analysis has been performed in order to evaluate the feasibility of solar generated steam injection method.

2.3 Steam Injection Method

Steam injection is one of the most widely used tertiary oil recovery technique in heavy, viscous oils. The process can be defined mainly to generate the steam on the surface,

sometimes in the downhole, and to inject the reservoir continuously or in cycles. In continuous steam injection also known as a “steamflooding” the oil recovery is 50-75% of the oil in place. In cycle steam injection also called as “huff and puff” or “steam soak” the steam is injected in production well at very high rate and waited to soak for a little time (a few weeks). The steam heats the producing zone close the wellbore and decreases the viscosity of oil on that area. Then, the well is allowed to production and waited until the production rate decreases again. The process is repeated until the well is not profitably produce. In steam soak method, the oil recovery is expected between 10-25% of the oil in place. [12]

The operation method of steamflooding depends on totally screening criteria. The most recent analysis was made by Chu (1985) to examine all past studies and analyze the data from 28 steamflooding process. Table 2.2 presents the main screening criteria of steamflooding.

Table 2. 2: Screening criteria for steam injection process (Chu,1985)

Oil Gravity	<35° API (9,5-35° API)
Oil Viscosity	>20 cp (450-1000 cp)
Composition	not critical
Oil saturation	>500 bbl/acre-ft (>40-50% PV)
Formation type	limestone
Net thickness	>20 feet
Average permeability	10-100md
Transmissibility	>100 md ft / cp
Depth	>200-4300 feet
Temperature	not critical

The depth and formation thickness of the reservoir are primarily effects on efficiency of oil recovery. The shallower and thicker formations are suggested due to minimize the heat losses. Moreover, the deeper formations, the influence of steam injection becomes less significant. [12]

In addition to the parameters mentioned above relative permeability is one of the significant factors of steamflooding process. Casse and Ramey (1979) described that absolute permeability term is based on the properties of saturation fluid itself and the overburden pressure. Temperature has no impact on absolute permeability of oil and gas. However, although temperature effect on absolute permeability of water is not remarkable and can be neglected in oil recovery calculations, with increasing temperature absolute permeability is observed to decrease. [12]

Relative permeability functions can be obtained using the residual saturations. Several relative permeability models for steam flooding methods were studied. Kumar et al. (1985) method is the most widely used method to describe the effect of residual saturation of relative permeability. [12]

Moreover, thermal properties of the rock should be also known in order to calculate heat losses during the steamflooding process. The main parameters required to calculate heat loss are thermal conductivity and diffusivity. Thermal diffusivity α (ft^2/hr) is the ratio of thermal conductivity and volumetric heat capacity. The heat capacity includes contribution of rock grains and contained fluids for the fluid saturated reservoir. [12]

For the heat loss calculation at the surface, about 20% of the heat loss occurs due to flue gas leaving the system from the stack, about 3-5% is lost due to well design and, significant percentage is lost due to the pipeline that is used to inject the steam to the injection well. [12]

The Equation 1.1 below expresses the heat loss per unit length of pipe:

$$"Q_{ls} = (T_b - T_a)/R_h" \quad (2. 1)$$

where

T_b = the bulk temperature of the fluid in the pump, °F

T_a = the ambient temperature, °F

R_h = the resistance to heat transfer, Btu/hr- °F-ft pipe⁻¹

$$R_h = 1/(2\pi rU)$$

where;

r = radius of the surface across which the heat transfer is occurring, ft

U = the overall heat transfer coefficient, Btu/hr- °F

For a surface pipe, R_h can be calculated as follows:

$$R_h = (1/2\pi) \left[\frac{1}{h_f r_i} + \frac{1}{h_{pi} r_i} + \left(\frac{1}{\lambda_p} \right) \ln \left(\frac{r_o}{r_i} \right) + \frac{1}{h_{po} r_o} + \left(\frac{1}{\lambda_{ins}} \right) \ln \left(\frac{r_{ins}}{r_o} \right) + \frac{1}{h_{fc} r_{ins}} \right] \quad (2. 2)$$

where;

h = film coefficient of heat transfer, Btu/hr-ft²- °F

f = indicating f between the fluid and inside pipe wall

po = across the contact between the outside pipe wall and the insolation

λ = thermal conductivity, Btu/hr-ft²- °F,

p = pipe wall

ins = insolation

The change in steam quality in the surface pump also written as:

$$"f_{sw} = f_{sg} - Q_{ls}L/mL_v" \quad (2. 3)$$

where;

f_{sw} = wellhead steam quality

f_{sg} = the generator discharge steam quality

L = pipe length, ft

m = mass flow rate of steam, lb/hr

L_v = average enthalpy of vaporization of steam, Btu/lb

Another significant area that heat loss occurs in is the wellbore. Wellbore heat loss is mainly depends on depth and steam injection rate. Also, other factors such as insulation of tubing, scale or dirt on tubing, cementing, casing pipe wall, and damaged zone are the parameters compromised the resistance of heat loss. [12]

2.3.1 Parameters That Effect Steamflooding

2.3.1.1 Porosity

High porosity reservoirs offer higher oil recovery per barrel of steam injected compared the smaller pore size reservoirs. The reason is that large pore sizes have higher pore connectivity that means more viscosity reduction and less heat loss to the rock matrix occur in the system. [12]

2.3.1.2 Reservoir Thickness

As reservoir thickness increases, studies show that the oil recovery is getting higher. Reservoir thickness has a significant impact on steam injection projects so it has to be taken into consideration while determining the parameters. Capillary pressure, vertical

temperature gradient and extent of steam override are determined by the reservoir thickness. Figure 2.5 shows the effect of reservoir thickness on steamflooding oil recovery. [12]

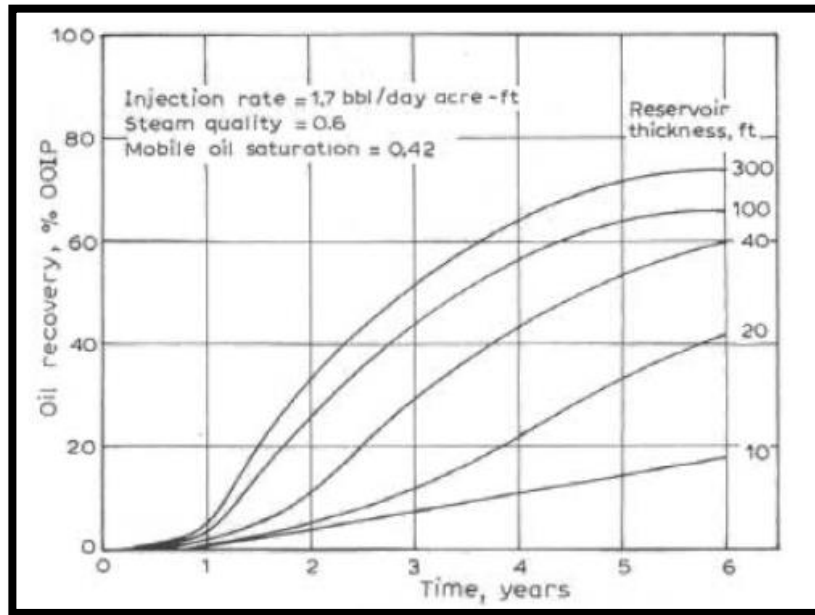


Figure 2. 5: Effect of reservoir thickness on steamflooding method [12]

2.3.1.3 Net / Gross Ratio

The net / gross ratio shows if any discontinuous shale part present in the reservoir. It has a negative effect on net productive thickness without any impact on vertical connectivity. Shale zones are generally water saturated and have a very high specific heat. Therefore, heat loss is less in shaly formations. [12]

2.3.1.4 Pattern Geometry

In most of the reservoir simulations, the well pattern geometry has no influence on oil recovery; however, in real life the limitation of well spacing and pattern geometry do exist. Higher producer to injector ratios give the higher productivity. Also, non-uniform spacing in pattern geometry such as nine-spot pattern brings less oil recovery due to lower sweep efficiency and earlier steam breakthrough. Figure 2.6 represents the geometry of common regular pattern floods (Craft & Hawkins, 1991) [12]

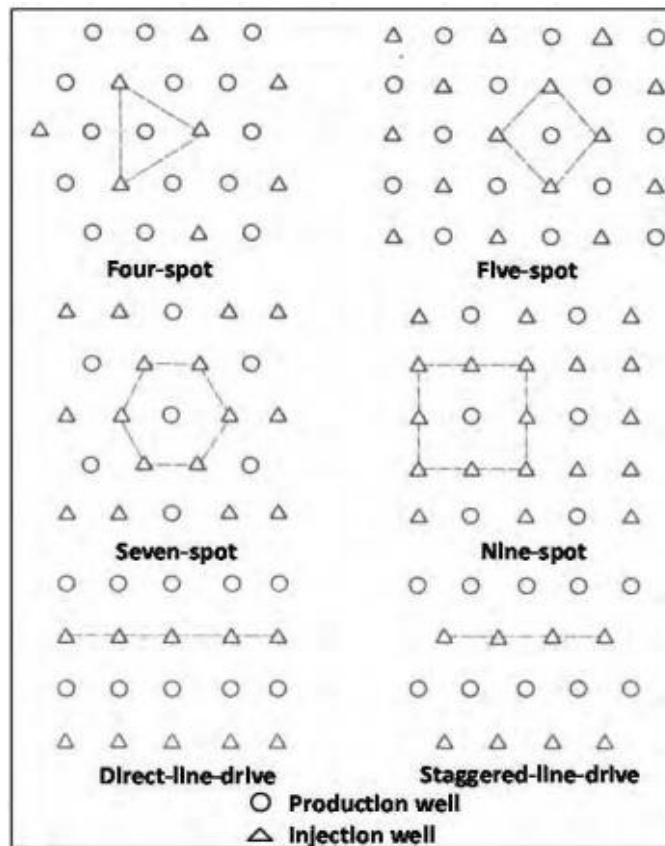


Figure 2. 6: Geometry of common regular pattern floods (Craft & Hawkins, 1991) [12]

2.3.1.5 Injection Rate

Injection rate is an important factor for steam injection process. Higher injection rates give higher oil recoveries due to minimize the heat loss. [12]

2.3.1.6 Steam Quality

“Steam quality is the proportion of saturated steam (vapor) in a saturated condensate (liquid)”. [13] As steam quality gets higher, the recovery increase also gets faster. Some studies show that with optimum steam quality could result in the highest productivity. Gomaa (1980) discovered that the optimum quality is about 40%; however, it depends on the characteristic of the operation. Higher steam quality suggests higher steam volume and lower steam viscosity. This situation shows a countereffect that results in better volumetric contact with the oil, though a lower displacement due to poorer mobility ratio. [12]

2.3.1.7 Heat Loss to Overburden and Underburden

The significant portion of the injected heat is passed on the formations existing above and below the pay which are called overburden and underburden. The amount of heat loss is based on the thermal characteristics of the rock and fluid. [12]

2.4 Steam Injection Modelling

In this study, a hypothetical solar application study has been conducted to show uses and benefits of the model. A pilot area of X field has been selected to apply the solar generated steam injection method. Several detailed research of X field on reservoir

properties and production analysis and the recent studies based on the steam injection application has been used to determine the application criteria of the solar field model. The following sections give the information about X field and steam injection model performed on the pilot area.

2.4.1 Field History

The first discovery of X field was in 1961. As seen in Figure 2.7 the peak production rate was observed as 9000 STB/D with approximately 120 wells in 1969. [14]

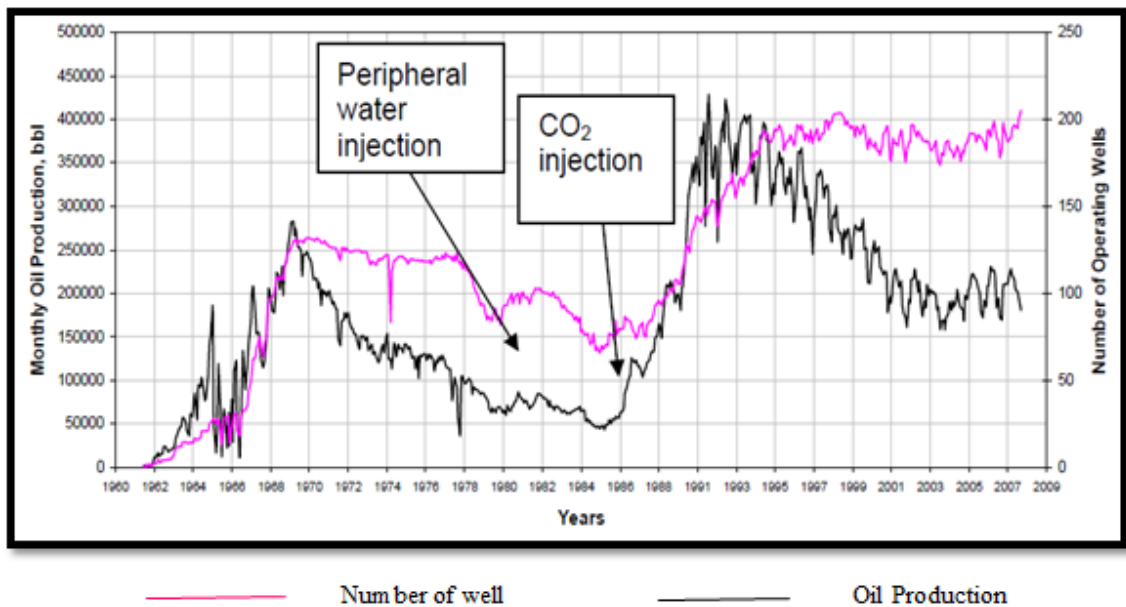


Figure 2. 7: Production history of the field [14]

As reservoir pressure declined to 400 psi from 1800 psi, secondary and tertiary methods consisting of waterflooding, CO₂ injection and steamflooding was applied in different time periods. Firstly, the waterflooding was implemented in the field between the years 1971 and 1978 and the recovery rate raised to 5% of OOIP. Then, CO₂ injection method was processed in 1986 and had been continued for 20 years. The peak production rate was reached to 14,000 bbl/day in 1990. In addition, with CO₂ injection water alternating gas (WAG) method and polymer gel treatments were implemented in latest years. [14]

2.4.2 Characteristics of X field

The reservoir is very heterogeneous and fissured limestone with a thickness varies from 60m to 80m. The field has about 17 km long and 2 to 4 km wide. The average porosity of the field is changing from 14% to 20% and the matrix permeability is ranging from 10 to 100md. The field contains very heavy oil of 9.5 to 13.5 API, and the viscosity ranging from 450 to 1000cp. The initial reservoir pressure and the bubble pressures were measured as nearly 1800 psi and 160 psig at depth of 4300 ft. The initial solution GOR was 18 SCF/STB. [14]

2.4.3 X Field Steam Pilot Study

The first steam injection application was performed in 1969 and had been continued for approximately 6 months. Five-spot pattern was implemented and Well-154 had performed as an injection well and Well-1, 14, 20, 41 were used as production wells. Figure 2.8 represents the location of five spot patterns. [14]

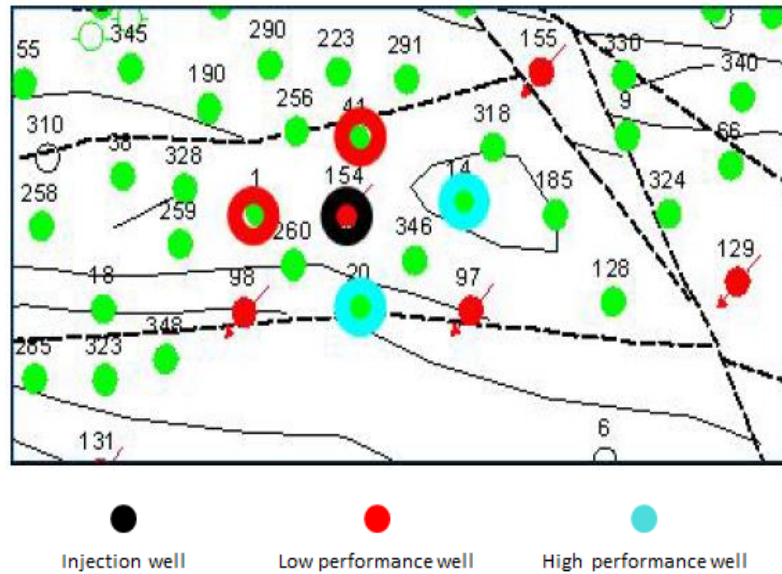


Figure 2. 8: Five spot steam drive pilot pattern [14]

Initial pressure was observed as 600 psi and it increased to 1550 psi after the 2 weeks of injection. The steam quality was 80% at the wellhead and it was observed to drop to 50% at the downhole. The performance of the wells with steam injection is shown in Figure 2.9. [14]

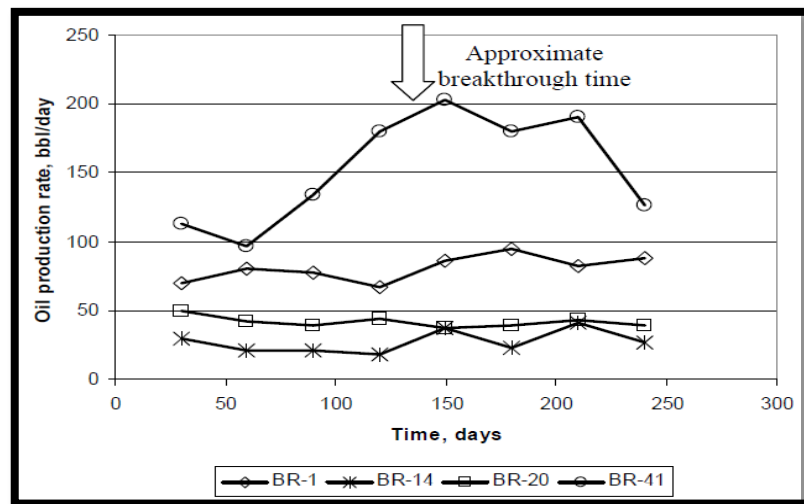


Figure 2. 9: Oil production rates of 4 wells during the steam injection application [14]

As it is seen in Figure 2.5, the best performance was obtained from Well- 41 as it was near a fault. Well-20 and Well-14 did not give the good results as Well-41. Although Well-41 had given the best performance during the steamflooding, after the breakthrough the sharpest decline was observed at this well. The significant experience gained from this pilot study was that the breakthrough was observed early and each well performed differently after the breakthrough. The reason could be due to the fact that the heterogeneous structure of the formation. [14]

2.4.4 Numerical Model Framework

In the developed sector model [15] the reservoir was a limestone. Porosity showed a range of from 14% to 20% and the matrix permeability was changing from 10 to 100md. The model consisted of 23x22x5 cartesian grids with a changing porosity (10.8% - 20%) and permeability (100md – 17.6 md). In addition, constant fracture porosity (1.5%) was defined to the model. [15]

The rock heat capacity was taken constant as 34.657 BTU / (ft³F) resembling a typical carbonate. The thermal conductivity of the rock, water, oil and gas were defined as 18.44, 8.6, 0.447 and 0.64 BTU/ (ft day F) respectively. The overburden heat loss was 31.76 BTU and underburden heat loss was 35.34 BTU. The injection pressure of the CO₂ was 1550 psi whereas steam injection pressure was 1800-2000 psi. The sensitivity analysis of steam quality between 0.50 and 0.95, steam temperature between 535°F and 635°F and steam injection rate between 250 and 2000 bpd were done. Initial reservoir temperature was taken as 150°F and the simulation run for 52 years. History match was done for 14, 41, 291, and 154 and 14, 41, 291 were defined as production well whereas 154 represented injection well. [15]

2.4.5 Semi Analytical Wellbore Model

In order to calculate pressure drop and heat losses in the wellbore, Fontanilla and Aziz (1982) semi analytical model was used. Table 2.2 shows the parameters that were used to describe the steam injection sector model:

Table 2. 3: Wellbore parameters that used in the model [16]

Tubing ID, m	0.050673
Tubing OD, m	0.060325
Insolation ID, m	0.0889
Insolation Thermal Conductivity, Btu/m-Day-°F	0.0219456
Heat Capacity of volumetric formation, Btu/ft ³ -°F	34.657
Casing ID, m	0.15707
Casing OD, m	0.17780
Well Diameter, m	0.2159
Depth, m	1.722.265
Heat Gradient, °F/m	0.0057912
Thermal Conductivity of Formation, Btu/m-Day-°F	7.132
Surface Temperature, °F	59

In addition to semi analytical wellbore model, to determine the design parameters, sensitivity analyses of steam quality, steam injection rate and steam temperature was done. The result of the study is represented in following Figure 2.10, 2.11, 2.12, and 2.13.

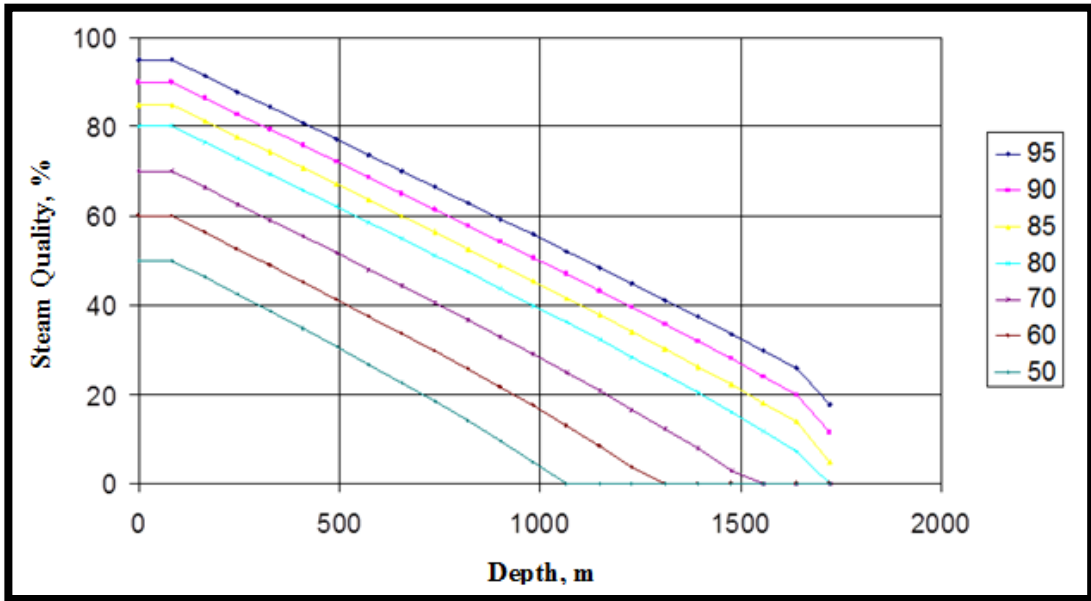


Figure 2. 10: Steam quality varies with depth based on the steam quality [16]

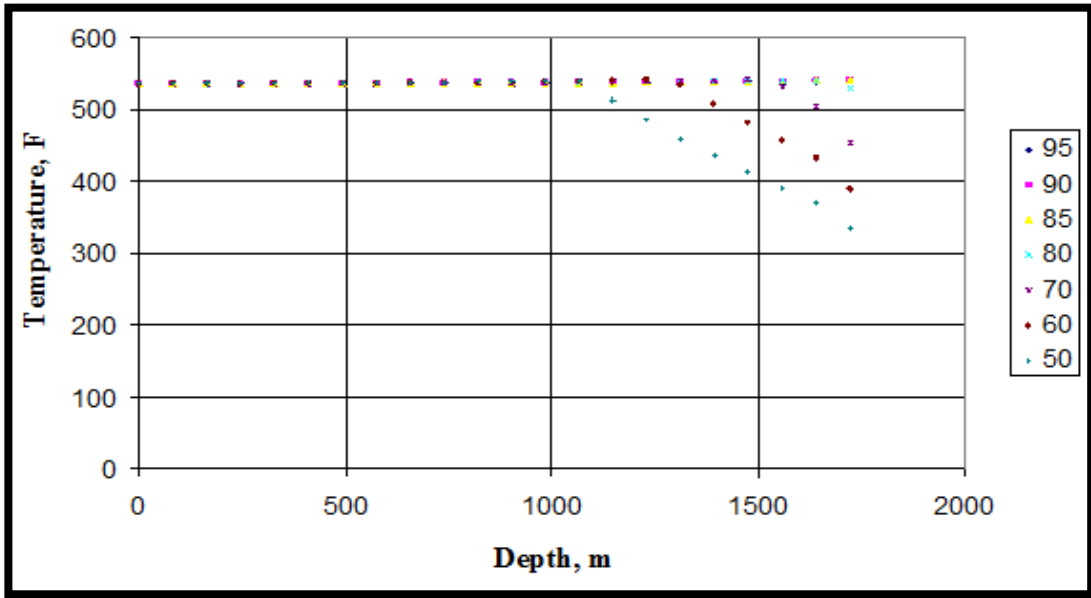


Figure 2. 11: Steam temperature varies with depth based on the steam quality [16]

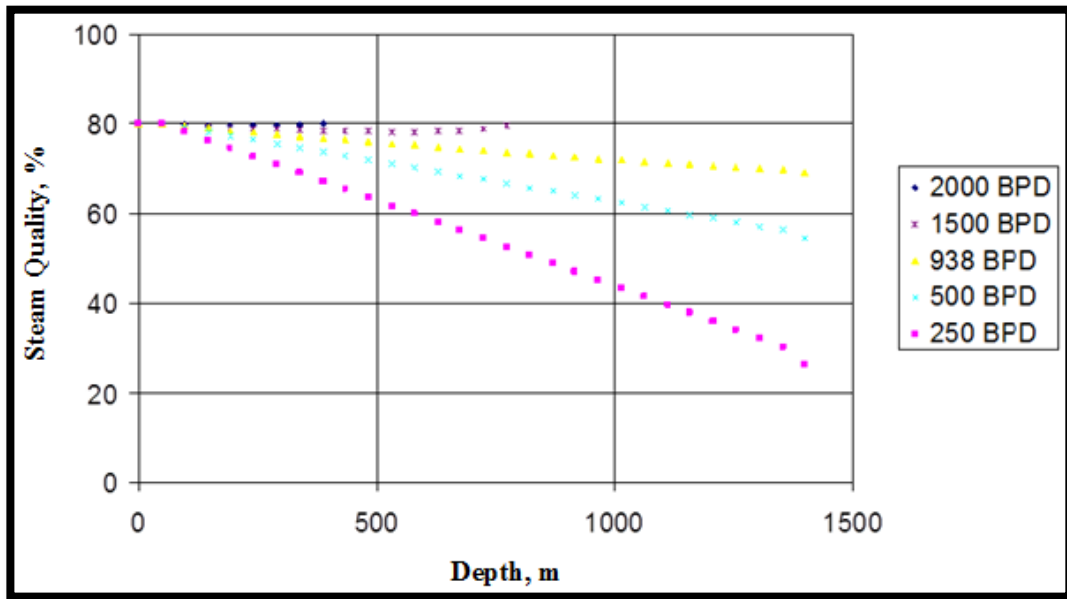


Figure 2. 12: Steam quality varies with depth based on the steam injection rate [16]

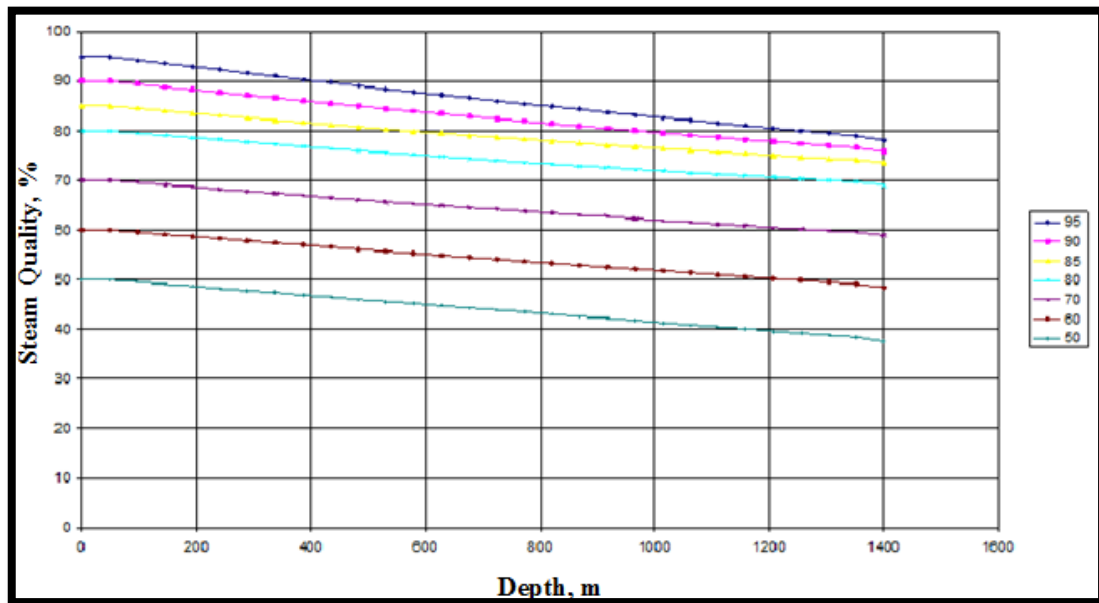


Figure 2. 13: Steam quality varies in vacuum insulated tubings [16]

Regarding the sensitivity analyses, in order to achieve maximum oil recovery the followings could be recommended;

- Vacuum insulated tubings (VIT) to decrease the heat loss in downhole
- 80% steam quality due to the fact that more than 80% has no impact on downhole steam quality.
- 1800-2000 psi steam injection pressure as more than 535 °F of steam temperature has no impact on downhole steam quality minimum recommended pressure; 1800 psi was selected and based on the pressure in thermodynamic condition, 622 °F was taken as steam temperature.
- 1000 cwebbl/day steam injection rate because more than this rate could result in high water cut and early breakthrough.

The following operational scenario has been used to mimic primary production and enhanced oil recovery period. According to steam injection pilot model, first Well-14 started production and after three years Well-41 was opened. Two years later, Well-154 was opened and the first steam injection was applied from this well after one year production period. The steam injection had been applied for 6 months. The last well Well-291 in the steam injection pilot model was commenced production 27 years later. The CO₂ injection method was started from Well-154 at the beginning of the 1991, and has been applied until today and will continue at the end of 2014. In the mid-2007 the field has undergone the steam injection while CO₂ application was still continue.

In this study, solar collectors are assumed to be put on the process for generating steam in 2008. The recommended parameters were taken into the solar model as determining factors. The details of the solar model will be presented in the following sections.

CHAPTER 3

STATEMENT OF THE PROBLEM

High fuel consumption is the main concern of thermal recovery applications in worldwide utilizations. Eliminating this issue significantly reduces CO₂ emission and fuel costs associated with solar technologies. This approach is a big progress over the conventional method of steam injection because it provides high amount of heat without burning extra fuel. Although solar generated thermal energy is a bleeding edge technology in oil industry, it has already proven its ability to generate steam in a lower cost and less environmental pollution.

This thesis aims to evaluate the existing X field whether solar generated steam injection project is able to solve the cost problems of the current steam injection applications in Batman region. In order to achieve this goal, a pilot area where steam injection was implemented in 1969 has been selected. In order to determine steam injection operation parameters, recent published studies have been used. Due to the amount of residual oil, the field has been extensively studied for the last 50 years and it has helped this study to obtain the information more accurate and easier. Solar field has been designed to fulfill the steam requirement of the pilot field. As solar energy can not be available all the time of the year, gas fired back up system has been used to maintain generating steam continuously all the years round till the end of the project.

CHAPTER 4

METHOD OF SOLUTION

4.1 Solar Generated Steam Injection Method

4.1.1 Overview of Concentrating Solar System

In order to understand the working principle of solar concentrating system, it is required to know some definitions used in the calculations.

Beam radiation also named direct radiation is defined as the solar radiation that shows no variance after passing through the atmosphere. Diffuse radiation as shown in Figure 4.1 is the sun's rays that change direction due to atmosphere effect before reaching to surface. Total solar radiation is the total radiation includes both beam and diffuse solar radiation. [3]

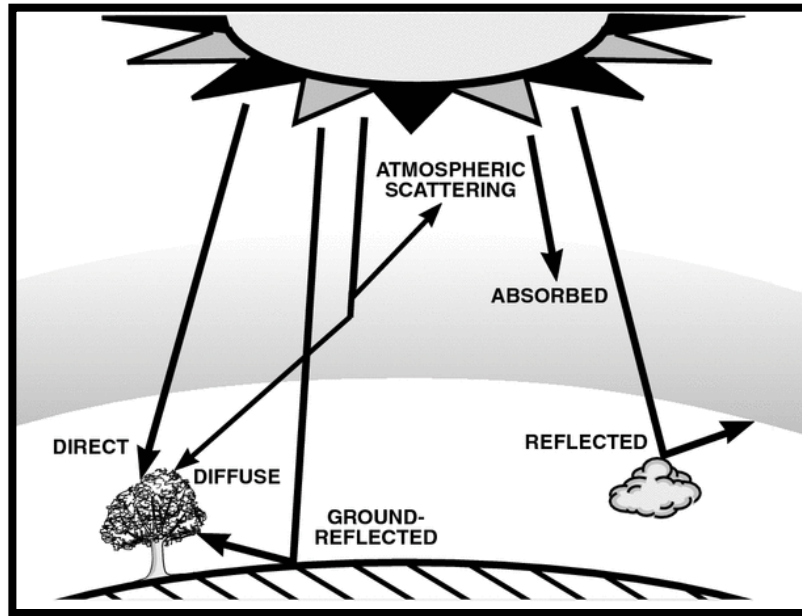


Figure 4. 1: Diffuse and Direct Radiation [17]

Irradiance, W/m^2 is the radiant energy received by unit area of the surface and Radiosity, W/m^2 is the radiant energy that leaves the surface due to emission, reflection and transmission. [3]

Since concentration technology uses only parallel rays, only beam radiation should be considered in calculation. Amount of radiation received by the surface is influenced by factors such as orientation of plane, position of sun and incoming beam radiation. These factors are described regarding to several angles as follows:

Latitude (φ) is the geographic location that shows the north or south position of a place on the Earth. $-90^\circ \leq \varphi \leq 90^\circ$

The declination angle (δ) represents the angular position of the sun at solar noon with respect to the plane of the equator. $-23,45^\circ \leq \delta \leq 23,45^\circ$. The Figure 4.2 shows the variation of declination angle throughout the year. [3]

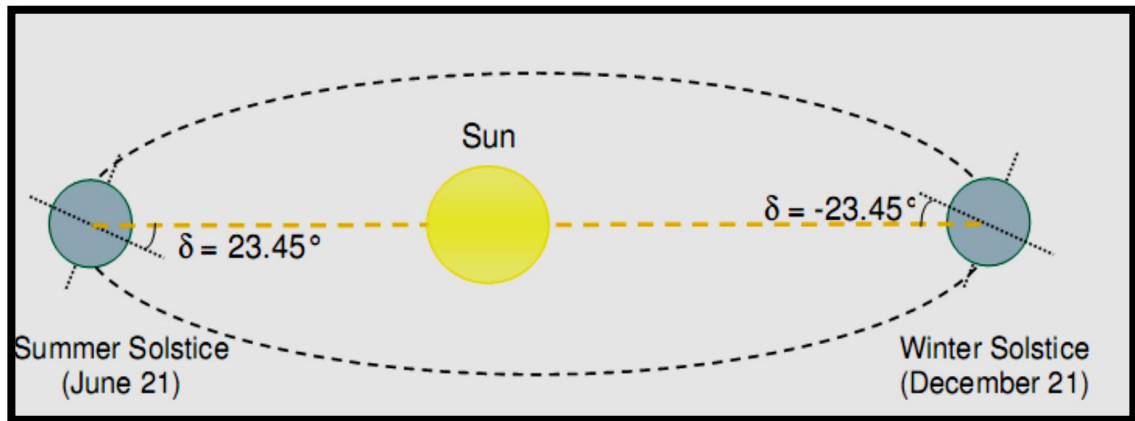


Figure 4. 2: The declination angle due to Earth's tilt [9]

It changes throughout the year over a range of $-23.45^\circ \leq \delta \leq 23.45^\circ$ and it is calculated with the following formula developed by P.I. Cooper in 1969:

$$\delta = 23.45 \sin \left(360 \frac{284+n}{365} \right) \quad (4. 1)$$

where;

n= day of the year

See Figure 4.3 for representing the declination variation during a year.

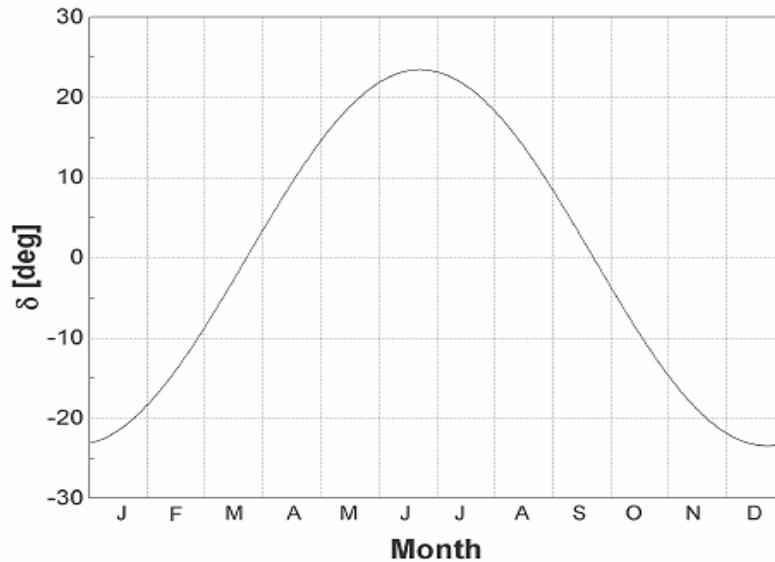


Figure 4. 3: Declination angle variation by month, from Equation 4.1

Slope (β) is the angle specify between the collector and the horizontal surface. $0^\circ \leq \beta \leq 180^\circ$

Zenith angle (θ_z) is the angle of incidence with respect to horizontal surface.

Solar altitude angle (α_s) is measured from the line of the sun to the horizontal.

Surface azimuth angle (γ) is the deviation of the projection on a horizontal plane of the normal to the surface from the local meridian, with zero being due south, east negative and west positive, $180^\circ \leq \gamma \leq 180^\circ$

Solar azimuth angle (γ_s) is the angular displacement from south of the projection of beam radiation on the horizontal plane. [3]

All angles are shown in Figure 4.4 below.

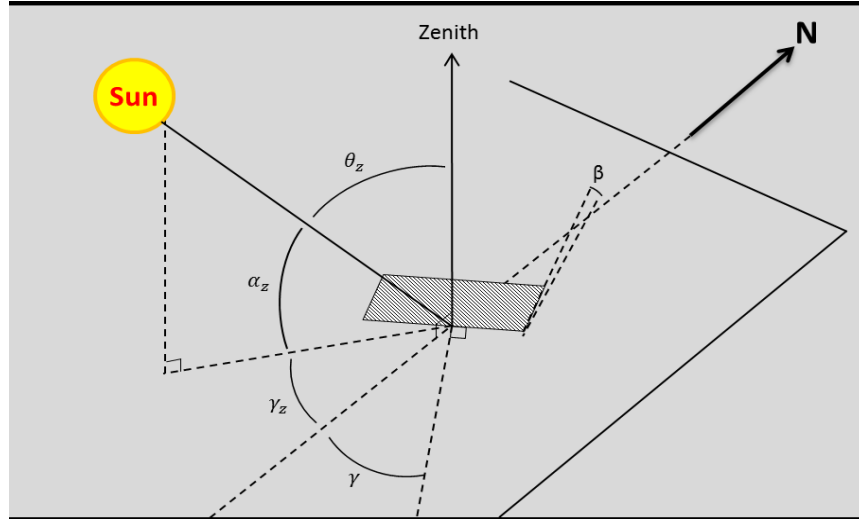


Figure 4. 4: Solar Angles [18]

4.1.2 Solar Generated Steam Injection Model

The basic representation of solar generated steam injection model is shown in Figure 4.5. The injected steam parameters which were used for solar modelling has been taken from the steam injection pilot study. Basically, direct normal insolation reaches to the collector and collectors heat the heat transfer fluid (HTF) while passing from the tube. Then, it enters the heat exchanger and heats the water (1000cwebbl/day) coming from the source. If the temperature of the water cannot reach 622°F, boiler starts to work and generates energy that is required to maintain steam injection. The percentage of usage of boiler and collector totally depends on the amount of direct normal insolation during a day.

The parts of the both solar generated steam injection and conventional steam injection models will be explained in the following sections.

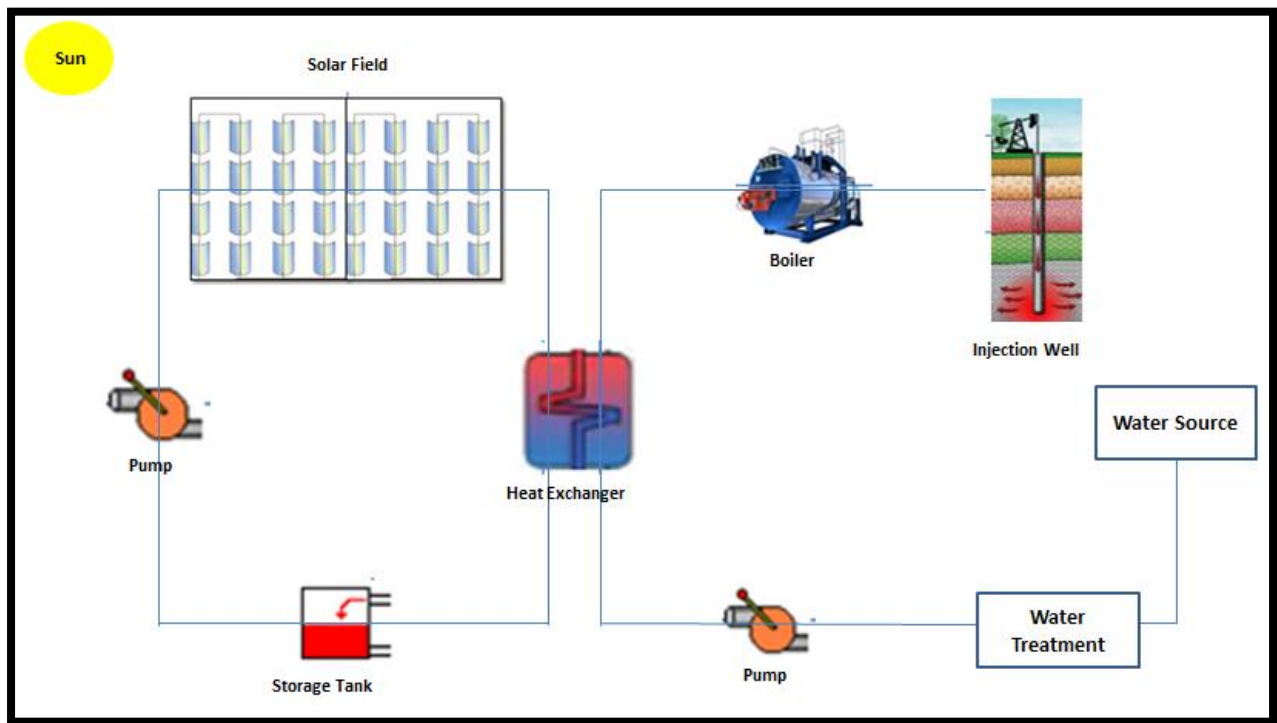


Figure 4. 5: Steam generating solar injection model

4.1.2.1 Solar Generated Steam Injection Model

4.1.2.1.1 Weather Data

Typical meteorological year (TMY) data sets between the years 1961 and 1990 were taken from the National Solar Radiation Data Base (NSRDB). These data sets are used in most of the economic analysis of the energy systems. NSRDB-TMY data files were replaced the TMY data derived from the 1952-1975 SOLMET / ERSATZ data base as more precise and latest data. SOLMET/ERSATZ was designed to provide the solar energy users with easy access to all appropriate historical meteorological data. [19]

Therefore, new data sets produced by NSRDB are called TMY2. The TMY2 data sets and manual were produced by the National Renewable Energy Laboratory's (NREL's) Analytic Studies Division under the Resource Assessment Program, which is funded and monitored by the U.S. Department of Energy's Office of Solar Energy Conversion. TMY data sets are based on the hourly values of solar radiation and other weather-related elements for a 1-year period. Also, it has daily and monthly options from individual years. The main reason to develop the TMY is to use in computer simulation of solar energy systems. The TMY2 solar based data sets were taken from 239 stations for the 30 year period from 1961-1990. There is no significant difference between the original TMY and TMY2 because both procedures of generating TMY and TMY 2 were almost same. [19]

The TMY2 procedure is an empirical approach that picks out the most appropriate properties of the months from different years period. For example, in NSRDB all September data in 30 years record are analyzed and the most representative and the most adjacent one is chosen to be built in TMY. The other months are selected using same methodology to obtain the whole year. Five main elements global horizontal radiation, direct normal radiation, dry bulb temperature, dew point temperature, and wind speed that are obtained from each station are taken into consideration to select 12 months. Other elements may or may not be typical but they are less significant to determine the desired months. [19]

In the method that was used by Sandia Laboratories, the selection is based on nine daily elements: the maximum, minimum, and mean dry bulb and dew point temperatures; the maximum and mean wind velocity; and the total global horizontal solar radiation. Last determination of a month is conducted by the examination of the monthly mean and median and the persistence of weather patterns. The procedure below is followed in order to obtain the selected month. [19]

In the 30 year period, five candidate months are selected based on the rule that their cumulative distribution functions (CDFs) are closest to the 30 years period CDFs. The comparison of 5 candidate months is made by the using Finkelstein- Schafer (FS) statistics method shown below: [19]

$$FS = \left(\frac{1}{n}\right) \sum_{i=1}^n \delta_i \quad (4. 2)$$

where,

δ_i = absolute difference between the long-term CDF and the candidate month CDF at x_i

n = the number of daily readings in a month

In order to take significant factors in to calculation, a weighted sum (WS) of the FS statistics is used to select the 5 candidate months that have the lowest weighted sums.

$$WS = \sum w_i FS_i \quad (4. 3)$$

where

w_i = weighting for index

FS_i = FS statistic for index.

Then, the selected 5 months are ordered based on the closeness of the month to the long-term mean and median.

The persistence of mean dry bulb temperature and daily global horizontal radiation are evaluated by determining the frequency and run length above and below fixed long-term percentiles. Then this data is used to determine the month to be included in TMY. The persistence criteria neglects the month with the longest run, the month with the most runs, and the month with zero runs.

The data obtained from TMY is shown in the Table 4.1.

Table 4. 1: Typical Meteorological Year Data [19]

Extraterrestrial Horizontal Radiation	Dry Bulb Temperature
Extraterrestrial Direct Normal Radiation	Dew Point Temperature
Global Horizontal Radiation	Relative Humidity
Direct Normal Radiation	Atmospheric Pressure
Diffuse Horizontal Radiation	Wind Direction
Global Horizontal Illuminance	Wind Speed
Direct Normal Illuminance	Horizontal Visibility
Diffuse Horizontal Illuminance	Ceiling Height
Zenith Luminance	Present Weather
Total Sky Cover	Precipitable Water
Opaque Sky Cover	Broadband Aerosol Optical Depth
Days Since Last Snowfall	Snow Depth

TMY2 format includes ten digit numbers. Every each digit represent different output such as local standard time, extraterrestrial horizontal radiation, diffuse horizontal radiation, direct normal radiation, direct normal illuminance, wind direction and speed, and dew point temperature i.e. [19]

2.1.1.1.1 Meteonorm - Worldwide interpolation of meteorological data

With the Meteonorm version 7 software it is possible to find all meteorological data from all regions of the world. However, in some parts there is no weather station to measure the data so Meteonorm uses interpolation to find the weather parameters of

these areas. In order to get measurements of a non-weather station area, the weather stations closest to the area in the question are used. The interpolation is done according to the following calculations:

The interpolation is carried out with a 3-D inverse distance model (Shepard's gravity interpolation) (Zelenka et al. (1992) (IEA Task 9), with additional North- South distance penalty (Wald and Lefèvre, 2001), where: [19]

$$G_h = \sum w_i \cdot [G_h(x_i) + (z_i - z_x) \cdot g_v] \quad (4.4)$$

$$w_i = [(1 - \delta_i)/\delta_i^2] / \sum w_k \quad \text{with} \quad (4.5)$$

$$\delta_i = d_i/R \quad \text{for } d_i < R \quad (4.6)$$

$$w_i = 0 \quad \text{otherwise}$$

$$d_i^2 = f_{NS}^2 \cdot \{s^2 + [v \cdot (z_i - z_x)]^2\} \quad (4.7)$$

$$f_{NS} = 1 + 0,3 \cdot |\varphi_i - \varphi_x| \cdot [1 + (\sin \varphi_i + \sin \varphi_x)/2] \quad (4.8)$$

where,

w_i = weight i

w_k = sum of overall weights

R = search radius (max. 2000 km)

v = vertical scale factor

s = horizontal (geodetic) distance [m]

z_i, z_x = altitudes of the sites [m]

i = number of sites (maximum 6)

φ_i, φ_x = latitudes of the points

g_v = vertical gradient

The other parameters such as temperature, wind, humidity and rain can be interpolated using similar procedures. In addition, some corrections can be done to reduce the local effect such as sea store.

In the project, the weather data of Batman region was taken from Meeonorm in TMY2 format. Since there is no weather station in Batman, the interpolation method was used. The radiation interpolation locations are: Diyarbakır (82km), Elazig Airport (180km), Van (203km), Malatya (273km)

The temperature interpolation locations are: Diyarbakır (82km), Kamisli (92km), Siirt (77km)

The results are presented in Figures 4.6, 4.7, 4.8, 4.9 and 4.10, and Table 4.2.

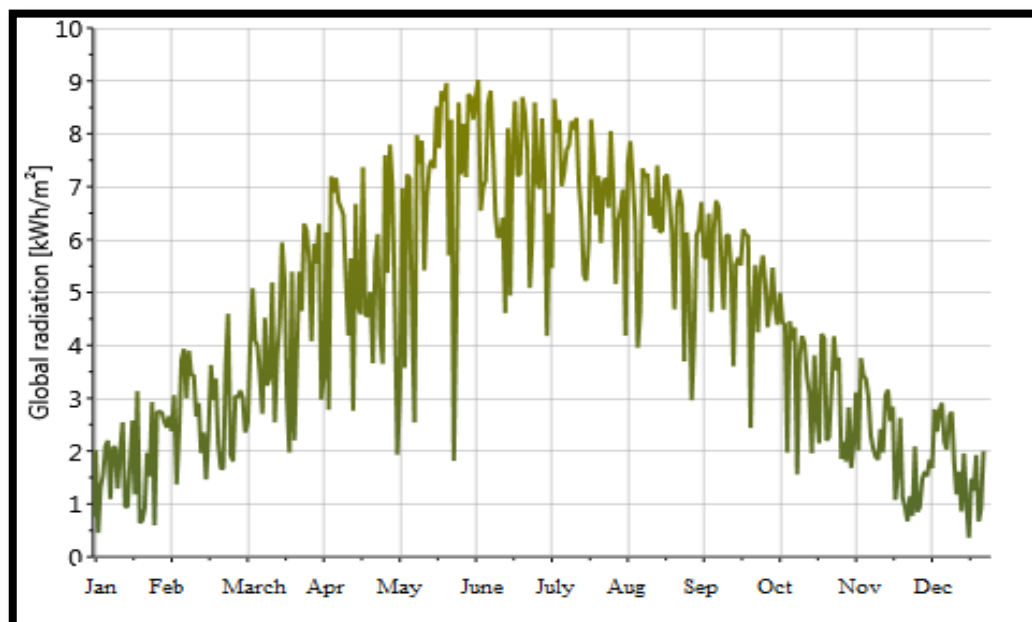


Figure 4. 6: Monthly Global Radiation

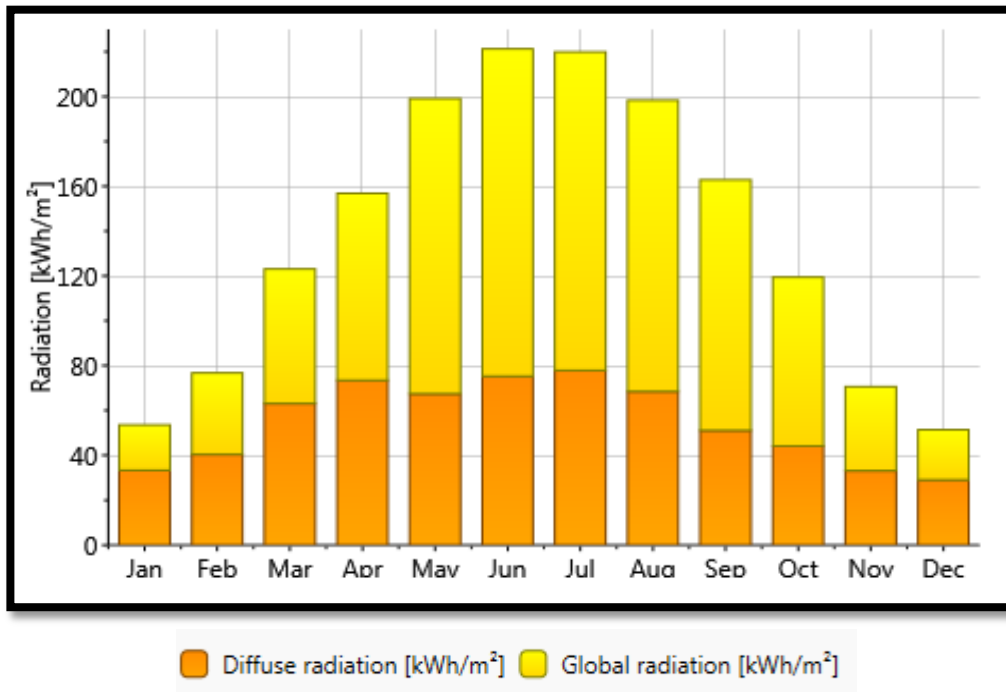


Figure 4. 7: Diffuse Radiation throughout the year

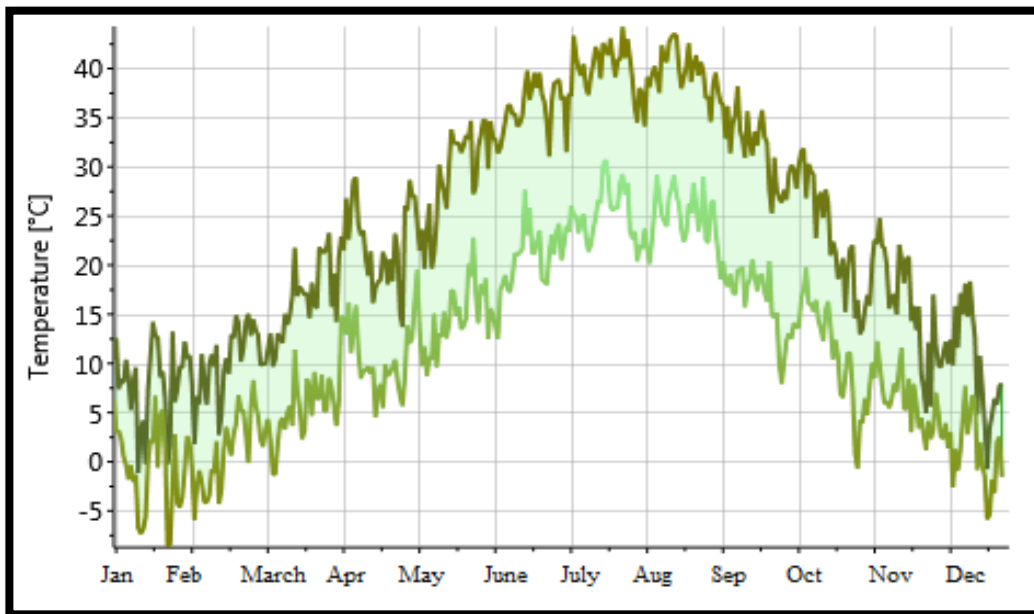
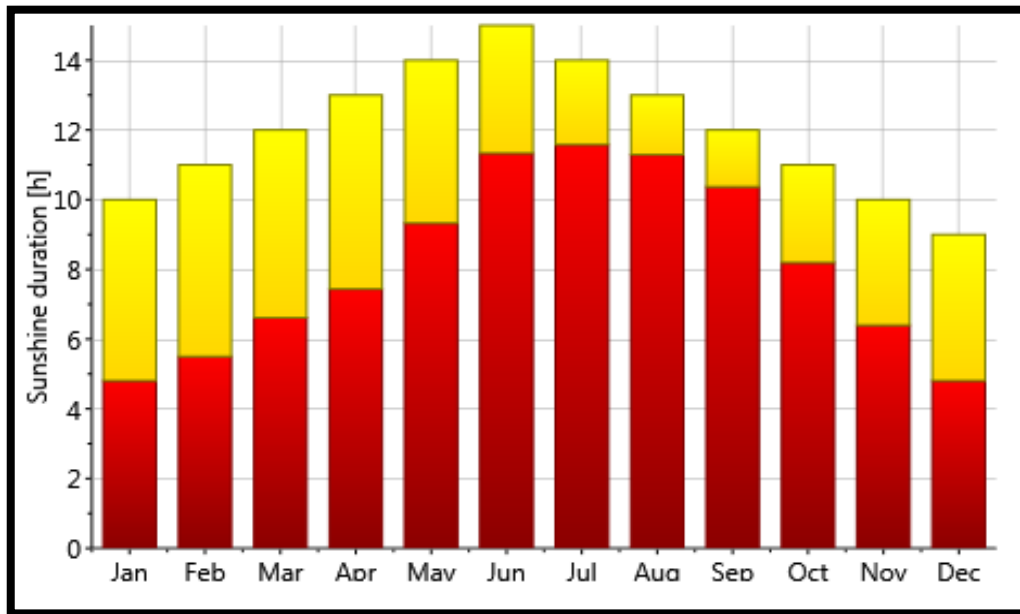


Figure 4. 8: Temperature variation throughout the year



■ Sunshine duration [h]
 ■ Astronomical sunshine duration [h]

Figure 4. 9: Sunshine duration throughout the year

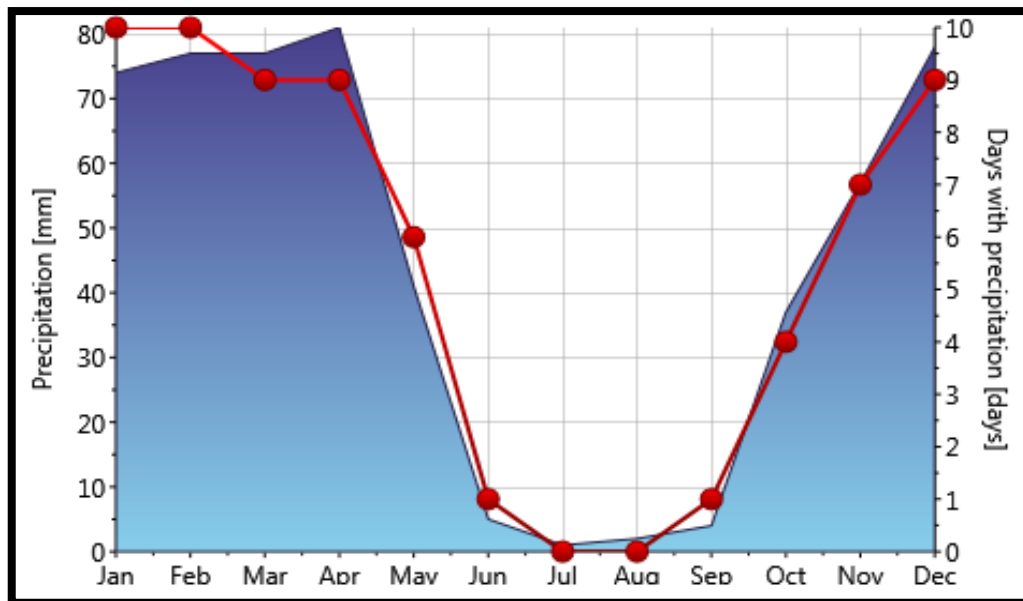


Figure 4. 10: Amount of precipitation throughout the year

Table 4. 2: Monthly average weather data

Month	Gh (kWh/m²)	Dh (kWh/m²)	Beam (kWh/m²)	Ta (°C)	FF (m/s)
January	54	33	21	3,5	3,8
February	77	40	37	5,2	3,9
March	123	63	60	9,9	3,8
April	157	73	84	15,4	3,6
May	199	67	132	21,3	3,6
June	221	75	146	28	3,9
July	220	78	142	32,7	3,4
August	198	69	129	32,2	3
September	163	51	112	26,7	2,7
October	119	44	75	18,9	2,8
November	71	33	38	11,3	2,9
December	51	29	22	5,7	3,5
Year	1650	657	993	17,6	3,4

Table 4. 3: Explanation of the terms

Abbreviation	Parameter	Unit
Month	Month	N/A
Gh	Global radiation horizontal	[kWh/m ² month]
Dh	Diffuse radiation horizontal	[kWh/m ² month]
Ta	Temperature	[°C]
FF	Wind speed	[m/s]

4.1.2.1.2 Parabolic Trough Concentrating Solar Collector

A concentrated solar collector consists of a concentrating parabolic mirror to focus the sunlight onto a tube that sits trough the center of it. The tube is a pipe in pipe assembly and the area between the outer glass tube and inner fluid filled absorber tube is mostly evacuated but sometimes may be filled with air or hydrogen. [20]

The heat transfer fluid (HTF) is pumped through to each collector and energy is transferred from the sun to the HTF. HTF (Therminol-VP1) is a mixture of biphenyl and diphenyl oxide and it is used for the vapor phase systems from 495 °F to 750°F. [21]

The mass of the fluid in the tube is accounted in the solar collector model. Also, the fluid properties that undergo a change with temperature depend on the solar field inlet and outlet temperature not the local temperature of itself. The model is based on the iso-volumetric sections of the fluid filled absorber tube called nodes. The number of nodes is determined by the user according to necessity of the model. For instance, larger number of nodes can be used in temperature distribution of the absorber tube to get more accurate results. On the other hand, sometimes it does not require such a big numbers depend on the relation between fluid velocity and volume of nodes. [20]

The differential equation that shows the temperature of fluid in one node as a function of time is: [20]

$$\frac{d(mu)}{dt} = \dot{Q}_{in} - \dot{Q}_{out} \quad (4. 9)$$

\dot{Q}_{in} is defined as the solar energy emitted by the absorber tube and transferred to the fluid and the fluid flowing in the node, whereas \dot{Q}_{out} is the energy loss from the fluid

to the environment with convection, conduction and radiation and the fluid flowing out of the node.

Therefore, Eq. 1 can be written as:

$$\frac{d(mu)}{dt} = \dot{Q}_{absorbed} + \dot{Q}_{fluid\ in} - \dot{Q}_{losses} - \dot{Q}_{fluid\ out} \quad (4. 10)$$

In most of the cases, the mass of the node and specific heat of the node are taken as a constant so the Eq.2 can be re-written as follow:

$$\frac{d(mu)}{dt} = mC_p \frac{dT}{dt} \quad (4. 11)$$

In this model, it is assumed that the volume of the node will not change but mass and internal energy does change with time and temperature so it will continue with the expansion of Eq.2.12

$$\frac{d(mu)}{dt} = m \frac{du}{dt} + u \frac{dm}{dt} \quad (4. 12)$$

In order to solve the temperature of node as a function of time, the equation is re-written as a function of dT/dt and applied chain rule on it.

$$\frac{d(mu)}{dt} = \frac{dm}{dT} * \frac{dT}{dt} \quad (4. 13)$$

$$m = \rho V \quad (4. 14)$$

Since volume is constant;

$$\frac{dm}{dT} = \frac{d(\rho V)}{dT} = V \frac{d\rho}{dT} \quad (4.15)$$

This model assumes that the density of the working fluid can be described as a quadratic function of temperature:

$$\rho = r_0 + r_1 T + r_2 T^2 \quad (4.16)$$

After combining Equations (4.15) and (4.16), it is derived for dm/dT :

$$\frac{dm}{dT} = \frac{d(\rho V)}{dT} = V \frac{d\rho}{dT} = V(r_1 + 2r_2 T) \quad (4.17)$$

Equation (4.17) is placed into Equation (4.13) and then derived.

$$\frac{dm}{dT} = V(r_1 + 2r_2 T) \frac{dT}{dt} \quad (4.18)$$

Same procedure will be applied for the du/dt . Using chain rule:

$$\frac{du}{dt} = \frac{du}{dT} * \frac{dT}{dt} \quad (4.19)$$

This model assumes that the internal energy of the working fluid can be described as a quadratic function of temperature:

$$u = u_0 + u_1 T + u_2 T^2 \quad (4.20)$$

It can be derived to get du/dT :

$$\frac{du}{dT} = (u_1 + 2u_2 T) \quad (4.21)$$

Expanding to Equation (4.13) with these derivations:

$$\frac{d(\mu)}{dt} = (uVr_1 + 2uVr_2T) \frac{dT}{dt} + (\mu u_1 + 2\mu u_2T) \frac{dT}{dt} \quad (4.22)$$

Finally, rearranging to Equation (4.22):

$$\frac{d(\mu)}{dt} = (uVr_1 + 2uVr_2T + \mu u_1 + 2\mu u_2T) \frac{dT}{dt} \quad (4.23)$$

Equation 4.23 is expanded and re-written as a function of temperature and time. Now, right side of the equation will be described.

Firstly, $\dot{Q}_{\text{absorbed}}$ is defined as: [9]

$$\dot{Q}_{\text{absorbed}} = AG_{\text{beam}}IAMf_{\text{endloss}}f_{\text{mirror}}f_{\text{dust}}f_{\text{bellows}}f_{\text{misc}}\tau_{\text{glass}}\alpha_{\text{coating}} \quad (4.24)$$

where

$\dot{Q}_{\text{absorbed}}$ = solar radiation absorbed by the receiver tubes [W/m²]

G_{beam} = DNI cos θ Row Shadow

DNI = direct normal insolation [W/m²]

θ = angle of incidence [deg]

IAM = incidence angle modifier [-]

Row Shadow = performance factor that accounts for mutual shading of parallel collector rows during early morning and late evening [-]

End Loss = performance factor that accounts for losses from ends of HCEs [-]

4.1.2.1.2.1 Direct Normal Insolation

The solar radiation receives from the sun is coming to the Earth surface by following a direct line. Some solar radiation is absorbed by the atmosphere but some of them reach

to the surface without changing. Direct Normal Insolation is the solar radiation that has not been scattered by the atmosphere. [3] Also it is called as a beam radiation. Figure 4.11 shows the direct normal insolation of Batman on both June 21, and December 21, 1995.

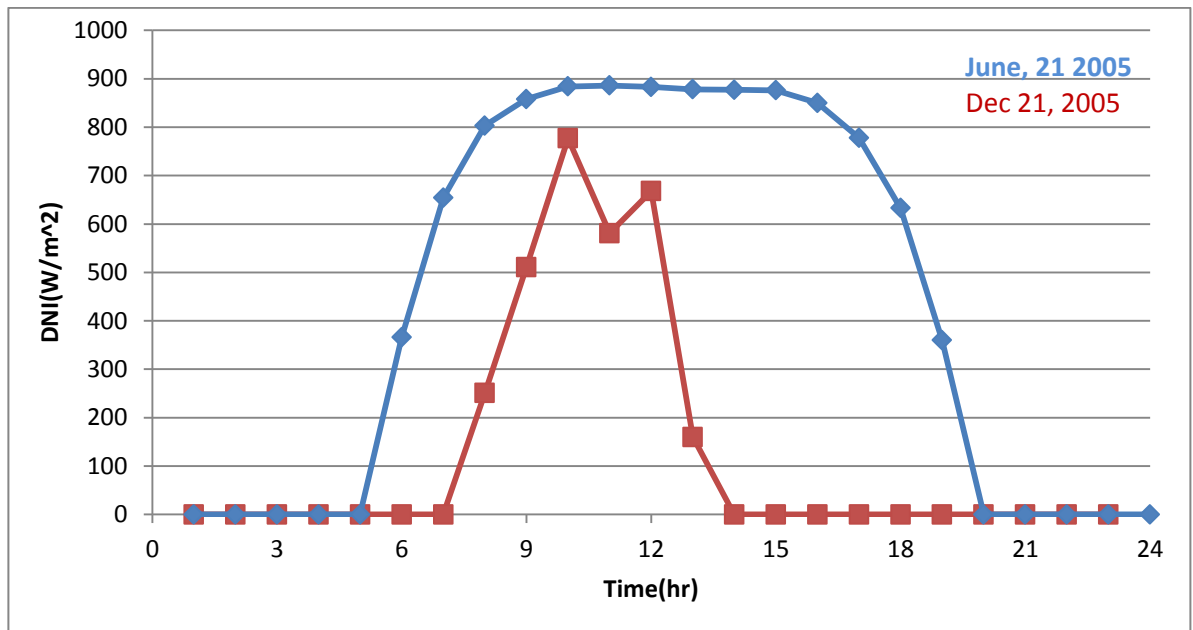


Figure 4. 11: Direct normal insolation of Batman on both June 21, and December 21, 2005

4.1.2.1.2.2 Angle of Incidence (θ)

Angle of incidence is defined as an angle between the beam radiation on a surface and the plane to that surface. [3] Angle of incident and other angles mentioned on the literature part will be used in following calculations.

The angle of incidence is changing during the day based on the sun's position and the tracking of the collector surface. It has a strong effect on performance of the collector.

The term hour angle is used to define angular displacement of sun. The hour angle is negative when the sun is east of the local meridian in other words when it is morning, positive when the sun is west of the local meridian (afternoon), and zero when it is noon. [3] It is defined as the Equation (4.25)

$$\omega = (\text{Solar Time} - 12) * 15^\circ/\text{hr} \quad (4.25)$$

where

$$\text{SolarTime} = \text{StandardTime} - \text{DST} + \frac{L_{st} - L_{loc}}{15} + E \cdot \frac{1\text{hr}}{60\text{min}} \quad (4.26)$$

DST = Daylight saving time adjustment (1 hr during daylight saving time, 0 hr during the standard time)

L_{st} = Standard meridian for the local time zone, deg

L_{loc} = The local meridian of the collector site, deg

E is the equation of time, used to correlate the values due to the Earth's path following while turning around the sun.

$$E = 229.18 * (0.000075 + 0.001868\cos(B) - 0.032077\sin(B) - 0.014615\cos(2B) - 0.04089\sin(2B)) \quad (4.27)$$

$$B = \frac{360}{365}(n - 1) \text{ (deg)} \quad (4.28)$$

n= day number of the year

Figure 4.12 shows the equation of time during the year.

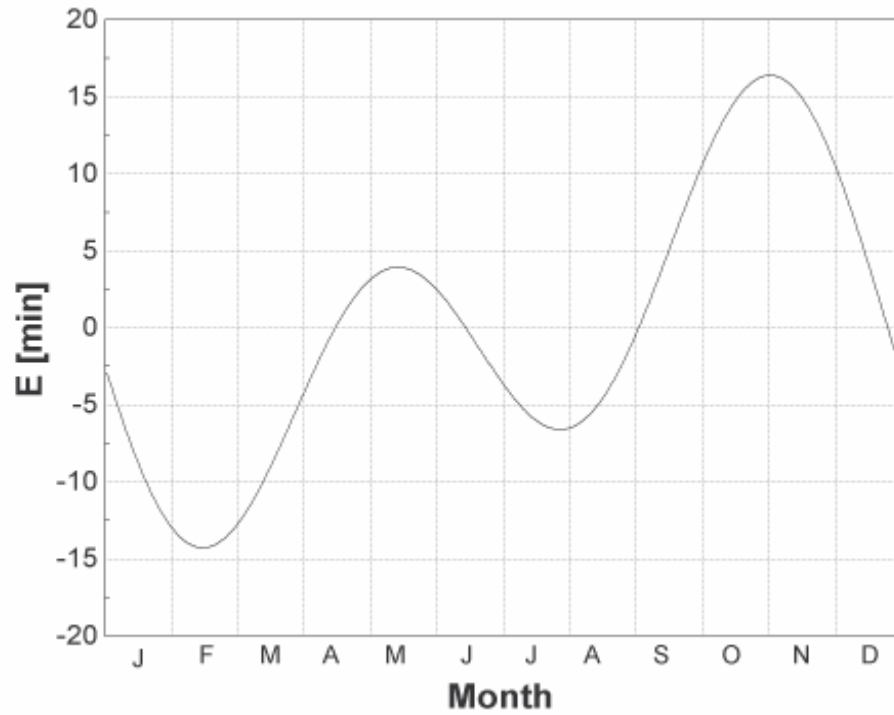


Figure 4. 12: Variation of equation of time throughout the year, from Equation 4.27

Lastly, in order to calculate angle of incidence, zenith angle should be defined. Zenith angle represents the angle between the sun line and the beam radiation. It is calculated as: [3]

$$\cos \theta_z = \cos \delta \cos \varphi \cos \omega + \sin \delta \sin \varphi \quad (4. 29)$$

In this model, north-south axis with continuous east-west tracking system will be used so angle of incidence is expressed by following: [3]

$$\cos \theta = \sqrt{\cos^2 \theta_z + \cos^2 \delta \sin^2 \omega} \quad (4. 30)$$

4.1.2.1.2.3 Incidence Angle Modifier (IAM)

While angle of incidence increases, there will be extra loss results in additional reflection and absorption by the glass envelope. IAM is used to remove these effects in calculations. IAM is expressed by an empirical fit to experimental data and it is specific for each type of collector. [9]

The equation of incidence angle modifier is given by Dudley:

$$\text{IAM} = b_0 + b_1 * \frac{\text{IncAng}}{\cos(\text{Inc Ang})} + b_2 * \frac{\text{IncAngle}^2}{\cos(\text{IncAng})} \quad (4.31)$$

4.1.2.1.2.4 Row Shadowing and End Losses

The position of the sun during the day can cause the shading problems in parallel rows especially in the morning and in the afternoon. The shading is mainly based on the collector position relative to the sun and the geometry of the collector.

In order to prevent loss due to shadowing, collectors are placed in parallel rows and between each parallel the distance is 15m in presented model. Shading effect is generally observed in early in the morning and afternoon. In the morning, due to collector has north-south axis with continuous east-west tracking system the eastern side of the system can receive all solar radiation but this eastern row will shadow the other rows in the west. During the midday, as the sun rises all collectors receive the sun and shading effect decreases and after reaching the zenith angle shading effect will be zero. It will continue to early in the morning but then again start to increase. Figure 4.13 shows the collector shading effect through a day. [9]

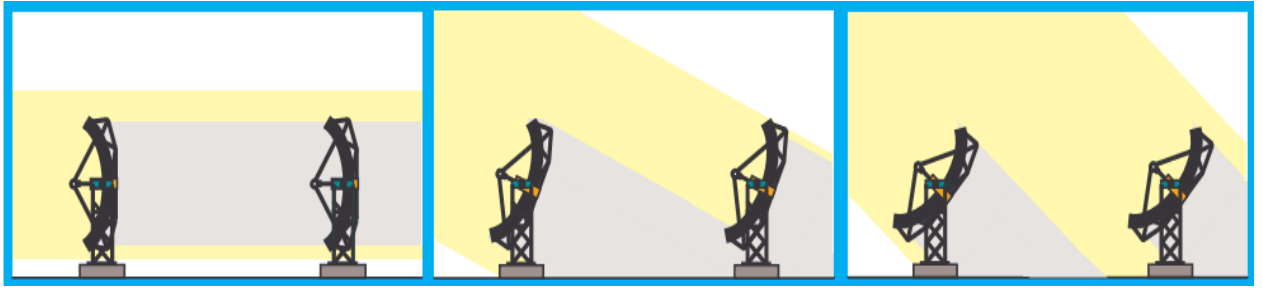


Figure 4. 13: Collector shading effect through a day [9]

With increasing shading, the performance of the collectors is decreasing due to limited receiving solar radiation. The width of the mirror aperture which receives incident radiation is defined as the “effective mirror width”. The row shadow factor is defined as a ratio of the effective mirror width to the actual mirror width. [9]

$$\text{RowShadow} = \frac{W_{\text{eff}}}{W} = \frac{L_{\text{spacing}}}{W} = \frac{\cos \theta_z}{\cos \theta} \quad (4.$$

32)

where

W_{eff} = effective width of mirror aperture, m

L_{spacing} = length of spacing between trough

W = collector aperture width

$\cos \theta_z$ = zenith angle

$\cos \theta$ = angle of incidence

End losses are observed at the two ends of the absorber tube since solar radiation is not reflected effectively from the mirrors due to incidence angle. The collector end losses are defined using an equation by Lippke (1995).

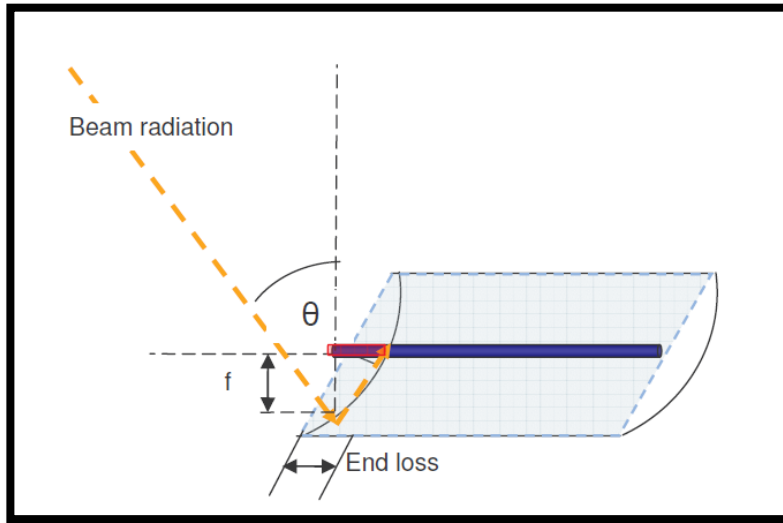


Figure 4. 14: Representation of end loss [9]

$$\text{End Losses} = 1 - \frac{f \tan \theta}{L_{SCA}} \quad (4. 33)$$

where,

f = focal length of the collectors

θ =incident angle

L_{SCA} = length of a single solar collector assembly

The lasting terms of the equation are shown below with description.

f_{mirror} = a factor which accounts for the geometric inaccuracies of the reflect mirror
(1=perfect mirror)

f_{dust} = a factor which accounts for dust on the glass receiver tube (1= no dust)

f_{bellows} = a factor which accounts for the shading of the mirror by the collector bellows
(1=no shading)

f_{misc} = a factor which accounts for miscellaneous losses from the collector system (1= no misc. losses)

τ_{glass} = the transmittance of the receiver glass to solar radiation (1=perfect transmission)

$\alpha_{coating}$ = the absorptance of the coating on the absorber tube (1=all incident radiation absorbed)

The rate of energy added by fluid entering the node is: [20]

$$\dot{Q}_{fluid\ in} = \dot{m}_{in}h_{in} \quad (4.34)$$

The rate of energy removed from the collector node by fluid is defined as:

$$\dot{Q}_{fluid,out} = \dot{m}_{out}h_{out} \quad (4.35)$$

In this model, the outlet flow rate is equal to the inlet flow rate minus the rate of change of mass of the node with respect to time.

$$\dot{m}_{out} = \dot{m}_{in} - \frac{dm}{dT} \quad (4.36)$$

However, since dm/dt term has a small effect on calculation of the outlet mass flow rate, it can be neglected in simulation models. Therefore,

$$\dot{m}_{out} = \dot{m}_{in} \quad (4.36)$$

The thermal losses from the working fluid to the environment including conduction, convection and radiation can be calculated with a simplified heat transfer method developed from the main heat transfer mechanism.

$$U' = a_0 + a_1T + a_2T^2 + a_3T^3 + DNI(a_4 + a_5T^2) \quad (4.38)$$

The ambient temperature of 25°C is used for this correlation. To calculate the heat loss coefficient per unit collector area, the model is divided by the collector aperture width and the temperature difference between the local fluid temperature and the assumed 25°C ambient temperature.

$$U_L = \frac{U'}{W(T-25)} \quad (4.39)$$

The heat loss from the fluid to the ambient is calculated as:

$$\dot{Q}_{\text{losses}} = U_L A (T - T_{\text{ambient}}) \quad (4.40)$$

Finally the energy balance of the outlet mass flow rate with the change in mass of the node calculation is:

$$\begin{aligned} (uVr_1 + 2uVr_2T + mu_1 + 2mu_2T) \frac{dT}{dt} = \\ AG_{\text{beam}} IAM f_{\text{endloss}} f_{\text{mirror}} f_{\text{dust}} f_{\text{bellows}} f_{\text{misc}} \tau_{\text{glass}} \alpha_{\text{coating}} + h_{\text{in}} - \dot{m}_{\text{in}} h - \\ U_L A (T - T_{\text{ambient}}) \end{aligned} \quad (4.41)$$

Since the outlet mass flow rate is equal to the inlet mass flow rate, the equation is rearranged:

$$\begin{aligned} \frac{dT}{dt} = \frac{AG_{\text{beam}} IAM f_{\text{endloss}} f_{\text{mirror}} f_{\text{dust}} f_{\text{bellows}} f_{\text{misc}} \tau_{\text{glass}} \alpha_{\text{coating}}}{(mu_1 + 2mu_2T + uVr_1 + 2uVr_2T)} + \\ \frac{\dot{m}_{\text{in}} h_{\text{in}}}{(mu_1 + 2mu_2T + uVr_1 + 2uVr_2T)} - \frac{\dot{m}_{\text{in}} h}{(mu_1 + 2mu_2T + uVr_1 + 2uVr_2T)} - \frac{U_L A (T - T_{\text{ambient}})}{(mu_1 + 2mu_2T + uVr_1 + 2uVr_2T)} \end{aligned} \quad (4.42)$$

In order to solve the equation, a second order Runge-Kutta method will be used to numerically solve the differential equation. The Runge-Kutta approach solves differential equations of the form:

$$\frac{dT}{dt} = g(T, t) \quad (4.43)$$

where $g(T, t)$ is a function of temperature and time. In this case, $g(T, t)$ represents the right side of the equation. The solution of Equation (4.41) takes the following form in the Runge-Kutta approach:

$$T_{k+1} = T_k + \frac{\Delta t}{N_{RK}} g\left(T_k + z, t_k + \frac{\Delta t}{2N_{RK}}\right) \quad (4.44)$$

Where the values of k are successive integers from 0 to N_{RK} and z is defined as:

$$z = \frac{\Delta t}{2N_{RK}} g(T_k, t_k) \quad (4.45)$$

Since there is no explicit dependence on time in the solution of the differential equation, the equation reduces to:

$$T_{k+1} = T_k + \frac{\Delta t}{N_{RK}} g\left(T_k + \frac{\Delta t}{2N_{RK}} g(T_k)\right) \quad (4.46)$$

The methodology to solve for T for a value of $N_{RK}=1000$ at time = $t + \Delta t$ is summarized in Appendix part.

The parameters and input of the parabolic collectors used in the model are below:

Table 4. 4: Parameters of the collector [20]

Name	Value	Unit
Width of Collector Aperture	5.79	m
Length of single collector	48	m
Inner diameter of absorber tube	0.07	m
Focal length for collector	1.8	m
Mirror accuracy	0.98	-
Reflectivity of mirror	0.93	-
Envelope transmittance	0.96	-
Absorptance of receiver coating	0.95	-
Number in collectors in series	15	-
Number of collector nodes	15	-

Table 4. 5: Input of the collector model [20]

Name	Value	Unit
Beam radiation on the tilted surface	0.0	kJ/hr.m^2
Incidence angle	0	degrees
Tracking efficiency factor	0.99	-
Mirror cleanliness factor	0.95	-
Receiver glass dusting factor	0.98	-
Bellows shading factor	0.97	-
Miscellaneous efficiency factor	0.96	-

4.1.2.1.3 Pump

In this model, pump is generated by a volumetric flow rate, a rated power and a control signal changing between 0 and 1. Volumetric flow rate is based on the rated flow rate and the control sign. Rated flow rate is defined by a polynomial whose coefficients are defined by user. [20]

Pump in the model provides user a feature to characterize the fluid whose enthalpy and density are either linear or quadratic functions of temperature. According to the coefficients provided by the users, the relationships between the temperature and the density and between the temperature and enthalpy can be obtained. [20]

As a first step, the density and the enthalpy of the fluid entering the pump are calculated as follows: [20]

$$h_{in} = h_0 + h_1 T_{in} + h_2 T_{in}^2 \quad (4.47)$$

$$\rho_{in} = r_0 + r_1 T_{in} + r_2 T_{in}^2 \quad (4.48)$$

where,

$h_0, h_1, h_2, r_0, r_1, r_2$ are all determined by the user in the model.

The volumetric and mass outlet flows are computed from:

$$\dot{v}_{out} = \gamma \dot{v}_{rated} \quad (4.49)$$

$$\dot{m}_{out} = \rho_{in} \dot{v}_{out} \quad (4.50)$$

The power is given by the relation:

$$\dot{p}_{pump} = \dot{p}_{rated}(p_0 + p_1\gamma + p_2\gamma^2 + \dots + p_n\gamma^n) \quad (4.51)$$

The coefficients are again provided by the user as desired. Also, number of coefficients is determined by the user but to make easier the calculation in most of the models $p_0 = 0$, $p_1 = 0$ and $p_2 = 1$ are used.

The pumping efficiency is calculated by user-provided values of overall and motor efficiency:

$$\eta_{pump} = \frac{\eta_{total}}{\eta_{motor}} \quad (4.52)$$

The shaft power is given by:

$$\dot{p}_{shaft} = \dot{p}_{pump}\eta_{motor} \quad (4.53)$$

The energy transferred by the pump to the fluid stream and to the environment is given by:

$$\dot{q}_{fluid} = \dot{p}_{shaft}(1 - \eta_{pump}) + f_{motorloss}(\dot{p}_{pump} - \dot{p}_{shaft}) \quad (4.54)$$

$$\dot{q}_{env} = \dot{p}_{pump} - \dot{q}_{fluid} \quad (4.55)$$

The outlet enthalpy is calculated then:

$$h_{out} = h_{in} + \frac{\dot{q}_{fluid}}{\dot{m}_{out}} \quad (4.56)$$

Table 4.6 shows the properties of pump model.

Table 4. 6: Pump Model [20]

Parameters	Value	Unit
Rated volumetric flow rate	132	m ³ /hr
Rated pump power	123	kW
Pump Efficiency	0.6	-
Motor Efficiency	0.9	-

4.1.2.1.4 Storage Tank

In this model, storage tank has a variable volume during the cycle and the fluid is assumed to be fully mixed in other words stratification is not considered in the model. The fluid properties change based on the temperature and a subroutine is used to define the effect of temperature on properties of the fluid. [20]

Initial conditions such as temperature and volume, heat loss coefficient, the inlet fluid temperature and flow rate are determined by the user. Unlike other models in TRNSYS, the user also provides the outlet flow rate from the storage tank. [20]

In most of the tank model the temperature effect is neglected in applications but since it is a solar based project where the temperatures vary during a day it cannot be ignored for this model. The model solves the resulting differential equation derived from the tank energy balance numerically inside the subroutine using the Runge-Kutta algorithm. The user can change the TRNSYS time step and the number of the Runge-Kutta steps to try and maximize the simulation speed. [20]

In addition, the model has a warning sign to check the fluid situation in the storage tank and gives signal if the fluid volume exceeds the capacity or if the tank completely empties. In the calculations, loss of coefficients are considered as equal in all over the tank and the concept of “wetted” loss coefficients and “dry” loss coefficients are not taken into consideration. [20]

The temperature of the fluid in the storage tank as a function of time is given by: [20]

$$\frac{d(\mu)}{dt} = \dot{Q}_{in} - \dot{Q}_{out} \quad (4.57)$$

The energy into the tank is related to the fluid flowing into the tank. The energy “out” is defined as the energy lost from the fluid to the environment through convection, conduction and radiation and the energy is related to the fluid flowing out of the tank. The rearranged energy equation is:

$$\frac{d(\mu)}{dt} = \dot{Q}_{fluid\ in} - \dot{Q}_{losses} - \dot{Q}_{fluid\ out} \quad (4.58)$$

Since the volume of the fluid, the mass of the fluid and the internal energy of the tank vary with the temperature and with time, the left side of the Equation (4.56) will be expanded as:

$$\frac{d(\mu)}{dt} = m \frac{du}{dt} + u \frac{dm}{dt} \quad (4.59)$$

Applying simple mass balance on the storage tank, dm/dt can be defined as:

$$\frac{dm}{dt} = \dot{m}_{in} - \dot{m}_{out} \quad (4.60)$$

At any time the mass of the tank is composed of the initial mass of the tank and the inlet and outlet flow rates:

$$m = m_i + \dot{m}_{in}t - \dot{m}_{out}t \quad (4. 61)$$

where;

$$m_i = \rho_i V_i \quad (4. 62)$$

The model assumes that the density of the working fluid can be described as a quadratic function of temperature:

$$\rho = r_0 + r_1 T + r_2 T^2 \quad (4. 63)$$

In order to define the temperature of the tank as a function of time, du/dt term is expressed by using chain rule:

$$\frac{du}{dt} = \frac{du}{dT} * \frac{dT}{dt} \quad (4. 64)$$

This model assumes that the internal energy of the fluid can be described as a quadratic function of temperature:

$$u = u_0 + u_1 T + u_2 T^2 \quad (4. 65)$$

It can be derived to get du/dT :

$$\frac{du}{dT} = (u_1 + 2u_2 T) \quad (4. 66)$$

In many cases, the internal energy is not a function of temperature; however, in this case the internal energy as a function of temperature can be derived by subtracting the product of the working pressure and the inverse of the density as a function of temperature. ($u=h-Pv$) [20]

Combining Equations (4.64) and (4.65)

$$\frac{du}{dt} = \frac{du}{dT} * \frac{dT}{dt} = (u_1 + 2u_2T) \frac{dT}{dt} \quad (4.67)$$

Finally, the equation can be re-written as:

$$\frac{d(mu)}{dt} = \dot{m}_{in}u - \dot{m}_{out}u + (mu_1 + 2mu_2T) \frac{dT}{dt} \quad (4.68)$$

The next step is to solve the heat flows as a function of temperature.

The rate of energy added to the node by the fluid entering the node is written as:

$$\dot{Q}_{fluid\ in} = \dot{m}_{in}h_{in} \quad (4.69)$$

The rate of the energy removed from the node by fluid exiting the node is written as:

$$\dot{Q}_{fluid\ out} = \dot{m}_{out}h \quad (4.70)$$

The model assumes that enthalpy of the fluid can be described as a quadratic function of temperature:

$$h = h_0 + h_1T + h_2T^2 \quad (4.71)$$

The thermal losses from the fluid to the ambient are defined with the coefficients for the multi-mode heat transfer remains a difficult process. To make easier this process, the coefficient can be used as an input to the model. This provides the user to calculate energy losses in the most flexible way. [20]

The heat loss from the fluid to the ambient can then be re-arranged as:

$$\dot{Q}_{\text{losses}} = U_L SA(T - T_{\text{ambient}}) \quad (4.72)$$

Finally, combining the all resultant terms in the full energy balance:

$$(\mu_1 + 2\mu_2 T) \frac{dT}{dt} = -\dot{m}_{\text{in}}u + \dot{m}_{\text{out}}u + \dot{m}_{\text{in}}h_{\text{in}} - \dot{m}_{\text{out}}h - U_L SA(T - T_{\text{ambient}}) \quad (4.73)$$

Therefore;

$$\frac{dT}{dt} = \frac{-\dot{m}_{\text{in}}u + \dot{m}_{\text{out}}u + \dot{m}_{\text{in}}h_{\text{in}} - \dot{m}_{\text{out}}h - U_L SA(T - T_{\text{ambient}})}{(\mu_1 + 2\mu_2 T)} \quad (4.74)$$

In order to solve the equation, a second order Runge-Kutta method will be used to numerically solve the differential equation. The Runge-Kutta approach solves differential equations of the form:

$$\frac{dT}{dt} = g(T, t) \quad (4.75)$$

where $g(T, t)$ is a function of temperature and time. In this case, $g(T, t)$ represents the right side of the equation. The solution of Equation (4.74) takes the following form in the Runge-Kutta approach:

$$T_{k+1} = T_k + \frac{\Delta t}{N_{RK}} g\left(T_k + z, t_k + \frac{\Delta t}{2N_{RK}}\right) \quad (4.76)$$

Where the values of k are successive integers from 0 to N_{RK} and z is defined as:

$$z = \frac{\Delta t}{2N_{RK}} g(T_k, t_k) \quad (4.77)$$

$$t_{k+1} = t_0 + k \frac{\Delta t}{N_{RK}} = k \frac{\Delta t}{N_{RK}} \quad (4.78)$$

The properties and the input of the storage tank is shown in Table 4.7

The methodology to solve for T at time = $t+\Delta t$ for a value of N_{RK} between 100 and 1000 is summarized in Appendix part.

Table 4. 7: Storage tank parameters [20]

Name	Value	Unit
Expansion tank volume	250	m ³
Tank surface area	150	m ²
Initial temperature	293	°C
Initial fluid volume	20	m ³
Tank heat loss coefficient	4	kJ/hr.m ² .K

4.1.2.1.5 Heat Exchanger

The working principle of heat exchanger is to develop heat transfer between two fluids with different temperatures separated by a solid wall. There are a few types of heat exchangers but the simplest one is a concentric tube shape with the parallel or opposite flow of movement of fluid. In the parallel flow construction, the hot and cold fluids enter the tube from the same side and continue the flow with the same direction through the end of the tube. In the counterflow arrangement, the hot and cold fluids enter the tube from the opposite side of the tubes and flow reverse direction to the end of the tube. Figure 4.15 shows the parallel and counterflow design of heat exchangers. [22]

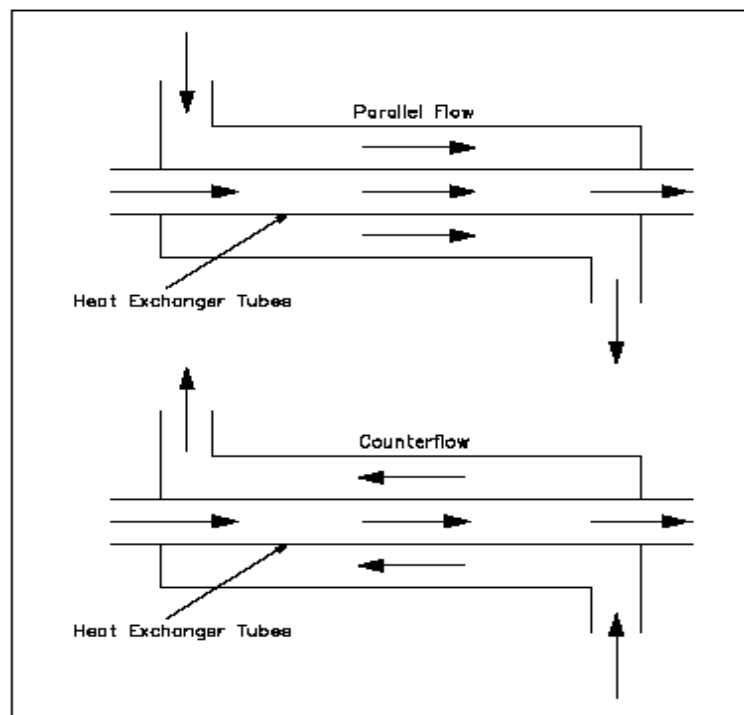


Figure 4. 15: The parallel and counterflow design of heat exchangers [23]

In order to calculate the performance of heat exchanger, the relation between the heat transfer rate and the quantities such as inlet and outlet temperatures, the overall heat transfer coefficient and the total surface area for heat transfer should be known. The energy balance between the hot and cold fluid is: [22]

$$q = \dot{m}_h(i_{h,i} - i_{h,o}) \quad (4. 79)$$

$$q = \dot{m}_c(i_{c,o} - i_{c,i}) \quad (4. 80)$$

where subscripts h and c designate to hot and cold, and i and o refer to inlet and outlet conditions.

The total heat transfer equation is calculated with the following assumptions:

- The heat transfer between the heat exchanger and the surroundings is negligible.
- Axial conduction along the tube is negligible.
- Potential and kinetic energy changes are ignored.
- The fluid specific heats are constant.
- The overall heat transfer coefficient is constant.

If there is no phase change during the heat transfer, the equations can be re-written then: [22]

$$q = \dot{m}_h c_{p,h}(T_{h,i} - T_{h,o}) \quad (4. 81)$$

$$q = \dot{m}_c c_{p,c}(T_{c,o} - T_{c,i}) \quad (4. 82)$$

The temperature difference between the hot and cold fluid is:

$$\Delta T = T_h - T_c \quad (4. 83)$$

Since ΔT is not constant during the time the balance equation is then:

$$q = UA\Delta T_m \quad (4. 84)$$

where U is the overall heat transfer coefficient and ΔT_m is an appropriate mean temperature difference.

4.1.2.1.5.1 The Counterflow Heat Exchanger

The Figure 4.16 shows the temperature distribution of hot and cold fluids in counterflow arrangement. On left side of the exchanger heat transfer occurs between the hotter portions of the two fluids on the other hand it occurs between the colder portions on the right side. In the counterflow heat exchanger the outlet temperature of the cold fluid may be more than the outlet temperature of the hot fluid. [22]

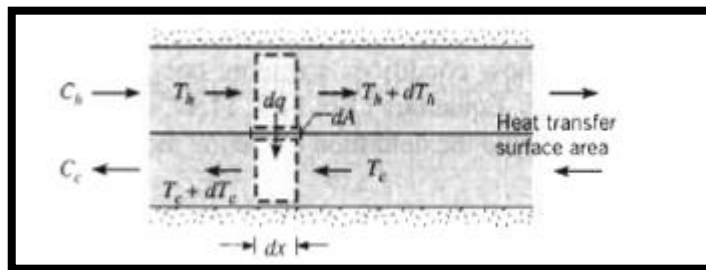


Figure 4. 16: Counterflow heat exchanger

Heat exchanger design was made by Aspen Exchanger Design & Rating V 7.2.1. according to required value for generating steam with heated oil coming from solar collector. Heat Exchanger specification is shown Appendix A.

4.1.2.1.6 Feedwater and Water Treatment

Feedwater treatment is an important factor in the efficiency of steam quality produced by steam generator. Before the steam generation application, some treatments should be done in order to adjust feedwater properties.

Hardness is one that should be zero at all times. Mostly, dual-ion-exchange system is used to handle with raw waters. It is one of the essential systems to achieve successful steam injection method. [24]

The other factor is total dissolved solid content of the feedwater. It can cause serious impact during the process of being softened of water as the sodium content increases. The steam generator tubing surface can be blocked by deposited solids. The ion-exchange system can also compensate this effect and prevent to damage the system.

The most common problem faced with steam generator is scaling. It was observed that to reduce the steam quality from 85% to 80% is enough for successful operations. Moreover, to keep oxygen concentration in recommended range is very important to prevent corrosion. [24]

The other important issue is to adjust pH of the feedwater. It helps to prevent corrosion and to keep silica in solution.

Feedwater should not involve hydrogen sulfide and oil and the content of iron should be below than 0,05 ppm. [24]

The Table 4.8 shows that feed water quality requirement for steam generation application.

Table 4. 8: Feedwater quality requirement for steam generation [24]

Total Hardness	< 1 mg/l CaCo ₃
Total Dissolved Solid	< 7000 ppm
Silica	< 100 – 150 mg/l
pH	< 7.0 – 9.5
Oxygen	0.01 – 0.02 mg/l
Oil	0
Hydrogen Sulfide	0
Iron	< 0.1 ppm

4.1.2.1.7 Pump

The function of feed pump is to elevate pressure to the specification point before the steam generation. 2 types of pump can be used as boiler feedwater pump which are reciprocating pump and centrifugal pump. The design of water pump is not the scope of this study it is not included.

4.1.2.1.8 Steam Generator

There are two types of steam generator preferred to use in steam injection operations depending on how many percentage of steam quality is required. Once through steam generator (OTSG) produces mostly 80-85% quality steam in spite of flush drum can produce 100% steam quality. In this application, OTSG was used since the required steam quality is 80%. [24]

The basic scheme of working principle of OTSG is shown Figure 4.17.

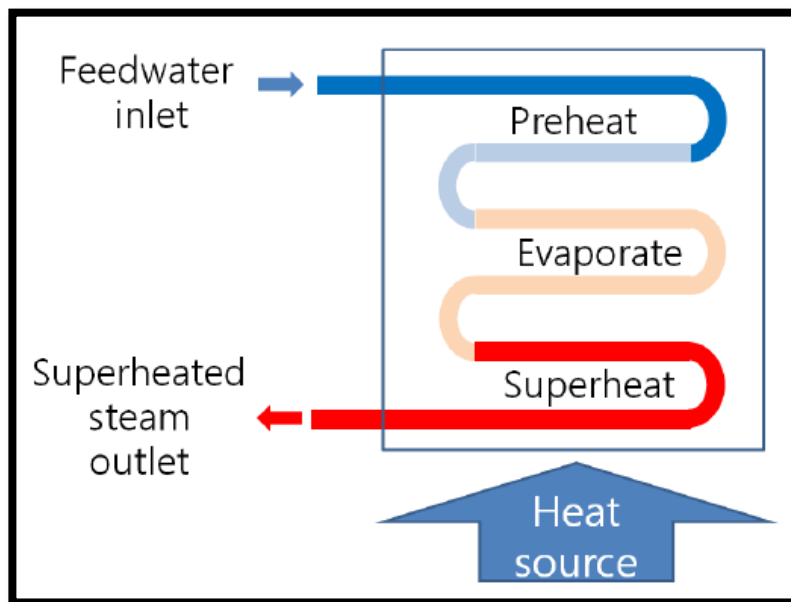


Figure 4. 17: Once through steam generator [24]

In order to obtain the steam, feedwater have to pass through three processes, preheating, evaporation, and superheating, in OTSG.

OTSG includes of convection section and radiation section (Figure 4.18)

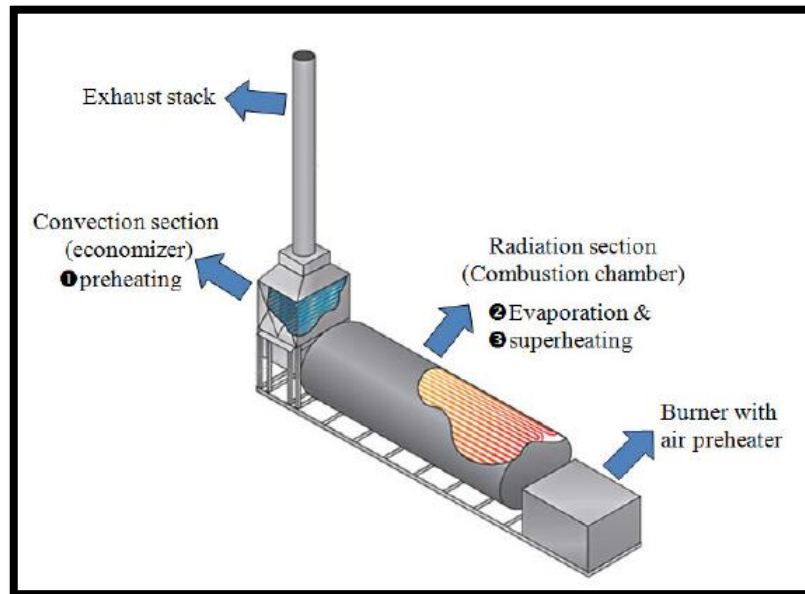


Figure 4. 18: Configuration of OTSG [24]

In convection section also called as economizer, feedwater is preheated by hot combustion flue gas. Between 35%-50% of heat is transferred in this section. In order to increase heat transfer efficiency in economizer, finned tubes are mostly preferred. However, it is recommended that to control sulphur content of the fuel as the fuel temperature goes down the dew point because of the excessive heat exchange. [24]

Evaporation and superheating are located in radiation section. In this section, selection of tube metallurgy is highly critical to avoid the tube failure. The length to diameter ratio of the radiant section is designed 3:1 to ensure the radiation intensity from the flame envelope relatively uniform. [24]

Control system is required for steam generation efficiency and operation and maintenance cost. Critical control factors are following:

- Steam temperature control
- Steam pressure control
- Steam flow rate control
- Feedwater flow rate control
- Fuel flow rate control
- Combustion control

In this application, operation design and regarding to operation parameters of the steam generator are stated in Figure 4.19 and Table 4.9.

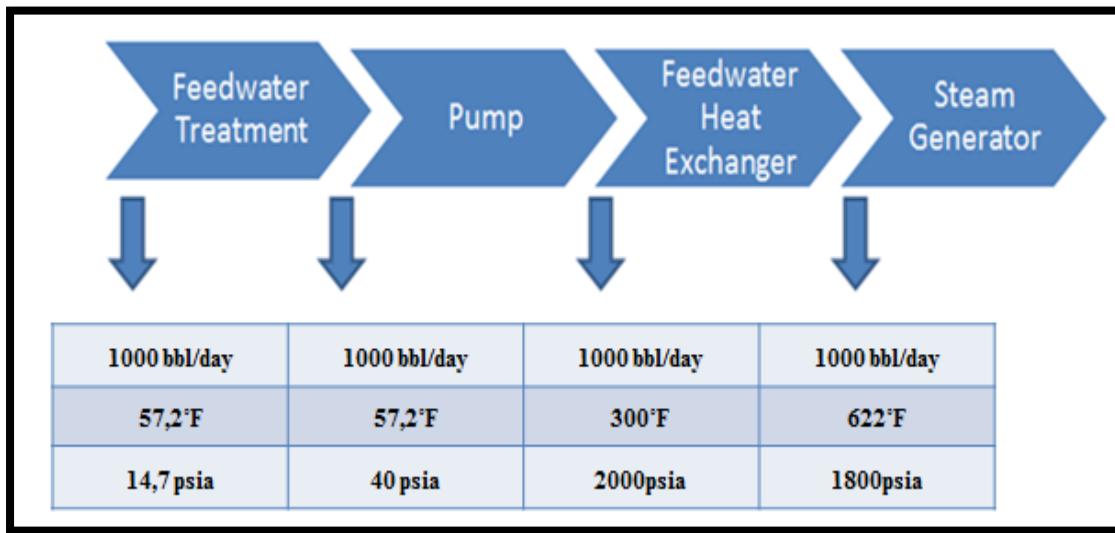


Figure 4. 19: Operation Design of Conventional Steam Injection

Table 4. 9: Operation design of steam generator

Fuel Type	Crude Oil / Natural Gas
Fuel Heating Value	17730 BTU/lb (HHV) / 910.6 BTU/scf (LHV)
Burner Heat Release (GF-HHV Basis)	31.0 MMBTU/hr
Burner Heat Release (GF-LHV Basis)	28.2 MMBTU/hr
Thermal Efficiency with Crude Oil	86%
Thermal Efficiency with Natural Gas	88%

As fuel type, crude oil was selected due to production of crude oil in the candidate area. The amount of required crude oil to produce steam will be calculated in the following section.

CHAPTER 5

RESULTS & DISCUSSION

5.1 Results

5.1.1 Solar Field Performance and Cost Analysis

5.1.1.1 Solar Field Performance Analysis

The aim of this study is to create a solar generated steam injection model that can be compared with the conventional steam injection applications in performance and cost analysis.

In order to achieve this specified goal, a pilot field has been selected. The main reason why this pilot area has been chosen is that steam injection method was applied in 1969 before. Reservoir modelling has been studied by using all field history and steam injection parameters. Several case scenarios have been evaluated and according to results, best case scenario has been decided to use to develop solar field model. The results are presented in Figure 5.1, 5.2, 5.3, 5.4.

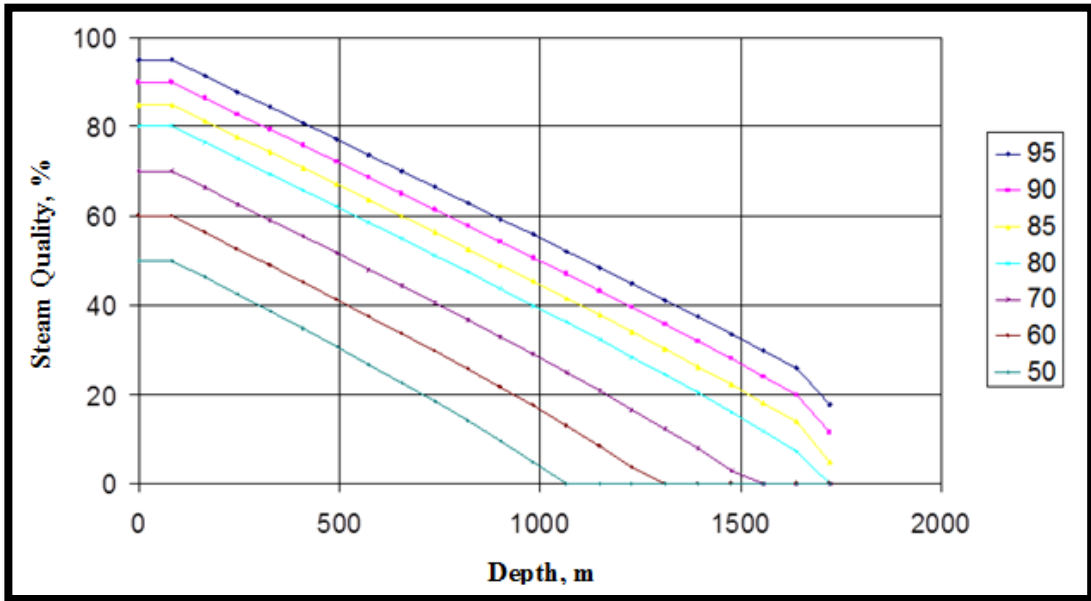


Figure 5. 1: Steam quality varies with depth based on the steam quality [16]

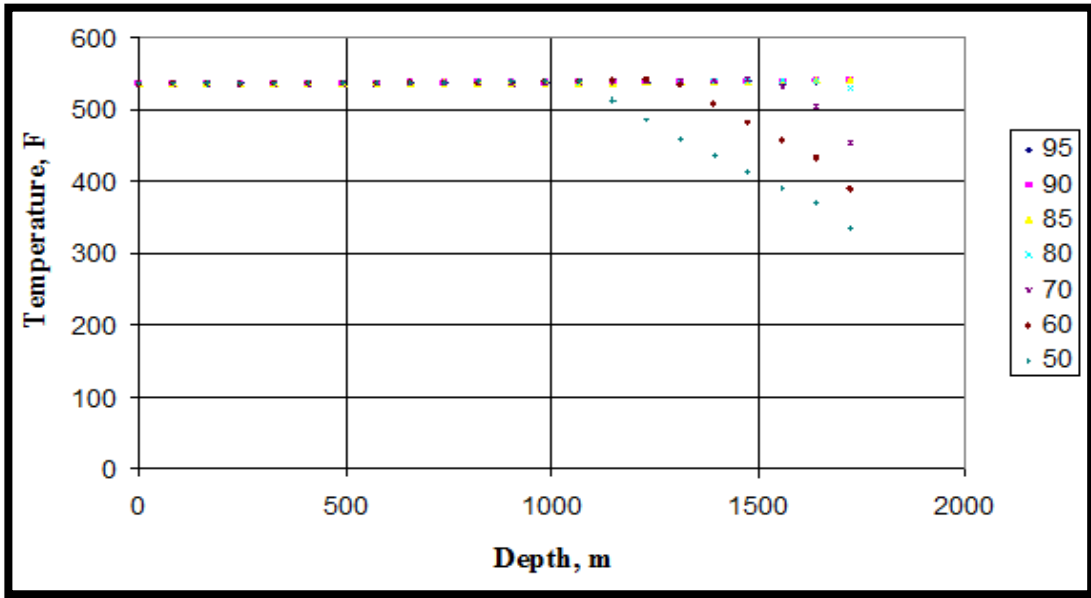


Figure 5. 2: Steam temperature varies with depth based on the steam quality [16]

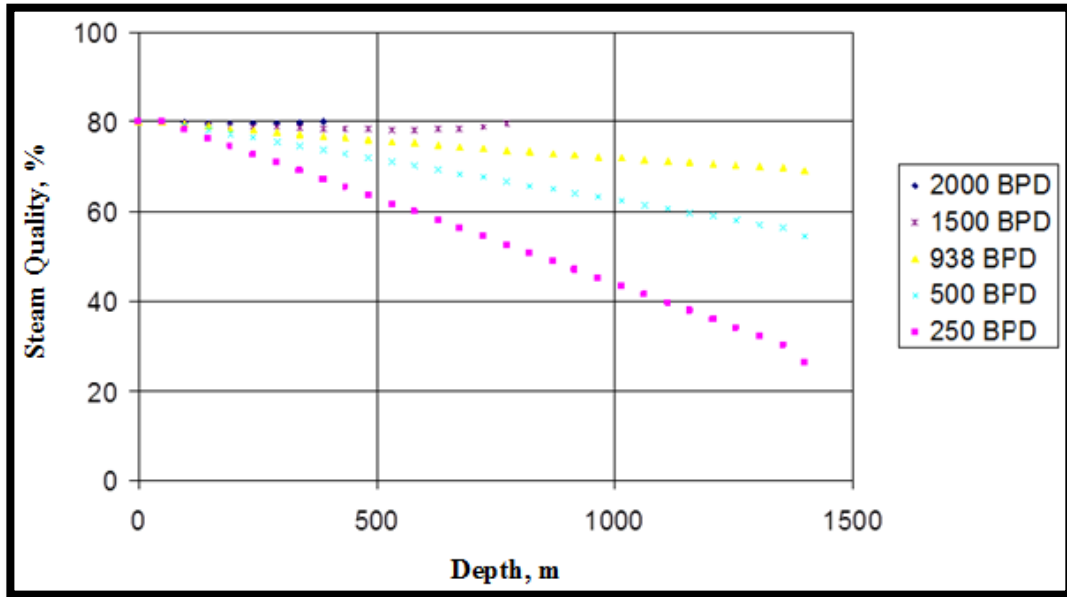


Figure 5. 3: Steam quality varies with depth based on the steam injection rate [16]

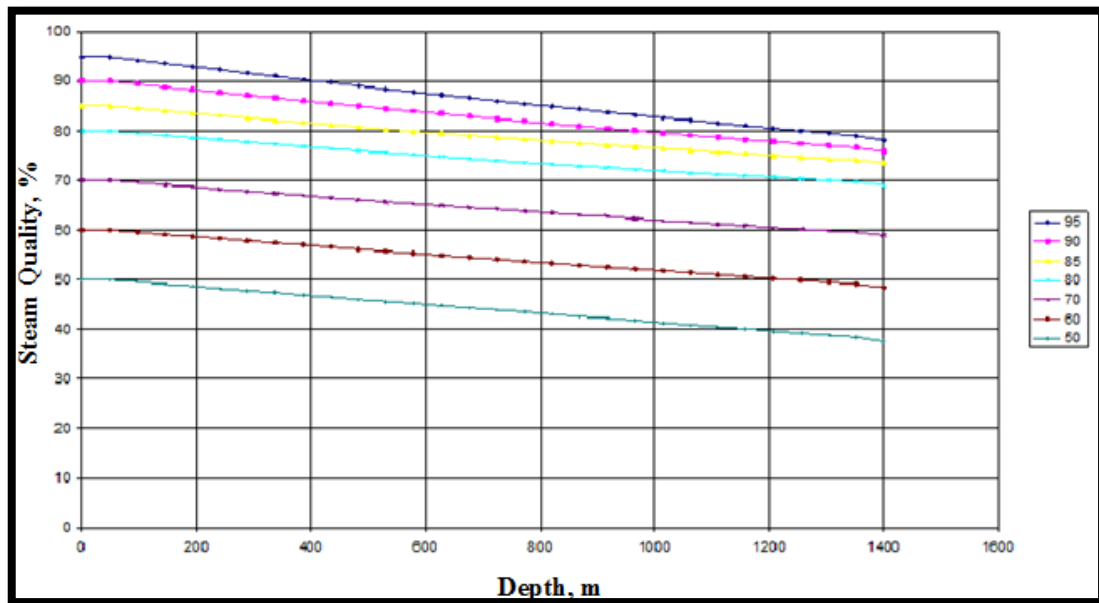


Figure 5. 4: Steam quality varies in vacuum insulated tubings [16]

Based on the results, steam injection implementing procedure has been determined.

- Steam injection rate is 1000 cwebbl/day.
- Steam pressure is 1800 psia.
- Steam temperature is 622 °F.
- Steam quality is 80%
- Vacuum insulated tubings (VIT) are used.

Solar field has been modelled in TRNSYS to meet steam injection application criteria. In this model, it has been assumed that if the system does not reach desired condition which is 1000 cwebbl/day steam at 622°F with 80% quality, with solar collector, boiler maintains to support the system to produce required steam at the time of cloudy days, nights and bad weather conditions. Table 5.1, 5.2, 5.3, 5.4, 5.5 represent solar field modelling properties.

Table 5. 1: Parameters of the collector [20]

Name	Value	Unit
Width of Collector Aperture	5.79	m
Length of single collector	48	m
Inner diameter of absorber tube	0.07	m
Focal length for collector	1.8	m
Mirror accuracy	0.98	-
Reflectivity of mirror	0.93	-
Envelope transmittance	0.96	-
Absorptance of receiver coating	0.95	-
Number in collectors in series	15	-
Number of collector nodes	15	-

Table 5. 2: Input of the collector model [20]

Name	Value	Unit
Beam radiation on the tilted surface	0.0	kJ/hr.m ²
Incidence angle	0	degrees
Tracking efficiency factor	0.99	-
Mirror cleanliness factor	0.95	-
Receiver glass dusting factor	0.98	-
Bellows shading factor	0.97	-
Miscellaneous efficiency factor	0.96	-

Table 5. 3: Pump Model [20]

Parameters	Value	Unit
Rated volumetric flow rate	132	m ³ /hr
Rated pump power	123	kW
Pump Efficiency	0.6	-
Motor Efficiency	0.9	-

Table 5. 4: Storage tank parameters [20]

Name	Value	Unit
Expansion tank volume	250	m ³
Tank surface area	150	m ²
Initial temperature	293	°C
Initial fluid volume	20	m ³
Tank heat loss coefficient	4	kJ/hr.m ² .K

After solar field modelling, the number of collectors has been determined based on the steam requirements. The required steam is 1000bbl/day and it is equal to approximately 6611 kg/hr at 622°F and 1800psi. Figure 5.5 shows that the amount of steam is produced by 1 parallel series, 15 collectors. The following Figure 5.5, 5.6, 5.7, 5.8, 5.9, 5.10, 5.11, 5.12, 5.13, 5.14 and 5.15 show the amount of steam produced based on the total number of series in the system.

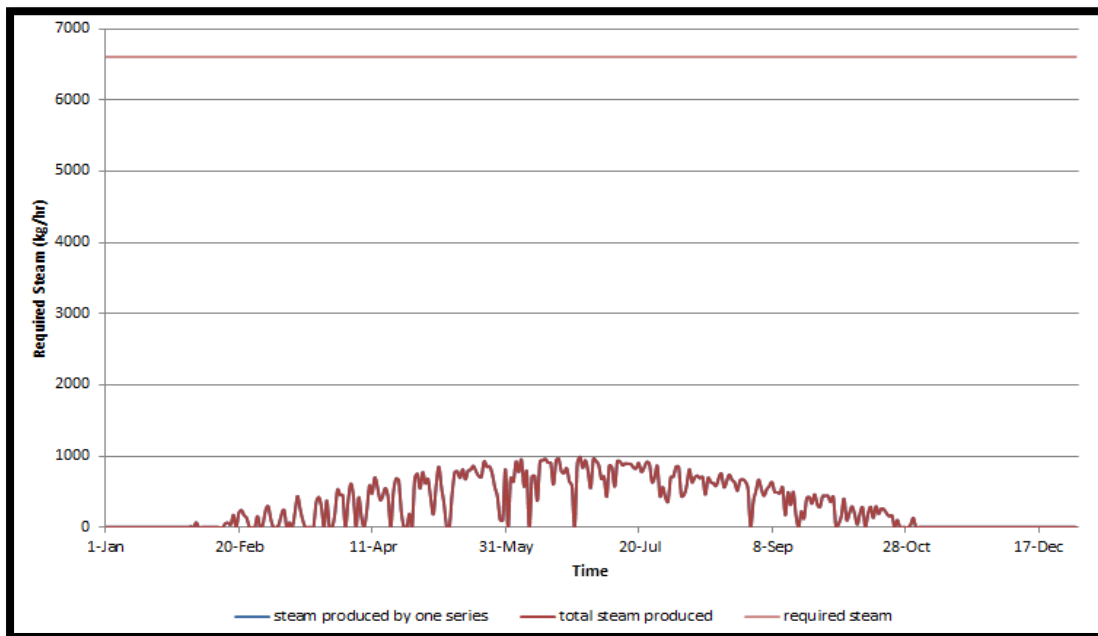


Figure 5. 5: Produced steam by 1 parallel series

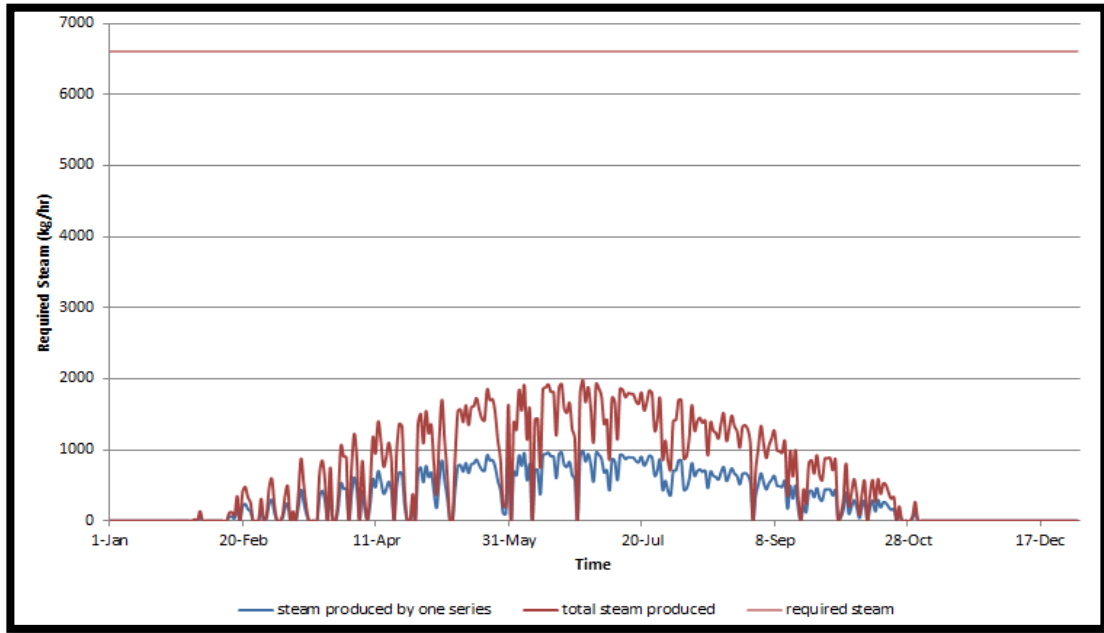


Figure 5. 6: Produced steam by 2 parallel series

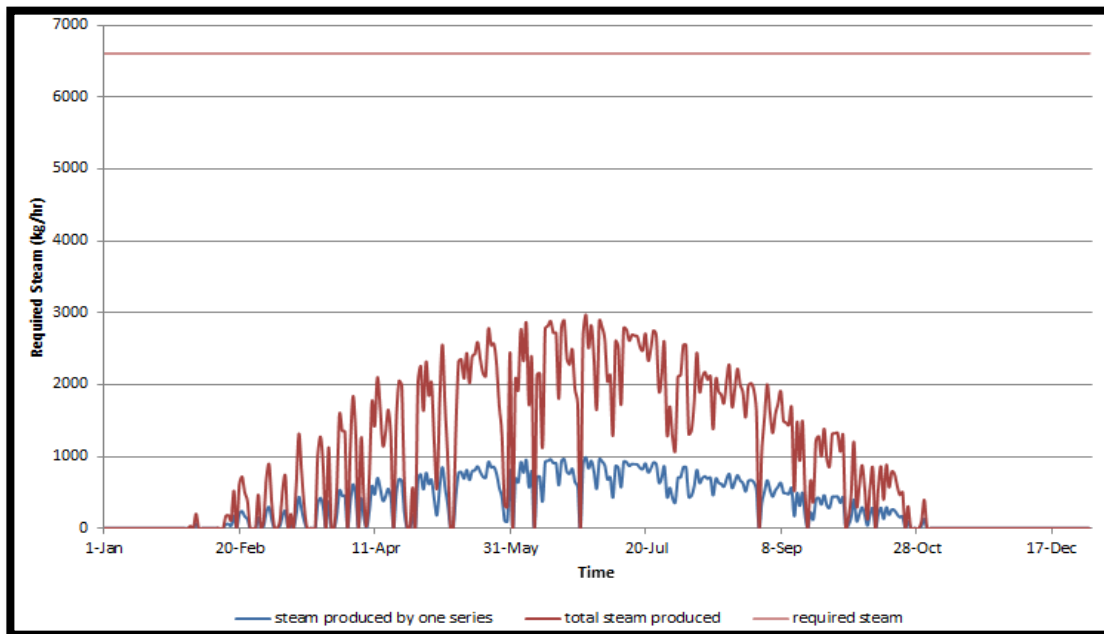


Figure 5. 7: Produced steam by 3 parallel series

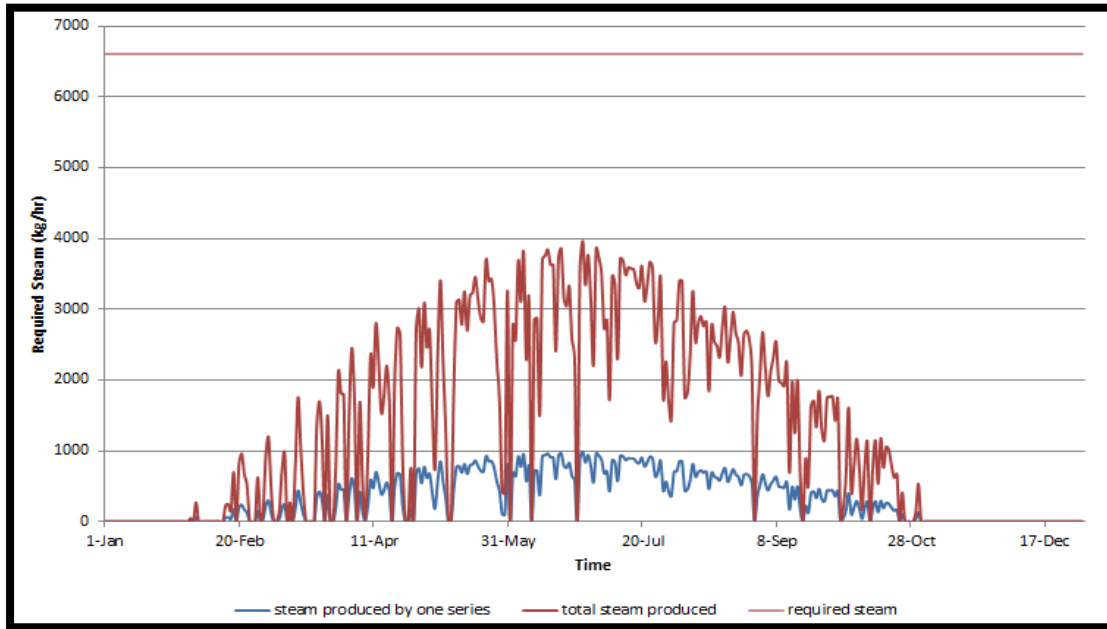


Figure 5. 8: Produced steam by 4 parallel series

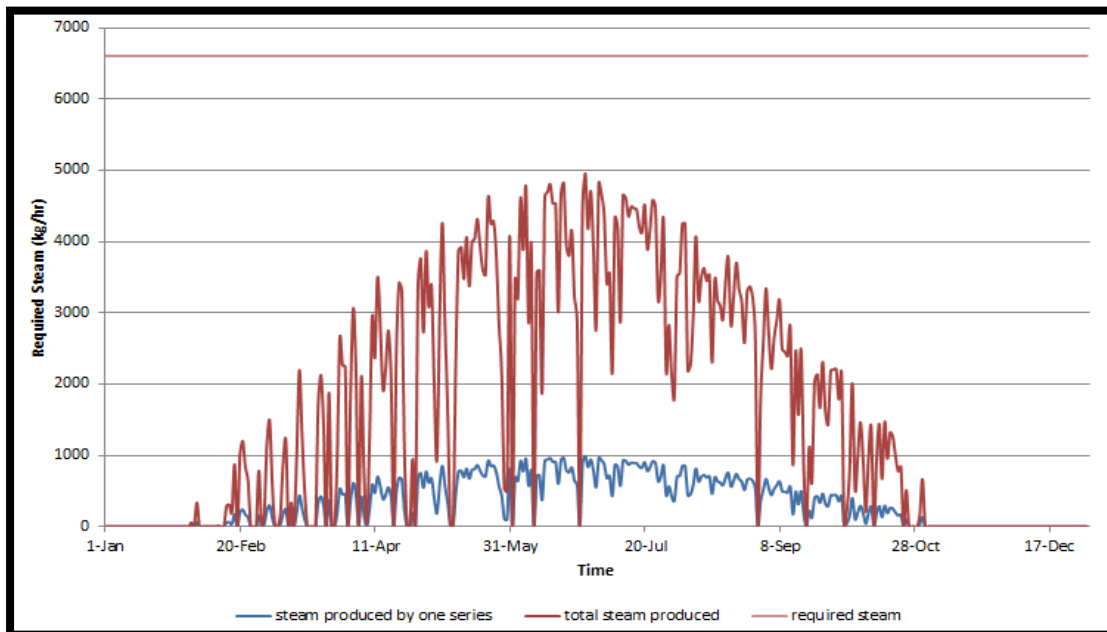


Figure 5. 9: Produced steam by 5 parallel series

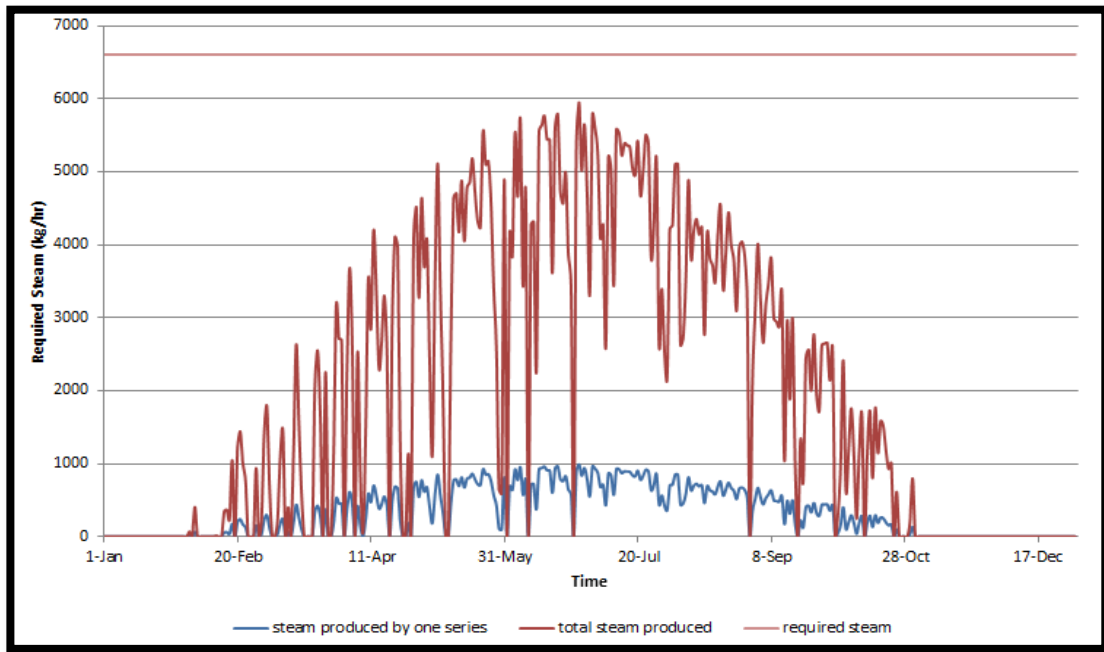


Figure 5. 10: Produced steam by 6 parallel series

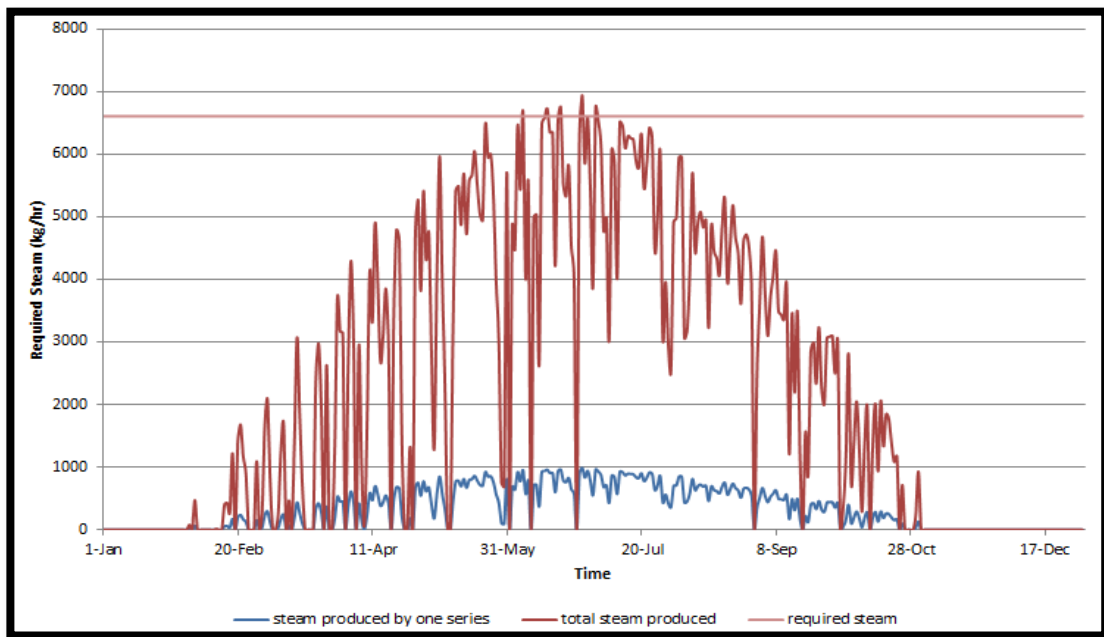


Figure 5. 11: Produced steam by 7 parallel series

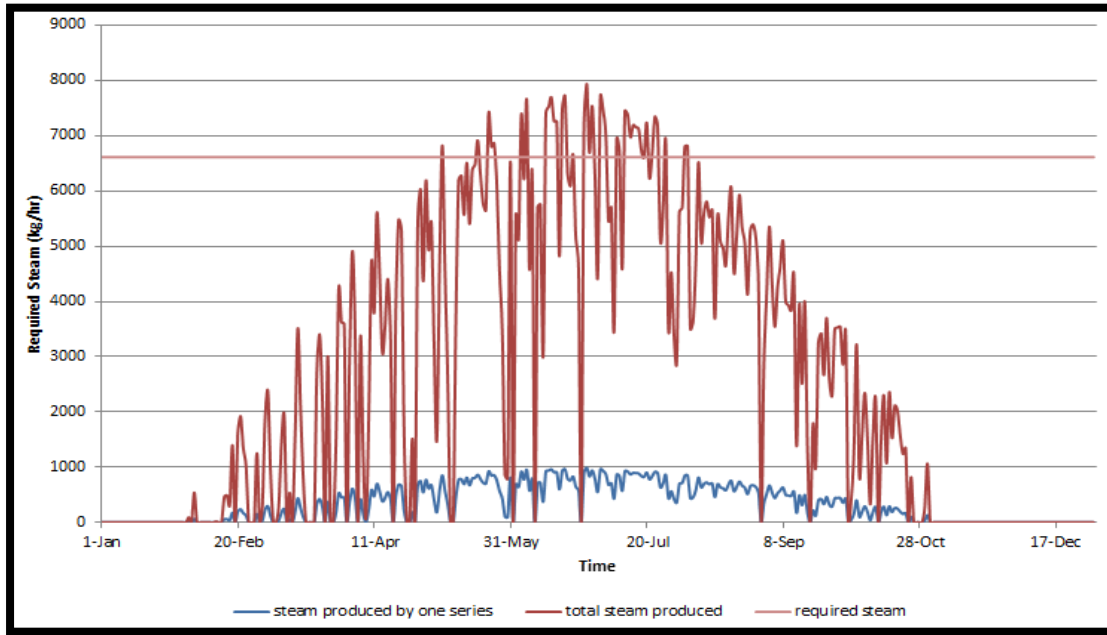


Figure 5. 12: Produced steam by 8 parallel series

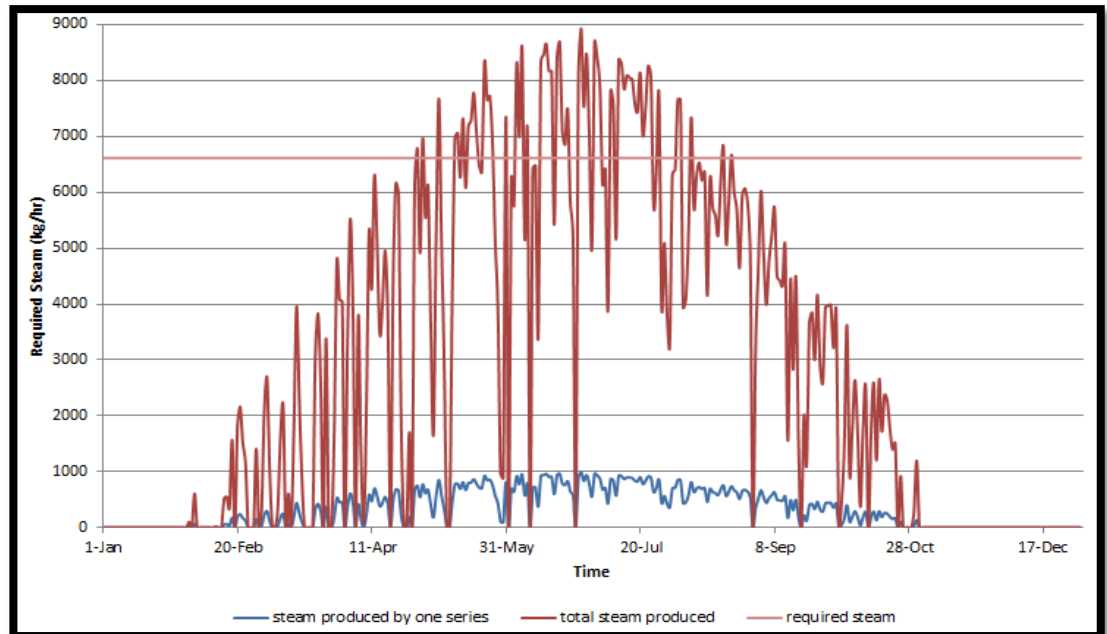


Figure 5. 13: Produced steam by 9 parallel series

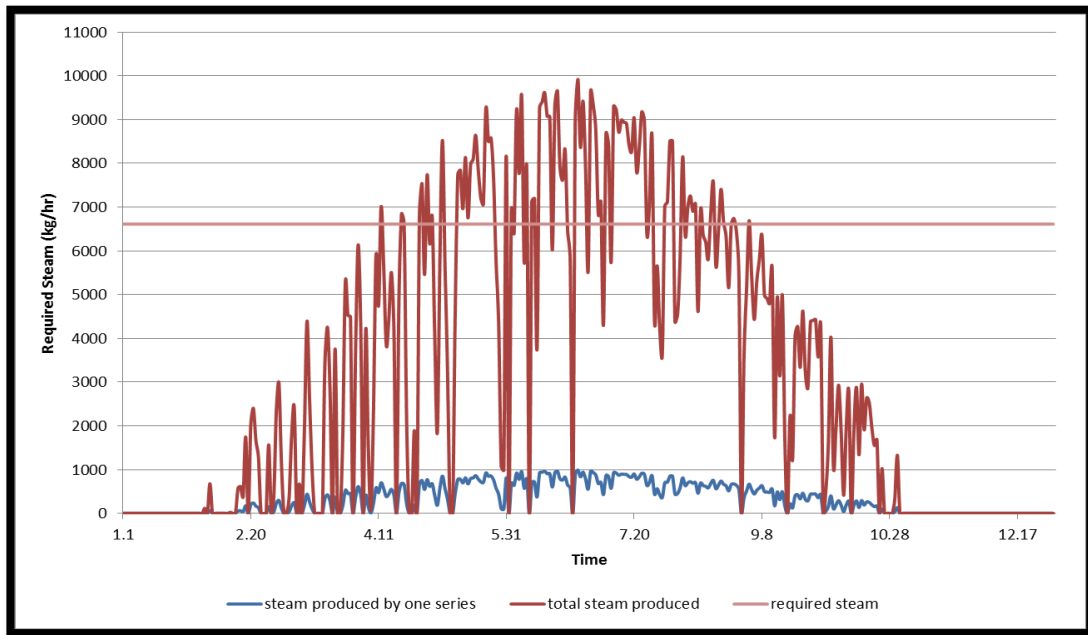


Figure 5. 14: Produced steam by 10 parallel series

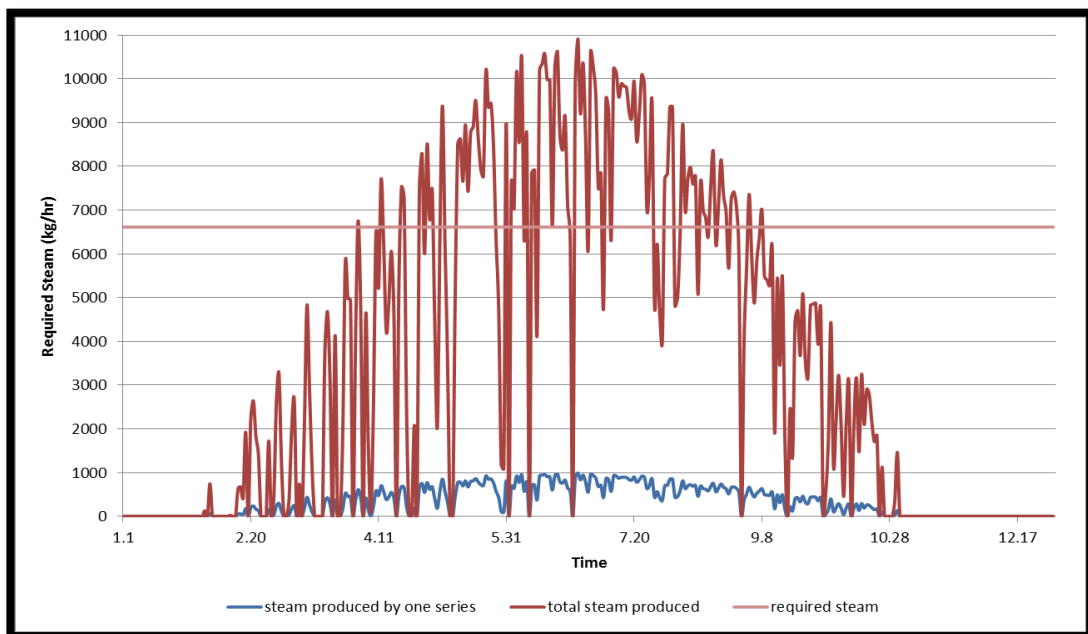


Figure 5. 15: Produced steam by 11 parallel series

As a conclusion Figure 5.16 shows the total analysis. It is clearly seen that the percentage of solar generated steam usage in the system does not show increase from 9 parallel series to 10 parallel series as it is like between each one before 9 parallel series. Therefore, to decrease the initial cost it was decided to use 9 parallel series in the model.

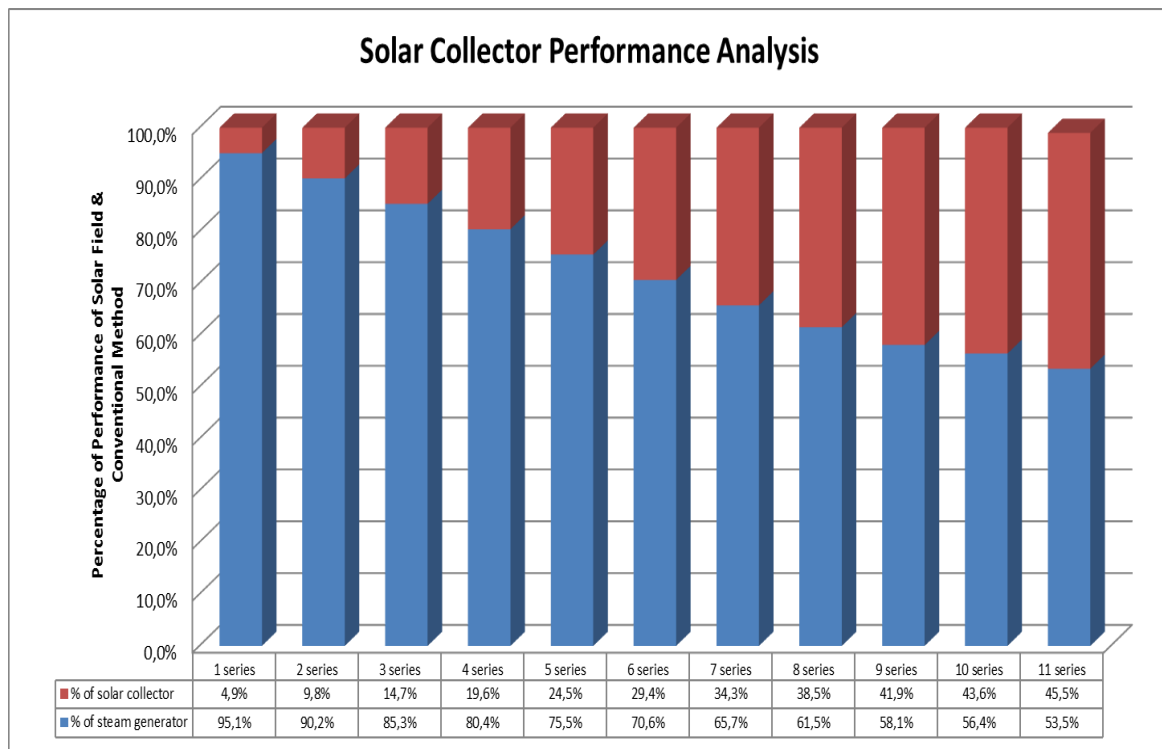


Figure 5. 16: Solar collector performance analysis

5.1.1.2 Cost Analysis

In this section, steam generation cost with solar thermal steam generating system will be discussed. As determined in previous section, the capital cost will be calculated for 9 parallel series and it means that 41,9% of steam is generated by solar collector whereas the rest of the steam is produced with only conventional method. In both cases, the capital cost does not contain the cost relevant to actual projects such as drilling cost, steam pipelines, etc. It is assumed that steam production is supported by solar collector system from 2008 till the end of the project. Operation parameters will not be changed as planned with conventional method. Therefore, the expected result shown by simulation will not change, either.

The calculation will be done according to the idea that by the beginning of 2008, solar collector has started to work and 41,9% of annual required steam has been generated by the parabolic trough collector system.

5.1.1.2.1 Capital Investment Cost

Based on the information from International Energy Agency (IEA, 2010) and National Renewable Energy Laboratory (NREL, Sargent and Lundy, 2003) the cost of concentrating solar power includes investment cost also called as CAPEX, operation and maintenance cost (O&M) and financing costs. However in the calculations financing cost will be added on CAPEX as it is not found separately in analysis. [25]

According to International Renewable Energy Agency (IRENA) publications it seems that the investment cost for parabolic trough solar collectors without storage are between 4500 USD/kw and 7150 USD/kw whereas with thermal storage it increases to between 5000 USD/kw and 10500 USD/kw. [25]

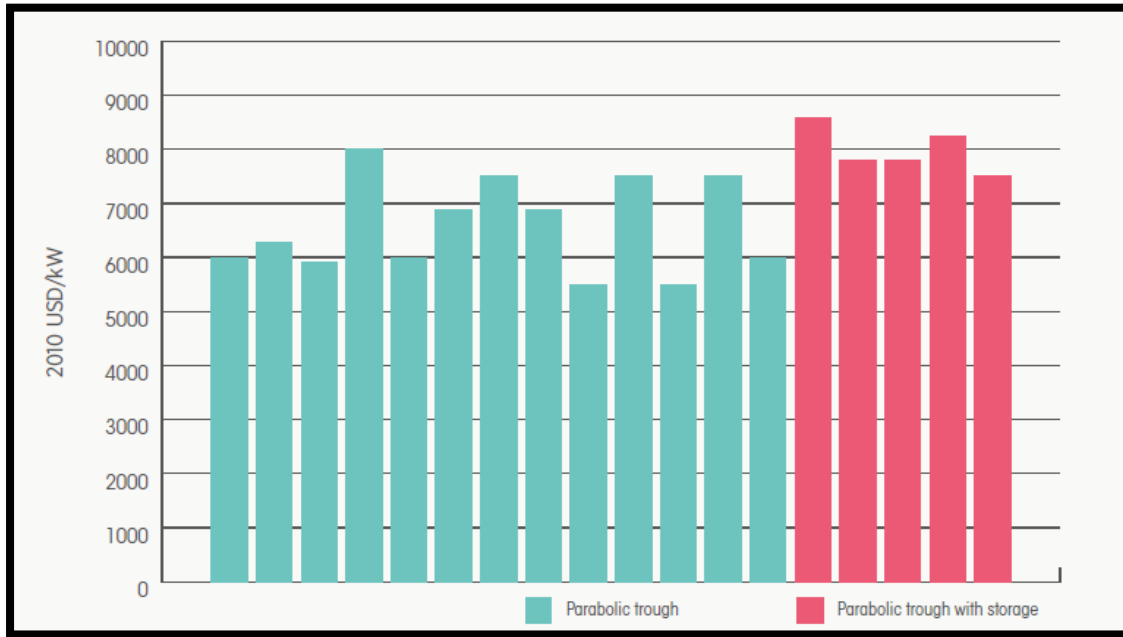


Figure 5. 17: Total installed cost for parabolic trough plant commissioned or under construction projects in 2010 and 2011 [25]

As part of the investment cost, solar field equipment cost has the highest component of the total cost. It takes between 35% and 49% of the project cost. (Fichtner, 2010; Turchi, 2010 and Hinkley, 2011) Moreover, the share of the thermal storage in total investment cost is between 9% for 4,5 hours storage and 20% for 13,5 hours storage of the total CAPEX. Figure 5.12 shows that the each breakdown of parabolic solar collector system cost. [25]

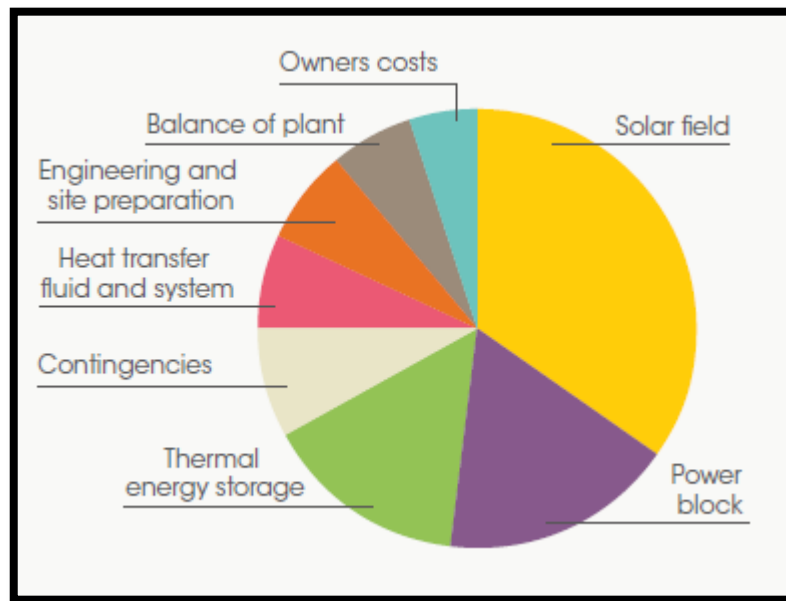


Figure 5. 18: Cost breakdown for parabolic trough collectors [25]

As it is given by the Figure 5.12, the solar field equipment represents the biggest part of the cost. Equipment cost includes metal support structure, the receiver, the mirrors, heat transfer system and heat transfer fluid. Second biggest part belongs to thermal storage with 10% of the total cost. Also, labour cost has a significant impact on the total cost.

5.1.1.2.2 Operation and Maintenance Cost

The operation cost includes mainly replacement of receivers and mirrors, mirror washing, water cost. Plant insurance also has significant effect on the cost and varies between 0,5% to 1% of the initial capital cost. By developing technology O&M cost decreases due to increasing in the quality of material of mirrors and receivers result in to reduce the requirement of change.

The total O&M cost is estimated around 0,015 USD/kWh with 0,003 USD/kwh variation cost depends on location. Care should be taken that this O&M percentage does not include the insurance. [25]

5.1.1.2.3 Economic Analysis of the Solar Generated Steam Injection

There is an direct proportion between operation cost and necessary energy for generating steam. In this model it was calculated as 14,67 MMBTU/hr and it is equal to 7474,43 kW.

As an example, the analysis of a power plant with 50 MW with a thermal storage capacity of 7,5 hours and solar field size 510 thousand m² is taken. The detailed breakdown of investment cost are given in Table 5.5.

The model that was used in this study has no storage capacity, around 7,5 MW and takes a space of 29,5 thousand m².

Table 5. 5: Breakdown of the investment cost of 50 MW PTC power plant [25]

Breakdown of Investment Cost		Cost 2010 (USD MM)	Share (%)
Labour cost: Site and solar field	Solar field	11,3	2,04
	Site preparation and infrastructure	21,2	3,83
	Steel construction	9,1	1,65
	Piping	6,4	1,16
	Electric installations and others	14,4	2,60
	TOTAL	62,4	11,28
Equipment: Solar field and HTF and system	Mirrors	23,1	4,18
	Receivers	25,9	4,68
	Steel constructions	39	7,05
	Pylons	3,9	0,71
	Foundations	7,8	1,41
	Trackers	1,6	0,29
	Swivel joints	2,6	0,47
	HTF system (piping, insulation, heat exchangers, pump)	19,5	3,53
	Heat transfer fluid	7,8	1,41
	Electronics, controls, electrical and solar equipment	9,1	1,65
	TOTAL	140,3	25,37
Thermal storage system	Salt	18,6	3,36
	Storage tanks	6,6	1,19
	Insulation materials	0,7	0,13
	Foundations	2,3	0,42
	Heat exchangers	5,1	0,92
	Pumps	1,6	0,29
	Balance of system	3,5	0,63
	TOTAL	38,4	6,94
Others	Project development	10,5	1,90
	Project management	28,1	5,08
	Financing	21,8	3,94
	Other costs (allowances)	10,5	1,90
TOTAL COST		312 MM USD	100%

In order to estimate the total investment cost of the project, a list of breakdown of the investment cost of a 50 MW parabolic trough power plant is used as an example. The project was constructed in 2010. As shown in the Table 5.5; thermal storage with 7,5 hours has 6,94% of the total investment cost. In the presented study, thermal storage has not been used so it was taken out from the total cost.

Moreover, total O&M costs of CSP plants in the longer run is calculated as 0.015USD/kWh so for this study, operation and maintenance cost is estimated as about 188 USD/hr with the variation of 22,4 USD/hr based on the location. Automated washer system decreases the repairment or replacement cost of the materials of the solar field. Work force shows also difference from country to country so it is expected to decline in the developing countries. As sum up, the total investment cost with O&M cost for this study is expected around 41 MM USD + 1,6 MM USD/year. [25]

On the other side, it will reduce the natural gas and crude oil consumption since solar collector system does not require fossil fuels for operation. As mentioned before, fossil fuel consumption will decrease 41,9% after solar generated steam method put in the progress.

Figure 5.19 shows amount of fuel consumption with solar generated steam injection method in X field in 1 year. As shown in the Figure 5.19 in January, November and December, steam is being produced by only steam generator.

Figure 5.20 gives a comparison of months for fuel consumption and fuel saving. Since the solar collector receives more DNI and there is more sunshine duration in summer, fuel saving is observed mostly in this duration.

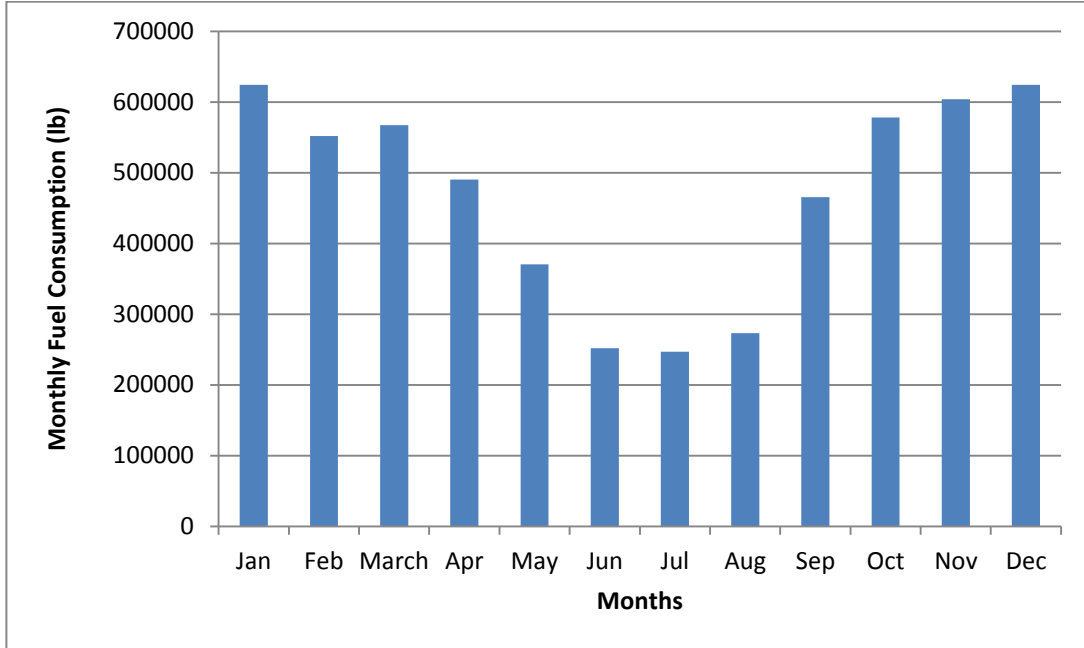


Figure 5. 19: Monthly Fuel Consumption

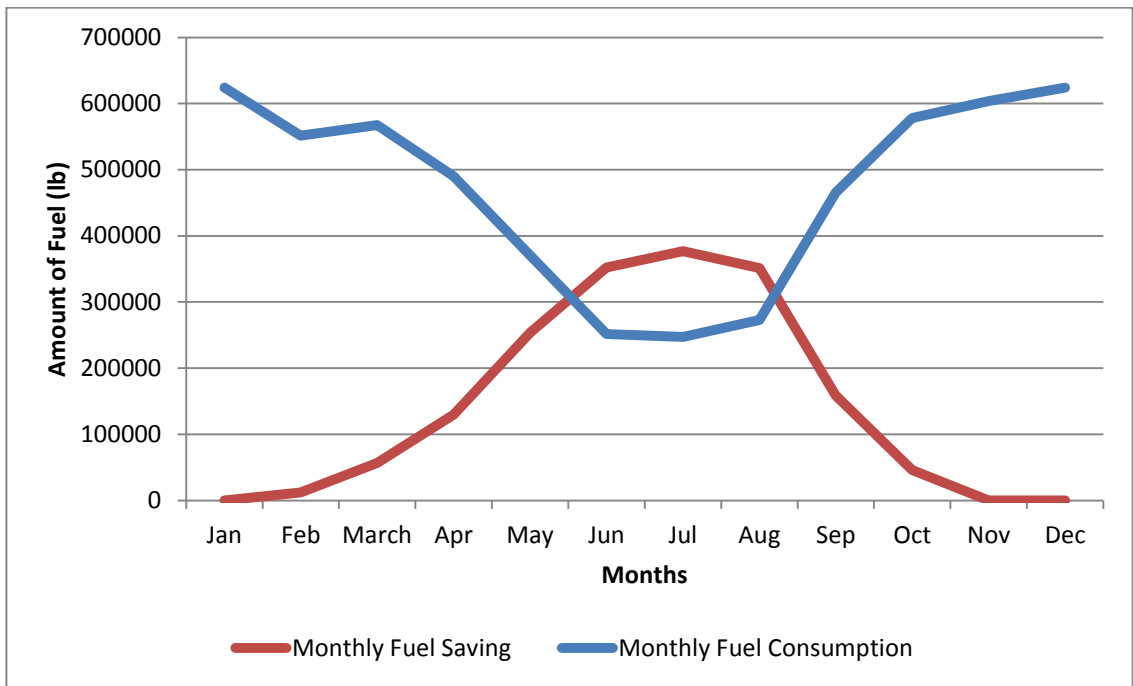


Figure 5. 20: Comparison of fuel saving and fuel consumption by months in 1 year

In order to calculate the cost reduction, the history and the forecast of crude oil price should be analyzed. According to International Energy Outlook 2013 made by U.S. Energy Information Administration, oil price will never be under 100\$/bbl after 2014. The history and forecast of the oil price is shown in Figure 5.21. [26]

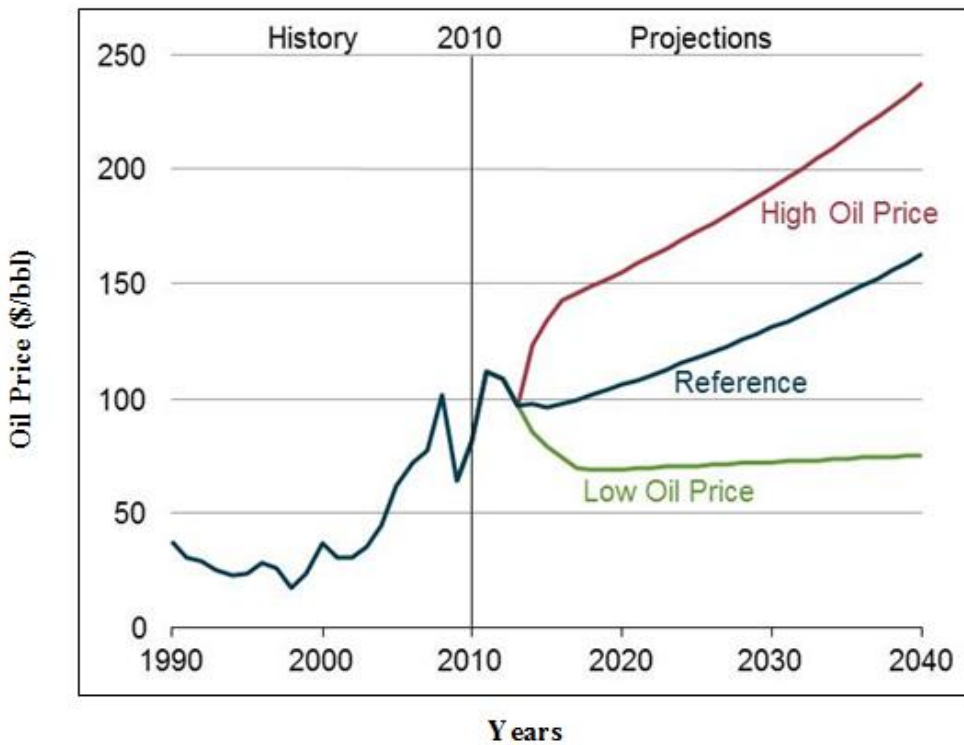


Figure 5. 21: History and forecast of the oil price [27]

In cost analysis reference data were taken to determine if solar generated steam injection method is feasible in defined condition. It is assumed that boiler uses 15° API crude oil as it is being produced in X field. Total fuel saving is one year is 1,7 MM lb and it approximately equals to 5145 bbl.

Table 5. 6: Yearly Saving with Solar Field

Years	\$/bbl	Fuel Saving by Year (\$)	Cost Saving by years (\$)
2008	\$ 100	\$ 512.727	\$ 512.727
2009	\$ 62	\$ 318.686	\$ 728.220
2010	\$ 80	\$ 409.534	\$ 1.137.754
2011	\$ 95	\$ 488.086	\$ 1.625.840
2012	\$ 94	\$ 483.817	\$ 2.109.657
2013	\$ 98	\$ 504.137	\$ 2.613.793
2014	\$ 101	\$ 519.569	\$ 3.133.363
2015	\$ 96	\$ 493.385	\$ 3.626.748
2016	\$ 97	\$ 498.992	\$ 4.125.740
2017	\$ 99	\$ 509.692	\$ 4.635.432
2018	\$ 101	\$ 520.598	\$ 5.156.030
2019	\$ 103	\$ 531.710	\$ 5.687.740
2020	\$ 106	\$ 543.078	\$ 6.230.818
2021	\$ 108	\$ 554.704	\$ 6.785.523
2022	\$ 110	\$ 566.588	\$ 7.352.111
2023	\$ 113	\$ 578.728	\$ 7.930.839
2024	\$ 115	\$ 591.126	\$ 8.521.965
2025	\$ 117	\$ 603.729	\$ 9.125.694
2026	\$ 120	\$ 616.693	\$ 9.742.386
2027	\$ 122	\$ 629.862	\$ 10.372.248
2028	\$ 125	\$ 643.340	\$ 11.015.588
2029	\$ 128	\$ 657.126	\$ 11.672.715
2030	\$ 130	\$ 671.170	\$ 12.343.885

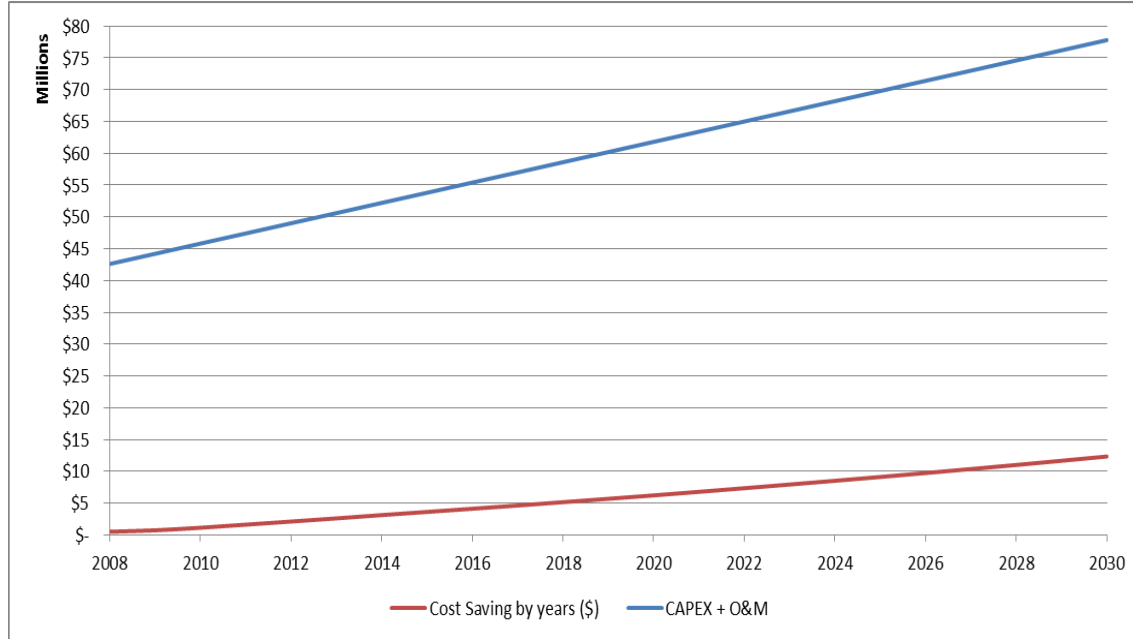


Figure 5. 22: CAPEX+O&M vs Cost Saving by Years

When saving cost is compared with CAPEX and M&O cost of the solar field (41 MM USD + 1,6 MM USD/year), it can be easily decided that solar generated steam project is not feasible for selected region.

5.2 Discussion

In this study, economic feasibility of solar generated steam injection method has been evaluated. Except than other assumptions mentioned before, many reasonable assumptions and simplifications has been made in solar modeling study.

It has been assumed that weather data will be same from 2008 till to the end of the project and the performance of pump, collector, steam generator does not change during the application and works well over the entire project period. The factors such as dirt

and humidity that reduces the performance of the concentrates solar collector has been neglected.

Oil prices that are produced from X field were assumed to be same as that was given in this study. As actual X field oil price is less than assumed price, cost saving would be less than mentioned although it has no impact on the result of the project.

Another assumption is that there is an available area where solar field can be constructed and any impact of land-use has been neglected. Moreover, due to reason that to move steam over a long distance causes heat loss, solar field are assumed to be very close to injection well.

CAPEX has been taken from a project that started to work in 2010 and this study was started in 2008 therefore cost difference has been ignored. Additionally, cost analysis has been done by forecasting oil price and solar field price that belong to 2010. Labor force is assumed to be same with the country where solar project has been applied.

CHAPTER 6

CONCLUSIONS

Recent experimental studies of the cooperation of solar and oil companies confirm that fuel cost of the steam injection process is declined when solar generated steam method is applicable. To better understand this phenomenon, feasibility study has been carried out in a pilot area of the selected oil field (X-field) in Turkey. A reservoir modelling of X field has been used as a reference and operation parameters of the steam injection has been drawn from that study. A solar field model has been developed in TRNSYS simulation and number of parabolic trough solar collector, capacity of heat exchanger and the other design parameters has been calculated based on the steam requirement. The results have clearly indicated that solar input is not enough to cover the necessity of the continuous steam injection process all the year round. Therefore, system has been supported with natural gas back up.

To investigate the ability of the project, an economic analysis has been conducted. It has been assumed that solar generated steam injection method has been performed since 2008. For comparison purposes, total investment cost and fuel savings have been calculated. Results demonstrated that, 41,9% of steam has been produced by solar field whereas the rest of the steam had to be produced by conventional method. The study can be summarized that fuel savings due to solar generated steam project has not compensated the total investment cost of the project with current oil price for selected oil field.

CHAPTER 7

RECOMMENDATIONS FOR FUTURE WORK

This presented study should be evaluated as a starting point for further studies in steam injection operations in Turkey. Parabolic trough collector system has a potential to decline the operating cost in generated steam with natural gas. In the future, this technology is promising to contribute the economy with existence of better solar insolation or higher oil prices.

Recommendations to improve on the presented study are following:

- The current model used Therminol VP-1 as a heat transfer fluid. The model can be improved to use water instead of Therminol VP-1 in order words, direct steam generation system can be applied to decline the operation cost.
- X field can be re-modeled in order to evaluate the cycle steam injection. If it works, the solar thermal generated steam technology can be applied alone; therefore, natural gas back-up will not be required.
- Its significant effect on reducing the CO₂ emission can be analyzed to benefit from government incentive on the investment cost.

REFERENCES

- [1] “Yenilenebilir Enerji Kaynaklari Nelerdir” [Online]. Available:
<http://www.bilgiustam.com/yenilenebilir-enerji-ve-kaynaklari-nelerdir/>.
[Accessed: 14-Jul-2014].
- [2] “The History of Solar” US Department of Energy [Online]. Available:
http://www1.eere.energy.gov/solar/pdfs/solar_timeline.pdf [Accessed: 14-Jul-2014].
- [3] J. A. Duffie and W. A. Beckman, Solar Engineering of Thermal Processes, 3rd ed.
Wiley, 2006.
- [4] “The History of Solar” US Department of Energy [Online]. Available:
http://www1.eere.energy.gov/solar/pdfs/solar_timeline.pdf [Accessed: 14-Jul-2014].
- [5] “Solar Energy” [Online]. Available: <http://www.earthlyissues.com/solar.htm>
[Accessed: 14-Jul-2014].
- [6] “Solar Paces” Energy Technology Network [Online]. Available:
http://www.solarpaces.org/CSP_Technology/csp_technology.htm
[Accessed: 14-Jul-2014].
- [7] "Ptc Technology Assessment Appendix A", NREL CA Solar Benefits, April 21,
2006.
- [8] The Potential for Low-Cost Electricity from Concentrating Solar Power Systems,
Price 1999

- [9] Patnode M. A., "Simulation and Performance Evaluation of Parabolic Trough Solar Power Plants", M.S. Thesis ,University of Wisconsin, Madison,2006.
- [10] "Enhanced recovery (EOR) methods in Russia: time is of the essence"
ERNST&YOUNG
- [11] Integrating Renewable Energy Resources Within the Oil Industry Concentrated Solar Power (CSP) & Enhanced Oil Recovery (EOR)
- [12] E.C. Donaldson, G.V. Chilingarian, T.F. Yen Enhanced oil recovery, II processes and operations, 1989
- [13] "Steam Quality – Plant Operations Require A High Steam Quality"
Steam System Best Practices [Online]. Available: <https://www.swagelok.com>
[Accessed: 14-Jul-2014].
- [14] Babadagli T., Sahin S., Kalfa U., Celebioglu D., Karabakal U., Topguder N., 2008, "Development of Heavy Oil Fractured Carbonate Bati Raman Field: Evaluation of Steam Injection Potential and Improving Ongoing CO2 Injection" SPE 115400, 2008 SPE Annual Technical Conference and Exhibition, Colorado, USA, 21-24 September
- [15] Akin S., Celebioglu D., Kalfa U., 2009 "Optimum Tertiary Steam-Injection Strategies for Oil-Water Fractured Carbonates" SPE 120168, 2009 SPE Western Regional Meeting, California, USA, 24-26 March
- [16] Akin S. "TPAO, Buhar Enjeksiyonu Sektör Model Simulasyonu" presented on 2007, October 9th

- [17] Assets Newport [Online]. Available:
<http://assets.newport.com/web250w-EN/images/1066.gif> [Accessed: 14-Jul-2014].
- [18] Uckun C. “Modeling and simulations of direct steam generation in concentrating solar power plants using parabolic trough collectors”, M.S. Thesis, Middle East Technical University, 2013
- [19] Global Change Master Directory, Discover Earth science data and services, NASA [Online].
Available: http://gcmd.nasa.gov/records/GCMD_gov.noaa.ncdc.C00047.html
[Accessed: 14-Jul-2014].
- [20] TESSLibs 17, Component Libraries for the TRNSYS Simulation Environment, High Temperature Solar Library Mathematical Reference , Volume 14, 2010
- [21] Therminol, Heat Transfer Fluids by Eastman [Online]. Available:
<http://www.therminol.com/products/Therminol-VP1> [Accessed: 14-Jul-2014].
- [22] Incropera, DeWitt, Bergman, Lavine “Fundamentals of Heat and Mass Transfer”, Sixth Edition, 2007
- [23] Engineer Edge, Parallel and Counter Flow Designs [Online]. Available:
http://www.engineersedge.com/heat_transfer/parallel_counter_flow_designs.htm
[Accessed: 14-Jul-2014].
- [24] Kwan Woong Gwak, Wisup Bae “A Review of Steam Generation for In-Situ Oil Sands Projects”, Geosystem Engineering, September 2010

- [25] International Renewable Energy Agency, “Renewable Energy Technologies: Cost Analysis Series” Volume 1: Power Sector Issue 2/5, June 2012
- [26] Independent Statistics & Analysis, US Energy Information Administration, Short-term Energy Outlook [Online]. Available:
<http://www.eia.gov/forecasts/steo/> [Accessed: 14-Jul-2014].
- [27] Independent Statistics & Analysis, US Energy Information Administration, Market Prices and Uncertainty Report [Online]. Available:
<http://www.eia.gov/forecasts/steo/uncertainty/> [Accessed: 14-Jul-2014].

APPENDIX A

HEAT TRANSFER FLUID (THERMINOL-VP1) PROPERTIES (21)

Table A. 1: Therminol-VP1 properties

Appearance	Clear, water white liquid
Composition	Biphenyl/diphenyl oxide (DPO) eutectic mixture
Maximum bulk temperature	400°C (750°F)
Maximum film temperature	425°C (800°F)
Normal boiling point	257.0°C (495.0°F)
Crystallizing point	12.0°C (54.0°F)
Flash point COC (ASTM D-92 / DIN 51376)	124°C (255°F)
Flash point PMCC (ASTM D-93 / DIN EN 22719)	110°C (230°F)
Autoignition temperature (ASTM E-659)	601°C (1114°F)
Autoignition temperature (ASTM D-2155)	621°C (1150°F)
Minimum liquid temperatures for transitional region flow, (NRe > 2000)	
10 ft/sec, 1 in tube (3.048 m/s, 2.54 cm tube)	151°C (304°F)
20 ft/sec, 1 in tube (6.096 m/s, 2.54 cm tube)	131°C (268°F)
Minimum vapor temperatures for fully developed turbulent flow (NRe > 10000)	
10 ft/sec, 1 in tube (3.048 m/s, 2.54 cm tube)	208°C (406°F)
20 ft/sec, 1 in tube (6.096 m/s, 2.54 cm tube)	181°C (358°F)
Coefficient of thermal expansion at 200°C	0.000979/°C (0.000544/°F)
Heat of vaporization at max. use temperature	206.0 kJ/kg (88.7 Btu/lb)
Kinematic viscosity at 100°C	99.00 mm ² /s (cSt)
Kinematic viscosity at 40°C	2.48 mm ² /s (cSt)

Table A.1 (continued)

Liquid density at 15°C	1068.0 kg/m ³ (8.91 lb/gal)
Liquid density at 25°C	1060.0 kg/m ³ (8.85 lb/gal)
Total acidity	<0.2 mg KOH/g
Average molecular weight	166
Pseudocritical temperature	499.0°C (930.0°F)
Pseudocritical pressure	33.1 bar (480.0 psia)
Pseudocritical density	327.00 kg/m ³ (20.40 lb/ft ³)
Sulfur content, ppm	<10 ppm
Copper corrosion	<<1a
Moisture content, maximum	300 ppm
Volume contraction upon freezing, %	6.27%
Volume expansion upon melting, %	6.69%
Surface tension in air at 25°C	36.6 dynes/cm

APPENDIX B

SOLAR FIELD DESIGN

B.1 Parabolic Trough Solar Collector

B.1.1 Nomenclature

Table B. 1: Nomenclature of Solar Collector

α	[0..1]	absorptance of the coating on the absorber tube
η	-	efficiency expressed as a fraction
ρ		density of the working fluid
θ	-	Angle of incidence of beam radiation upon the collector surface
Δt	hours	the TRNSYS timestep
τ_{glass}	[0..1]	transmittance of the glass envelope to the concentrated beam radiation
a	several	coefficient in the correlation of heat loss per unit length
A	m^2	gross collector area defined by collector length and aperture width
b	several	coefficient in the incident angle modifier correlation
Cp	kJ/kg.K	specific heat of the fluid in the node
Cp,in	kJ/kg.K	specific heat of the fluid entering the node
DNI	kJ/hr.m ²	direct normal solar radiation
F	m	the focal length of the collector
$f_{bellows}$	[0..1]	function that accounts for shading of the mirror by the bellows

f_{dust}	[0..1]	function that accounts for losses due to the dust on the glass receiver
$f_{endloss}$	[0..1]	function that accounts for the end losses from the solar collector
f_{mirror}	[0..1]	function that accounts for the geometric inaccuracies of the parabolic mirror
f_{misc}	[0..1]	function that accounts for miscellaneous losses from the system
$f_{tracking}$	[0..1]	function that accounts for the inaccuracies of the tracking system
g	C/hr	the function that equals dT/dt ($dT/dt = g(T,t)$)
G_{beam}	kJ/hr.m^2	incident beam solar radiation on the parabolic mirrors per unit area including the effects of collector row shading
h	several	coefficient in the enthalpy correlation of the fluid as a function of temperature
IAM	-	incident angle modifier
L	m	the length of one collector along the length of the mirror
m	kg	mass of the fluid in the node
m_{in}	kg/hr	mass flow rate of fluid entering the node
m_{out}	kg/hr	mass flow rate of fluid exiting the node
n	-	integer in the Runge-Kutta solution
$\dot{Q}_{absorbed}$	kJ/hr	solar energy transferred to the working fluid
$\dot{Q}_{fluid,in}$	kJ/hr	energy transfer via fluid flow into the node
$\dot{Q}_{fluid,out}$	kJ/hr	energy transfer via fluid flow out of the node
\dot{Q}_{losses}	kJ/hr	energy lost from the working fluid to the environment
r	several	coefficient in the density correlation of the fluid as a function of temperature

t	hours	time
T	C	temperature of the fluid in the node
T_{in}	C	temperature of the fluid entering the node
u	several	coefficient in the correlation of internal energy of the fluid
U_L	$\text{kJ/hr.m}^2.\text{K}$	heat transfer coefficient between the device and the surrounding air (function of temp.)
U'	kJ/hr.m	heat loss coefficient from the fluid to environment per unit length of collector
V	m^3	volume
W	m mirror	the aperture width of the collector mirror
z	C	a variable in the Runge-Kutta solution to the differential equation $dT/dt = g(T,t)$

B.1.2 Methodology

A value of NRK=1000 seems to work well for time steps between 1 second and 1/10th of an hour (typical timesteps for this problem) The methodology to solve for T at time = $t+\Delta t$ can then be summarized as:

1. Calculate $g(T_0)$ using either Equation 4.41 depending on the mass outlet mode, where T_0 is the temperature of the fluid at the beginning of the time step.
2. Multiply this value by the TRNSYS time step and divide by 2 times the number of Runge-Kutta steps.
3. Multiply the results from step 1 by the result from step 2 and then add the product to the result from step 1. Refer to this value as T' .

4. Calculate $g(T')$ using either Equation 4.41 depending on the mass outlet mode.
5. Multiply the value from step 4 by the TRNSYS time step and divide by the number of Runge-Kutta steps.
6. Add the value from step 5 to the initial temperature (T_0) to get our estimate of T at time = $n\Delta t/N_{RK}$ where $n=1$ for this iteration. Refer to this new temperature as T_{new}
7. Calculate $g(T_{new})$ using either Equation 4.41 depending on the mass outlet mode.
8. Multiply the value from step 7 by the TRNSYS time step and divide by 2 times the number of Runge-Kutta steps.
9. Multiply the results from step 7 by the result from step 8 and then add the product to the result from step 8. Refer to this value as T' .
10. Calculate $g(T')$ using either Equation 4.41 depending on the mass outlet mode.
11. Multiply the value from step 10 by the TRNSYS time step and divide by the number of Runge-Kutta steps.
12. Add the value from step 11 to temperature T_{new} to get our estimate of T at time = $(n+1)\Delta t/N_{RK}$. Refer to this new temperature as T_{new} and set $n = n+1$
13. Repeat steps 7 through 12 ($N_{RK} - 1$) times to arrive at the estimate of the nodal fluid temperature at time = $t+\Delta t$

B.1.3 Default Settings

Table B. 2: Default setting of TRNSYS

Collector aperture width	m	5	The width across the collector mirror from one edge to the other.
Collector length	m	50	The length along ONE of the identical solar collectors (length is defined as along the absorber tube direction)
Absorber tube diameter	m	0.07	The inner diameter of the fluid-filled absorber tube.
Focal length	m	1.8	The effective focal length of the collector; the distance from the absorber tube to the center of the parabolic mirror.
Mirror accuracy	(0..1)	0.98	The modifier which accounts for the geometric inaccuracies of the mirrored surface (1=perfectly focusing mirror)
Mirror reflectivity		0.93	The reflectivity of the mirrored surface (1=perfectly reflective).
Envelope transmittance		0.93	The transmittance of the glass receiver tube to solar energy at normal incidence (1=all radiation passes through)
Absorptance of receiver coating		0.93	The absorptance of the coating on the absorber tube of the receiver.
Initial fluid temperature	C	100	The temperature of the fluid in the absorber tube at the beginning of the simulation.
Number in series	-	8	The number of identical collectors connected in a series arrangement that will be modeled by this component.
Number of collector nodes	-	5	The number of iso-volumetric nodes that the collector absorber tube will be broken into along the flow direction. The more nodes the greater the accuracy at low-flow conditions but the longer the simulation run-time.

Number of Runge-Kutta steps	-	1000	The number of small steps that will be taken each TRNSYS timestep to solve the dT/dt differential equation. This value should be chosen with care; too small and the calculations may diverge, too large and numerical instabilities may be introduced.
Outlet flow calculation mode	-	0	The mode for calculating the outlet flow rate from the collector: 0 the outlet mass flow rate is set to the inlet mass flow rate (less accurate but more stable), 1 = the outlet mass flow rate is the inlet mass flow rate + dm/dt
IAM coefficient b_0	-	1	The coefficient b_0 in the IAM correlation: $b_0 + b_1 \frac{\theta}{\cos(\theta)} + b_2 \frac{\theta^2}{\cos(\theta)}$
IAM coefficient b_1	$\frac{1}{\text{Degrees}}$	0,000884	The coefficient b_1 in the IAM correlation: $b_0 + b_1 \frac{\theta}{\cos(\theta)} + b_2 \frac{\theta^2}{\cos(\theta)}$
IAM coefficient b_2	$\frac{1}{\text{Degrees}^2}$	-0,00005369	The coefficient b_2 in the IAM correlation: $b_0 + b_1 \frac{\theta}{\cos(\theta)} + b_2 \frac{\theta^2}{\cos(\theta)}$
Collector heat loss coefficient a_0	kJ/h.m	-34.0669188	The coefficient a_0 in the collector heat loss per unit length correlation: $U' = a_0 + a_1 T + a_2 T^2 + a_3 T^3 + \text{DNI}(a_4 + a_5 T^2)$
Collector heat loss coefficient a_1	kJ/h.m.K	1.09066176	The coefficient a_1 in the collector heat loss per unit length correlation: $U' = a_0 + a_1 T + a_2 T^2 + a_3 T^3 + \text{DNI}(a_4 + a_5 T^2)$
Collector heat loss coefficient a_2	kJ/h.m ² .K ²	-0.0049925988	The coefficient a_2 in the collector heat loss per unit length correlation: $U' = a_0 + a_1 T + a_2 T^2 + a_3 T^3 + \text{DNI}(a_4 + a_5 T^2)$
Collector heat loss coefficient a_3	kJ/h.m ² .K ³	0.0000249452748	The coefficient a_3 in the collector heat loss per unit length correlation: $U' = a_0 + a_1 T + a_2 T^2 + a_3 T^3 + \text{DNI}(a_4 + a_5 T^2)$
Collector heat loss coefficient a_4	m	0.0764961	The coefficient a_4 in the collector heat loss per unit length correlation: $U' = a_0 + a_1 T + a_2 T^2 + a_3 T^3 + \text{DNI}(a_4 + a_5 T^2)$
Collector heat loss coefficient a_5	m/K ²	0.0000001128818	The coefficient a_5 in the collector heat loss per unit length correlation: $U' = a_0 + a_1 T + a_2 T^2 + a_3 T^3 + \text{DNI}(a_4 + a_5 T^2)$
Fluid density coefficient r_0	kg/m ³	1074	The coefficient r_0 in the fluid density correlation: $\rho = r_0 + r_1 T + r_2 T^2$

Fluid density coefficient r_1	kg/m ³ K	-0.6367	The coefficient r_1 in the fluid density correlation: $\rho = r_0 + r_1 T + r_2 T^2$
Fluid density coefficient r_2	kg/m ³ K ²	-0.0007762	The coefficient r_2 in the fluid density correlation: $\rho = r_0 + r_1 T + r_2 T^2$
Fluid enthalpy coefficient h_0	kJ/kg	-18.66	The coefficient h_0 in the fluid enthalpy correlation: $h = h_0 + h_1 T + h_2 T^2$
Fluid enthalpy coefficient h_1	kJ/kg.K	1.498	The coefficient h_1 in the fluid enthalpy correlation: $h = h_0 + h_1 T + h_2 T^2$
Fluid enthalpy coefficient h_2	kJ/kg.K ²	0.001377	The coefficient h_2 in the fluid enthalpy correlation: $h = h_0 + h_1 T + h_2 T^2$
Fluid internal energy coefficient u_0	kJ/kg	-19.00	The coefficient u_0 in the fluid enthalpy correlation: $u = u_0 + u_1 T + u_2 T^2$
Fluid internal energy coefficient u_1	kJ/kg.K	1.498	The coefficient u_1 in the fluid enthalpy correlation: $u = u_0 + u_1 T + u_2 T^2$
Fluid internal energy coefficient u_2	kJ/kg.K ²	0.001377	The coefficient u_2 in the fluid enthalpy correlation: $u = u_0 + u_1 T + u_2 T^2$
Inlet fluid temperature	C	293	The temperature of the fluid entering the first solar collector in series.
Temperature of the surroundings	C	15	The temperature of the surroundings in which the collectors are located (for thermal loss calculations).
Incidence angle	deg	0	The angle of incidence of beam radiation upon the collector surface.
Tracking efficiency factor	(0..1)	0.99	The factor to account for tracking inaccuracies: 1 = perfectly tracked
Mirror cleanliness factor	(0..1)	0.95	The factor to account for the mirror not being perfectly clean: 1 = perfectly clean

Receiver dust factor	(0..1)	0.98	The factor to account for dust on the receiver glass: 1 = no degradation due to dust
Bellows shading factor	(0..1)	0.97	The factor to account for shading of the mirror by the collector support structure: 1 = no shading of the mirror by the bellows
Misc. efficiency factor	(0..1)	1	The factor to account for otherwise unaccounted for losses: 1 = no other losses

B.2 Pump

B.2.1 Nomenclature

Table B. 3: Nomenclature of Pump

h_{in}	kJ/kg	The enthalpy of fluid entering the pump
h_{out}	kJ/kg	The enthalpy of fluid exiting the pump
$h_0 h_1 h_2$	various	User-provided coefficient relating fluid enthalpy to fluid temperature
$r_0 r_1 r_2$	various	User-provided coefficient relating fluid enthalpy to fluid temperature
T_{in}	°C	The temperature of fluid entering the pump
T_{out}	°C	The temperature of fluid exiting the pump
ρ_{in}	kg/m ³	The density of fluid entering the pump
\dot{v}_{out}	m ³ /h	The volumetric flow rate of fluid being delivered by the pump
\dot{v}_{rated}	m ³ /h	The volumetric flow rate of fluid being delivered by the pump at its rated condition

\dot{m}_{out}	kg/hr	The mass flow rate of fluid exiting the pump
\dot{p}_{rated}	kJ/hr	The power consumed by the pump at its rated condition
\dot{p}_{pump}	kJ/hr	The power consumed by the pump current condition
\dot{p}_{shaft}	kJ/hr	The pump shaft power at current condition
η_{total}	[0..1]	The overall pump efficiency
η_{motor}	[0..1]	The overall motor efficiency
η_{pump}	[0..1]	The efficiency of the actual pumping process
$p_0 p_1 p_n$	various	User provided coefficient relating pump power to dimensionless control signal
$f_{motorloss}$	[0..1]	The fraction of the pump motor inefficiencies that contribute to a fluid temperature increase in the pump
\dot{p}_{rated}	kJ/hr	The energy added by the pump to the fluid stream
\dot{p}_{rated}	kJ/hr	The energy added by the pump to the environment
γ	[0..1]	The pump control signal

B.3 Storage tank

B.3.1 Nomenclature

Table B. 4: Nomenclature of Storage Tank

ρ	kg/m ³	density of the working fluid
Δt	hours	the TRNSYS timestep
g	C/hr	the function that equals dT/dt (dT/dt = g(T,t))
h	several	coefficient in the enthalpy correlation of the fluid as a function of temperature

m	kg/hr	mass of the fluid in the tank
m_i	kg/hr	initial mass of the fluid in the tank
m_{in}	kg/hr	mass flow rate of fluid entering the tank
m_{out}	kg/hr	mass flow rate of fluid exiting the tank
n	-	integer in the Runge-Kutta solution
$Q_{fluid,in}$	kJ/hr	energy transfer via fluid flow into the tank
$Q_{fluid, out}$	kJ/hr	energy transfer via fluid flow out of the tank
Q_{losses}	kJ/hr	energy lost from the working fluid to the environment
r	several	coefficient in the density correlation of the fluid as a function of temperature
SA	m^2	tank surface area for thermal loss calculations
t	hours	time
T	C	temperature of the fluid in the tank
T_i	C	Initial temperature of the fluid in the tank
T_{in}	C	temperature of the fluid entering the tank
u	several	coefficient in the correlation of internal energy of the fluid
U_L	kJ/hr.m ² .K	heat transfer coefficient between the tank and the surrounding air
V	m ³	volume

B.3.2 Methodology

1. Calculate $g(T_0, t_0)$ using Equation 4.73 T_0 is the temperature of the fluid at the beginning of the time step and $t_0=0$ at the beginning of the time step.
2. Divide the TRNSYS time step by the number of Runge-Kutta steps and call this value Δt_{RK} .
3. Multiply the value found in step 1 by the value found in step 2 and divide by two to get z .

4. Evaluate Equation 4.73 at $T = T_0 + z$ and at time = $\Delta t_{RK}/2$
5. Multiply the result of step 4 by Δt_{RK} and add to T_0 to get our new estimate of T_1
6. Calculate $g(T_1, t_1)$ using Equation 4.73. T_1 is the temperature of the fluid that we calculated in the previous step and $t_1 = 1 * \Delta t_{RK}$
7. Multiply the result of step 6 by Δt_{RK} to find our new estimate of z
8. Evaluate Equation 4.73 at $T = T_1 + z$ and at time = $1 * \Delta t_{RK} + \Delta t_{RK}/2$
9. Multiply the result of the previous step by Δt_{RK} add to T_1 to get our new estimate of T_2
10. Calculate $g(T_k, t_k)$ using Equation 4.73. T_k is the temperature of the fluid that we calculated in the previous step and $t_k = k * \Delta t_{RK}$
11. Multiply the result of step 10 by Δt_{RK} to find our new estimate of z
12. Evaluate Equation 4.73 at $T = T_k + z$ and at time = $k * \Delta t_{RK} + \Delta t_{RK}/2$
13. Multiply the result of the previous step by Δt_{RK} add to T_k to get our new estimate of T_{k+1}

Repeat steps 10 through 13 multiple times to find T_{NRK} . T_{NRK} represent the numerical solution of Equation 4.73 (and the temperature of the fluid in the tank) at the end of the current TRNSYS time step.

B.3.3 Default Settings

Table B. 5: Default Setting of TRNSYS for Storage Tank

Tank volume	m ³	250	The capacity of the storage tank.
Tank surface area	m ²	300	The surface area of the storage tank for thermal loss calculations.
Initial fluid temperature	C	100	. The temperature of the fluid in the expansion tank at the beginning of the simulation.
Initial fluid volume	m ³	100	The volume of the fluid in the storage tank at the beginning of the simulation.
Number of Runge-Kutta steps	-	100	The number of small steps that will be taken each TRNSYS timestep to solve the dT/dt differential equation.
Fluid density coefficient r ₀	kg/m ³	1074	The coefficient r ₀ in the fluid density correlation: $\rho = r_0 + r_1 T + r_2 T^2$
Fluid density coefficient r ₁	kg/m ³ K	-0.6367	The coefficient r ₁ in the fluid density correlation: $\rho = r_0 + r_1 T + r_2 T^2$
Fluid density coefficient r ₂	kg/m ³ K ²	- 0.0007762	The coefficient r ₂ in the fluid density correlation: $\rho = r_0 + r_1 T + r_2 T^2$
Fluid enthalpy coefficient h ₀	kJ/kg	-18.66	The coefficient h ₀ in the fluid enthalpy correlation: $h = h_0 + h_1 T + h_2 T^2$
Fluid enthalpy coefficient h ₁	kJ/kg.K	1.498	The coefficient h ₁ in the fluid enthalpy correlation: $h = h_0 + h_1 T + h_2 T^2$
Fluid enthalpy coefficient h ₂	kJ/kg.K ²	0.001377	The coefficient h ₂ in the fluid enthalpy correlation: $h = h_0 + h_1 T + h_2 T^2$
Fluid internal energy coefficient u ₀	kJ/kg	-19.00	The coefficient u ₀ in the fluid enthalpy correlation: $u = u_0 + u_1 T + u_2 T^2$
Fluid internal energy coefficient u ₁	kJ/kg.K	1.498	The coefficient u ₁ in the fluid enthalpy correlation: $u = u_0 + u_1 T + u_2 T^2$
Fluid internal energy coefficient u ₂	kJ/kg.K ²	0.001377	The coefficient u ₂ in the fluid enthalpy correlation: $u = u_0 + u_1 T + u_2 T^2$
Inlet fluid temperature	C	293	The temperature of the fluid entering the tank.
Temperature of the surroundings	C	15	The temperature of the environment in which the tank is located (for thermal loss calculations)

APPENDIX C

HEAT EXCHANGER DESIGN

Table C. 1: Heat Exchanger Properties

Size	10-240	in	Connected in		1 parallel	5 series
Surf/unit(eff.)	1360	ft ²	Shells/unit		5	Surf/shell (eff.)
						272
						ft ²
PERFORMANCE OF ONE UNIT						
Fluid allocation			Shell Side		Tube Side	
Fluid name			oil		water	
Fluid quantity, Total		lb/h	46000		15000	
Vapor (In/Out)	lb/h	0	0	0	12052	
Liquid	lb/h	46000	46000	15000	2948	
Noncondensable	lb/h	0	0	0	0	
Temperature (In/Out)	°F	734	75	57	623.41	
Dew / Bubble point	°F			623.73	623.73	
Density	Vapor/Liquid	lb/ft³	44.227	66.222	62.366	4.095/40.023
Viscosity		cp	0.1524	3.8587	1.1971	0.024/0.086
Specific heat		BTU/(lb F)	0.6185	0.3721	1.0022	2.217/1.230
Thermal conductivity		BTU/(ft h F)	0.045	0.079	0.338	0.051/0.272
Latent heat		BTU/lb				483.8
Pressure (abs)		psi	60	55	1830	1825.81
Velocity		ft/s	10.89		12.69	
Pressure drop, allow./calc.		psi	5	153.73	30	4.19
Heat exchanged	14873087	BTU/h			MTD corrected	2913.03
						°F